WEBB, Gerald Ph.D. Civil

SYNOPSIS

The behaviour of a clay soil beneath moving rigid wheels was obtained with the aid of a cine-radiographic technique, which uses high intensity, short duration x-ray pulses to observe the movement of small tracer objects imbedded in the clay matrix.

A visioplasticity method was used to compute the soil velocities and finally the strain-rate invariants. The plastic work rate calculated from these invariants after the examination of basic plasticity equations, was equated to the deformation energy, the beneath wheel component of soil-wheel interaction.

Examination of the energy balance of the soil-wheel system, taking into account the energy dissipated at the soil-wheel interface showed that good predictions of the drawbar pull - the usually accepted soil-vehicle criterion - was obtained.

DEFORMATION OF A CLAY SOIL BENEATH MOVING RIGID WHEELS - WEBB

DEFORMATION OF A CLAY SOIL BENEATH MOVING RIGID WHEELS

by

G. L. W. WEBB

A thesis submitted to the Faculty of
Graduate Studies and Research in
partial fulfillment of the requirements
for the degree of Doctor of Philosophy

Department of Civil Engineering
and Applied Mechanics,
McGill University,
Montreal, Quebec.

September, 1968

TABLE OF CONTENTS

ACKNOWLEDGEMENTS

The author acknowledges his indebtedness to:-

Dr. R. N. Yong, his Research Director, who made countless suggestions and provided invaluable advice throughout the experimental programme and in the preparation of this thesis.

Mr. J. D. Fitzpatrick-Nash, who participated in the entire experimental programme and contributed many useful ideas.

Mr. B. Cockayne and his staff for assistance in the modification of the existing facility.

Mr. L. J. Vroomen, Department of Mechanical Engineering, for his assistance in the instrumentation of the test facility, and to the Department of Mechanical Engineering for the loan of numerous items of equipment.

The De Havilland Aircraft of Canada Ltd. for some financial support and for providing the test wheels used during this study.

Dr. R. Japp and several research students of the Soil Mechanics Lab. who assisted in the performance of special tests.

My wife, Marilynn, for typing this thesis.

This study on the interaction between moving rigid wheels and a clay soil represents one phase of an overall study on soil-vehicle interaction being conducted under contract arrangement with the Defence Research

Telecommunications Establishment of Canada (Geophysics Section), negotiated through the Department of Defence Production. Mr. T. A. Harwood, Chief, Geophysics Section DRTE is the Project Officer for this study.

NOTATION

A	area of contact
b	wheel width (inches)
C	cohesion lbs/square inch
D	wheel diameter (inches)
$\mathcal{D}$	deformation energy
F	drawbar pull (lbs)
j	horizontal soil deformation
k	yield stress in shear(lbs/square inch)
K	soil deformation modulus
K_c, K_ϕ, n	Bekker soil parameters
L	horizontal distance travelled by wheel (inches)
M	net torque moment developed by wheel (in./lbs)
p	nominal ground pressure (lbs/square inch)
R	rolling resistance
R_b	compaction resistance
R_c	bulldozing resistance
r	wheel radius (inches)
s	normal wheel slip rate
S	shear stress (lbs/square inch)
t	characteristic time (seconds)
Δu	instantaneous soil velocity
u	X velocity in spatial coordinates = $V_c \longrightarrow \Delta u$
v	Y velocity in spatial coordinates
V	soil velocity (inches/second)

V_c	carriage (translational) velocity
V_s	true slip velocity
w	gravimetric moisture content
W	vertical wheel load (lbs)
X	interfacial energy (in.lbs/sec)
y_b	sinkage to bow wave
y_o	dynamic or rolling sinkage (inches)
y_r	rut depth
η	torque energy coefficient
λ	ratio of characteristic prototype to model wheel length
Λ	pull energy coefficient
γ	soil density (lbs/cub. in.)
ρ	density (lbs.sec^2/in.^{4})
ρ'	Chudakov-Phillips coefficient of rolling resistance
ρ''	dissipated energy coefficient
ρ°	coefficient of rolling resistance
$\hat{\sigma}$	best estimate of population standard deviation
ϕ	soil friction angle
ϖ	angular wheel velocity (rad./sec.)
$\bar{\varpi}$	angular wheel velocity (rev/sec.)

$\epsilon_x, \epsilon_y, \epsilon_z$	normal strains
$\dot{\epsilon}_x, \dot{\epsilon}_y, \dot{\epsilon}_z$	strain rate
$\bar{\dot{\epsilon}}$	strain rate intensity, (or effective strain rate)
$\gamma_{xy}, \gamma_{zx}, \gamma_{zy}$	shearing strains
$\dot{\gamma}_{xy}, \dot{\gamma}_{zx}, \dot{\gamma}_{zy}$	shearing strain rates
I_2	second invariant of strain-rate tensor
u_x, u_y, u_z	displacements
u, v, w	velocity components
$\sigma_x, \sigma_y, \sigma_z$	normal stresses
$\tau_{xy}, \tau_{zx}, \tau_{zy}$	shearing stresses
$\sigma'_x, \sigma'_y, \sigma'_z$	deviatoric stresses
J_2	second invariant of stress tensor
$\bar{\sigma}$	stress intensity (effective stress)
$\dot{W}$	plastic work rate
X, Y	X-Y components of body force

<u>ABBREVIATIONS</u>

B.D.C.	Bottom Dead Center
I.S.T.V.S.	International Society of Terrain Vehicle Systems
L.V.D.T.	Linear Voltage Displacement Transducer
S.F.D.	Source to Film Distance
S.O.D.	Source to Object Distance

LIST OF FIGURES

LIST OF TABLES

CHAPTER 1

INTRODUCTION

Many centuries have elapsed since it was discovered that the force necessary to move an object along the ground was much smaller if the object was equipped with wheels. In the off-road vehicle mechanics field the ability to predict the force necessary to maintain motion in a towed system, or the force that must be developed in a powered system to maintain motion and perform useful drawbar work is of prime importance.

The theoretical or semi-empirical methods available at the present time do not provide a quantitative measure of soil-vehicle interaction. It is obvious that the beneath-wheel component of soil-vehicle interaction has received insufficient attention in the past, and a greater effort should be directed towards the prediction of the soil response behaviour under vehicular loading if adequate soil-vehicle theories are to be formulated.

REVIEW OF EXISTING THEORIES

Rolling Resistance Theories

Bekker (1956), (1960) laid the foundation upon which most soil-vehicle mechanics theories have been developed. He postulated that the pressure beneath a wheel was similar to the pressure below a loaded plate and proposed the following soil pressure-sinkage relationship, namely:-

$$p = \left[\frac{K_c}{b} + K_\phi \right] z^{n} \qquad 1\text{-}1$$

where p is pressure

K_c, K_ϕ and n are 'soil' parameters

b is the wheel width

z is the sinkage

The parameters K_c, K_ϕ and n are determined experimentally from two plate penetration tests. The method is described by Bekker (1959). Reece (1965) showed that Equation (1-1) did not provide the proper pressure sinkage relationship and proposed the following equation:-

$$p = \left[K'_c C + K'_\phi \gamma b \right] \left(\frac{z}{b}\right)^{n} \qquad 1\text{-}2$$

where C = cohesion

γ = soil density

This equation is dimensionally correct and Wills (1966) has shown from tests on sands and clays with plates of varying aspect ratios that an equation similar to Equation (1-2) was in closer agreement with experimental data, but did not necessarily give consistent results. The K'_c and K'_ϕ terms are analagous to N_c and N_γ terms used in conventional bearing capacity formulas and Uffelmann (1961) has used the formula p = 5.7C in his treatment of cohesive soils.

Bekker further assumed that the work expended by the wheel in rut formation is constant and independent of slip. Normal slip (s) can be expressed by the following relation:-

$$s = 1 - \frac{V_C}{r\omega} \qquad 1\text{-}3$$

where V_C = Carriage velocity

r = Wheel radius

ω = Angular velocity of wheel

He equated the work producing this rut to the work expended in forcing a plate vertically into the soil to a depth corresponding to the sinkage. This work is named the compaction resistance, R_c. For an axle load W and a wheel diameter D, Bekker used Equation (1-1) to derive an expression for the wheel sinkage z_o:-

$$z_o = \left[\frac{3W}{(3-n)\,(\frac{K_c}{b} + K_\phi)\,\sqrt{D}}\right]^{\frac{2}{2n+1}} \qquad 1\text{-}4$$

and for compaction rolling resistance, R_c:-

$$R_c = \frac{1}{(n+1)\;(\frac{K_c}{b} + K_\phi)^{\;(1/2+1)}}\left[\frac{3W}{(3-n)\sqrt{D}}\right]^{\frac{2n+2}{2n+1}} \qquad 1\text{-}5$$

For cohesive soils, Uffelmann has obtained the following formulas for sinkage, z_o:-

$$z_o = \frac{W^2}{(5.7C)^2 b^2 D} \qquad 1\text{-}6$$

and for compaction rolling resistance, R_c:-

$$R_c = \frac{W^2}{5.7CbD} \qquad 1\text{-}7$$

It is now generally accepted that sinkage is not independent of slip for sands, (see Reece (1966), Yong et al (1967)) and therefore static plate bearing tests cannot be expected to apply to the entire slip range. For cohesive soils, slip-sinkage is much smaller and Uffelmann (1961) has shown for a wide rigid wheel that slip sinkage was nonexistent. However, tests on tires conducted by Wismer (1965) show some slip sinkage.

Bulldozing resistance due to bow wave formation ahead of the wheel becomes important for loose soils and wide wheels. Bekker approximated the bulldozing resistance, R_b, by the following formula:-

$$R_b = \frac{b \sin(\alpha+\phi)}{2 \sin\alpha \cos\phi} \left[2zC\,Kc + z^2K_\gamma\right] + \frac{\pi t^3}{540}\gamma(90-\phi)$$

$$+ \frac{C\pi t^2}{180} + Ct^2 \tan\left(45+\frac{\phi}{2}\right) \qquad 1\text{-}8$$

where $Kc = (Nc-\tan\phi)\cos^2\phi$

$K_\gamma = \left(\frac{2N}{\tan\phi} = 1\right)\cos^2\phi$

$t = 2\tan^2(45-\phi/2)$

α = Angle of approach. For a rigid wheel α is approximated.

Equation (1-8) actually gives the resistance of soil behind a grouser at some angle of attack. The second, third and fourth terms on the right hand side give the resistance to shear at the edges of the grouser and are usually small when compared with the first term. Hegedus (1960) has simplified Equation (1-8) and suggested the following equation:-

$$R_b = (2zCK_b + z^2 K_\theta \gamma)b \qquad 1\text{-}9$$

K_b and K_θ are 'soil' dependent properties. Methods for calculating them are given by Hegedus.

Drawbar Pull

As mentioned before, the basis of all soil-vehicle interaction studies is the ability to predict the useful drawbar work that can be performed by the system. Bekker postulated that the drawbar pull represents the difference between the gross tractive effort or thrust developed by the system and the rolling resistance of the wheel. This can be written as:-

$$F = H - R \qquad 1\text{-}10$$

where F = Drawbar pull

H = Gross tractive effort or thrust

R = Rolling resistance

The thrust H was equated to the force required to shear the ground along the contact area A. Using Coulomb's Law, the thrust at zero slip can be expressed as:-

$$H = A\,(C + p \tan \phi) \qquad 1\text{-}11a$$

where Shear Stress, $S = C + p \tan \phi$

If W is the vehicle load, the thrust becomes:-

$$H = A\left(C + \frac{W}{A} \tan \phi\right)$$

$$H = AC + W \tan \phi \qquad 1\text{-}11b$$

The shear stress, S is assumed to be slip dependent and the following equation can be written for the shear stress:-

$$S = (C + p \tan \phi) \quad (1 - e^{-j/K}) \qquad 1\text{-}12$$

K, the Deformation Modulus is obtained from a stress strain curve of the material, while j is the soil deformation in the horizontal direction.

Other attempts have been made to predict the thrust developed by a slipping wheel, among these are the works of Janosi (1961), Sela (1964), Poletayev (1964) and Wong and Reece (1967).

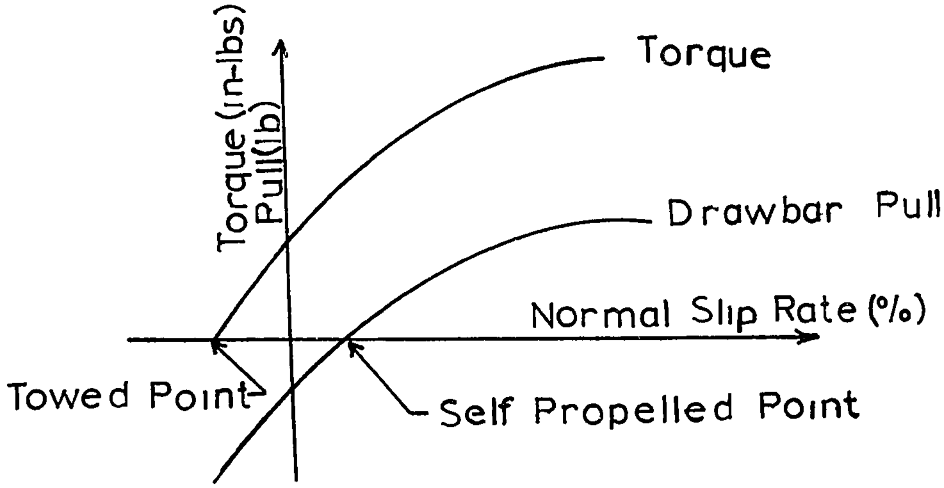

Figure 1-1:- Measured Torque and Pull. Wheel on Clay

Figure 1-1 shows a typical curve of the measured drawbar pull and torque versus normal slip rate for a wheel on clay. For wheels on sand the curves have the same shape except that there is a distinct peak point in the draw pull curve.

Energy Considerations

The soil-vehicle problem has also been studied from an energy viewpoint. Schuring (1966) considering the equilibrium of a wheel suggested the following formula:-

$$M\omega \quad = \quad F\, V_C \quad + \quad \frac{E}{L}\, V_C \qquad 1\text{-}13$$

Torque Energy = Pull Energy + Dissipated Energy

Torque Energy - This is the work done by the driving Torque M and can be calculated as $M\omega$ where ω is the angular velocity in radians. In systems with internal resistance, the driving torque to propel the wheel along the ground is obtained by subtracting the moment to overcome the internal resistance from the total torque.

Pull Energy - The work done by the horizontal axle force (drawbar pull). F can be negative or positive depending on whether the wheel is self propelled or is being towed. The quantity can be expressed as $F\, V_C$ where V_C is the carriage velocity.

Dissipated Energy - $\frac{E}{L}$ represents the energy loss per unit distance travelled by the wheel axle.

The dissipated energy is then expressed as the difference between the torque energy and the pull energy.

$$\frac{E}{L}(V_c) = M\omega - F\,V_c \tag{1-14}$$

Using the definition of normal slip, $s = 1 - (V_c/r\omega)$, the angular velocity ω can be expressed as:-

$$\omega = \frac{V_c}{r(1-s)} \tag{1-15}$$

Substituting for ω in Equation (1-14) we can write:-

$$\frac{E}{L}(V_c) = M\left[\frac{V_c}{r(1-s)}\right] - F\,V_c \tag{1-16}$$

Rearranging, Equation (1-16) becomes:-

$$\frac{E}{L}(V_c) = \frac{V_c}{1-s}\left[\;F\,s + \frac{M}{r} - F\right] \tag{1-17}$$

Expressions are then derived for M, F and axial load, W. These are written in terms of radial and tangential stresses and finally these stresses were transformed into vertical and horizontal stresses. Using these expressions it was then shown that the dissipated energy could be expressed as:-

$$E = \frac{L}{1-s}\left[F\,s + r\,b\int_{\theta_1}^{\theta_2} p\,\theta\,d\theta\right] \tag{1-18}$$

where p = vertical stress on interface

b = wheel width

$\theta_1 - \theta_2$ defines contact surface

Comparison of Equations (1-17) and (1-18) shows that:-

$$\frac{M}{r} - F = r\,b\int_{\theta_1}^{\theta_2} p\;\;\theta\;\;d\theta = R \tag{1-19}$$

The quantity R is defined as the energy dissipated per unit distance travelled by the wheel axle.

Schuring asserts that Equation (1-19) is similar to Bekker's compaction resistance formula for a slipless wheel where the rolling resistance is equated to the work done in making a vertical rut. This formula can be written as follows:-

$$R_c = b\ L \int_{o}^{z_o} p\ dz \qquad 1\text{-}20$$

Equation (1-18) can then be expressed as:-

$$E = \frac{L}{1-s} \left[R V_t + Fs \right] \qquad 1\text{-}21$$

To define E, R and F must be evaluated. Schuring suggests the use of the Bekker-Bernstein pressure-sinkage relationship to define the pressure beneath the wheel and finally the R term. The inadequacy of these formulations has been discussed previously. To calculate F, a stress-displacement relation is assumed and the equilibrium of stresses around the wheel is considered.

The calculation of both F and R for a slipping wheel to evaluate the dissipated energy seems to be an unnecessary exercise, since the calculation of F only, provides an answer to the vehicle mechanics problem.

Equation (1-19) can also be written as:-

$$E = \frac{L}{1-s} \left[Fs + W\rho^{o} \right] \qquad 1\text{-}22$$

where ρ^{o} is a coefficient of rolling resistance

The term ρ^{o} is dependent on several input parameters and it is assumed that this portion of the dissipated energy follows a Coulombic concept. Methods for evaluating ρ' are suggested but they are approximate.

Phillips (1961), using a formulation of Chudakov (1950) suggested a formula of the form:-

$$\frac{E}{L} = \rho' W \qquad 1\text{-}23$$

ρ' is a Coulombic coefficient and is considered to define the entire dissipated energy. Expressions for ρ' are derived by suggesting a new definition for "rolling radius" of the wheel and a line of action for the vertical soil reaction. Leflaive (1966) obtained a dimensionless relationship by dividing Equation (1-14) by WV_c and rearranging it to give:-

$$\frac{E/L\ V_c}{WV_c} = \frac{M\omega}{WV_c} - \frac{FV}{WV_c}$$

$$\rho'' = n - \Lambda \qquad 1\text{-}24$$

Dissipated Energy Coefficient = Torque Energy Coefficient − Pull Energy Coefficient

Here again the entire dissipated energy coefficient is given a "Coulombic nature" by the division by W.

BEHAVIOUR OF SOIL BENEATH WHEELS

The stresses at the wheel soil interface have been obtained by the use of various devices. Freitag et al (1965) installed several transducers around the periphery of tires and converted the readings into normal and shear stresses. Pressure distributions have been obtained at the interface by Hegedus (1965) while pressure and shear stress distribution have been obtained by Uffelmann (1961), Onafeko (1965) and Onafeko and Reece (1967). These measurements have been useful in showing that the maximum radial pressure occurs ahead of the bottom dead centre, and that negative shear stresses can exist for towed wheels. Their usefulness has been limited because correlations between the measured values and values predicted from postulated theories are lacking.

McKibben (1938) observed the material paths of sand particles beneath a driven wheel. Wong and Reece (1966) used a glass sided box to observe the behaviour of soil beneath rigid wheels. The behaviour of sand beneath rigid wheels was investigated using a cine-radiographic technique at the soils lab at McGill University. Partial analysis of this data has been presented by Yong and Osler (1966), Boyd and Windisch (1966) and Yong et al (1967). The translational paths qualitative in the first two studies and quantitative in the last study mentioned above showed a distinct horizontal component. Most rolling resistance theories neglect this aspect of soil deformation and assume vertical rut formation.

PURPOSE OF STUDY

In the majority of studies mentioned previously, the beneath-wheel component of soil vehicle interaction has been accounted for by empirical relations which do not adequately describe the response behaviour of soil under vehicular loading.

The energy balance method seems to offer a solution for the soil-vehicle interaction problem. However the forces and factors that affect the energy balance of the system must be analysed from a more rational viewpoint. The torque energy and the pull energy are clearly defined, however new methods for the estimation of the dissipated energy must be formulated.

This dissipated energy term can only be formulated if the entire deformation pattern is analysed. The dissipated energy term must include the following:-

i) The energy used up in deforming the soil vertically and horizontally. This will be shown as the Deformation Energy; $\mathfrak{D}$.

ii) The energy dissipated by the frictional stresses at the wheel-soil interface. It should be noted here that the "wheel-soil interface" is a very thin region close to the spinning wheel and does not extend to the bottom of the deformed medium. This will be called the Interfacial Energy; X.

To define the interfacial frictional stresses at the wheel-soil interface the laws of friction must be examined. These are discussed in Chapter II.

Proposed Energy Balance Equation

For a rigid wheel travelling with uniform velocity and with zero slip at the wheel-soil interface, the energy balance equation can be written as:-

$$\underset{\text{Torque (Input) Energy}}{M\omega} = \underset{\text{Pull Energy}}{FV_c} + \underset{\text{Deformation Energy}}{\mathcal{D}} \qquad 1\text{-}25$$

For the general case of a slipping wheel, the energy balance equation can be written as:-

$$\underset{\text{Torque Energy}}{M\omega} = \underset{\text{Pull Energy}}{FV_c} + \underset{\text{Deformation Energy}}{\mathcal{D}} + \underset{\text{Interfacial Energy}}{X} \qquad 1\text{-}26$$

The ability to predict F is a useful criterion in soil vehicle studies. In Equation (1-25) if the deformation energy can be estimated, the pull, F can be determined, whereas in Equation (1-26) estimates of the deformation and interfacial energy are necessary.

Certain misconceptions which might arise from the division of the dissipated energy will be discussed briefly. Phillips (1961) states that a number of authors argue that the power loss to the ground is divisible into separate parts (i) that which is due to slip and (ii) that which is due to deformation of the wheel and gound. He quite correctly asserts that coefficients derived from such relationships are not very useful because of the arbitrary definition of slip, and the methods for calculating deformation energy are not precise. Reece (1961) comments that in the study of the mechanics of a wheel on soil, slip losses (due to horizontal deformations) and rolling losses (due to vertical deformations) should be computed separately. The deformation energy as specified above defines the work in deforming the soil vertically and horizontally. There is both horizontal and vertical movement of the soil under all conditions. The interfacial energy might be considered a slip loss (not according to Reece's definition since there are horizontal movements down to the bottom of the deformed zone) because it represents the energy quantity produced by the frictional stresses at the interface, multiplied by the slip velocity V_s. The definition of slip velocity is exact however in this thesis, since rigid wheels are used and the visioplasticity methods provide the true soil velocity. In calculating slip velocity on each segment of the interface the relation below is used:-

$$V_s = r\omega - (\text{Carriage Velocity, } V_c + \text{Instantaneous Soil Velocity, } \Delta u)$$

$$V_s = r\omega - \text{ Soil Velocity, } V.$$

The normal slip velocity ($r\omega-$ Carriage Velocity, V_c) is not used to calculate the interfacial energy.

SEARCH FOR NEW THEORIES

Considerable research has been conducted by workers in the field of metals seeking theories that will adequately describe various metal forming processes. It must be accepted that the behaviour of soil beneath wheels bears some resemblance to some of the metal forming processes such as strip rolling, extrusion or material behaviour under a punch. The slip line method has been extensivley used for the plane strain case and allows the determination of local stresses and velocity distribution in the plastic zone for rigid, perfectly plastic materials. Upper bound limit solutions have also been formulated. These two methods however suffer from lack of uniqueness.

Visioplasticity Method - A method for obtaining Deformation Energy.

Visioplasticity is a technique for visualizing the plastic flow of a material by determining the particle velocity vectors.

For an extrusion process, Thomsen and Lapsley (1954) obtained the displacement by photographing the changes in a grid etched on the meridian plane of an axi-symmetric lead billet. From the displacements the field was evaluated and used to compute the strain rates and finally the internal stress distribution.

The cine-radiographic method developed at McGill University provides particle displacements through the use of a matrix of small tracer-objects imbedded in the soil. The location of these tracer-objects at successive deformation stages is obtained on film through the use of short duration, high intensity, x-ray pulses. This radiographic data is used to compute the velocity vectors and strain rate invariants. From the strain rate invariants the plastic work rate can be computed. If certain conditions are satisfied, the plastic work rate can be equated to the rate of deformation of the soil.

In the absence of any theory for soil-vehicle interaction, it was envisaged that an initial two dimensional study of the behaviour of soil beneath rigid wheels using the visioplasticity method would be a big step forward and it could be later extended to the three dimensional case. The entire developement of the visioplasticity method is given in Chapter II.

USE OF MODELS

The use of models in soil-vehicle studies and the extension of results to prototype behaviour is a very attractive proposition because of the relative ease in testing and also because of economics. Most existing scaling theories, theoretical or otherwise do not properly incorporate the beneath wheel component of soil-vehicle interaction in the system parameters. Certain basic relationships for prototype behaviour have been developed from model testing, however the extension of model results to prototype behaviour is still a haphazard exercise. In the absence of any adequate scaling theory, it was decided to vary the input parameters systematically and an attempt would be made to establish basic relationships.

SCOPE OF STUDY

This study can be divided into two parts. In Part I the deformation behaviour of a clay soil beneath two driven rigid wheels will be obtained by the use of a cine-radiographic technique. Clay soils are most often encountered in nature and present the most difficulties. A better knowledge of their behaviour under vehicular motion is necessary before soil-vehicle mechanics can be studied on a more rational basis.

The measurement of the surficial and above ground parameters, namely Load, Torque, Drawbar-pull, Carriage Velocity, Sinkage and Angular Velocity is also included in Part I.

In Part II the information obtained above will be used to:-

i) Calculate the Deformation Energy, that is the energy expended in deforming the soil vertically and horizontally using a visioplasticity method.

ii) Examine the energy balance of the entire system.

iii) Formulate a theory which explains soil-vehicle interaction in the light of the above.

CHAPTER 2

OBSERVED WHEEL PERFORMANCE

The main body of this thesis will concern itself with the analytical treatment of the soil-vehicle interaction problem. To enhance the continuity of this section the following have been placed in appendices at the end of this thesis.

Appendix I	- TEST FACILITY	- Description and Calibration of Components.
Appendix II	- EXPERIMENTATION	- Modifications to Existing Facility.
		- Radiographic Considerations.
		- Clay Compaction and Control.
		- Test Bed Geometry.
		- Testing Schedule.
Appendix III	- TEST TECHNIQUE AND DATA REDUCTION	- Transfer of Radiographic Data
		- Computer Programs.

A resume of the experimentally obtained surficial and above ground parameters will be presented here, (see Table 2-1). Some of the information discussed is obtained

TABLE 2-1

SURFICIAL LOADING INFORMATION

	Carr. Veloc.	Ang. Veloc.	Normal Slip	Torque	Pull	Dynamic Sinkage	Rut Depth	M/C
Test No.	V_c in./sec	ω rad./sec	s %	M in.lbs.	F lbs.	y_o ins.	y_r in.	w %
Model Wheel 23.5 lbs. D = 9.0 ins. b = 2.5 ins.								
15	5.54	2.387	48.39	97.01	8.45	0.70	0.18	53.7
16	5.68	1.257	1.73	47.68	-26.18	0.95	-0.12	53.8
17	5.63	1.445	13.18	74.00	-12.93	0.75	-0.06	53.7
18	5.78	1.885	32.31	76.78	2.98	0.51	0.35	53.7
19	5.45	1.508	18.45	67.10	- 8.96	0.72	0.15	54.7
20	5.59	2.953	57.52	102.99	9.67	0.63	0.15	54.6
21	5.63	2.953	57.94	106.07	9.40	0.70	0.18	54.3
22	5.73	1.131	-12.17	9.76	-35.82	0.62	-0.18	53.8
23	5.82	2.575	49.86	102.04	7.19	0.56	0.06	53.4
24	5.82	2.199	41.42	88.00	7.19	0.80	0.00	54.7
25	5.87	4.775	72.81	99.65	9.57	0.70	0.38	54.6
Prototype Wheel 34 lbs. D = 13.5 ins. b = 3.75 ins.								
28	5.63	2.236	60.37	198.47	17.45	0.31	0.00	52.9
44	5.82	1.257	29.89	148.02	3.13	0.30	0.00	53.1
Prototype Wheel 51 lbs. D =13.5 ins. b = 3.75 ins.								
30	5.78	1.696	50.18	214.61	15.27	0.61	0.20	54.5
32	5.73	1.257	32.14	173.86	5.86	0.73	-0.05	53.9
33	5.59	.941	14.52	146.04	- 6.47	0.74	0.00	53.5
34	5.73	1.005	17.50	153.99	- 4.35	0.76	0.20	54.6

Table 2-1 Cont'd

Test No.	V_c	ω	s	M	F	y_o	y_r	W
35	5.59	0.817	2.37	80.94	-15.71	0.69	0.20	54.6
36	5.68	0.754	- 9.64	8.39	-25.59	0.67	0.10	54.6
37	5.78	2.513	66.30	233.99	20.52	0.55	0.10	54.4
38	5.78	3.833	77.82	238.47	22.17	0.67	0.15	54.9
39	5.63	1.068	21.91	157.47	- 2.70	0.74	0.05	53.2
43	5.82	1.256	31.02	172.37	4.94	0.55	0.05	52.0
48	8.83	1.958	31.94	188.10	3.43	0.62	0.10	53.3
49	7.28	1.508	29.72	179.83	1.38	0.60	0.00	53.2
50	4.88	1.151	35.95	173.37	2.34	0.58	-0.10	53.0
51	3.94	1.817	29.43	170.39	2.56	0.56	-0.10	52.6
Prototype Wheel 68 lbs. D = 13.5 ins. b = 3.75 ins.								
31	5.78	2.073	58.57	229.02	16.76	0.90	0.20	54.2
42	5.78	1.257	32.67	189.27	5.55	0.83	0.25	52.9
45	5.78	1.382	36.70	201.69	10.69	0.79	0.00	53.8
Prototype Wheel 79 lbs. D = 13.5 ins. b = 3.75 ins.								
40	5.59	2.236	60.70	263.81	15.80	1.15	0.25	53.6
41	5.78	0.942	7.82	206.17	-32.01	1.39	0.00	54.2
46	5.68	1.068	19.75	244.93	-17.43	1.18	0.00	54.0
47	5.68	1.131	26.78	252.88	-13.14	1.00	0.10	54.6

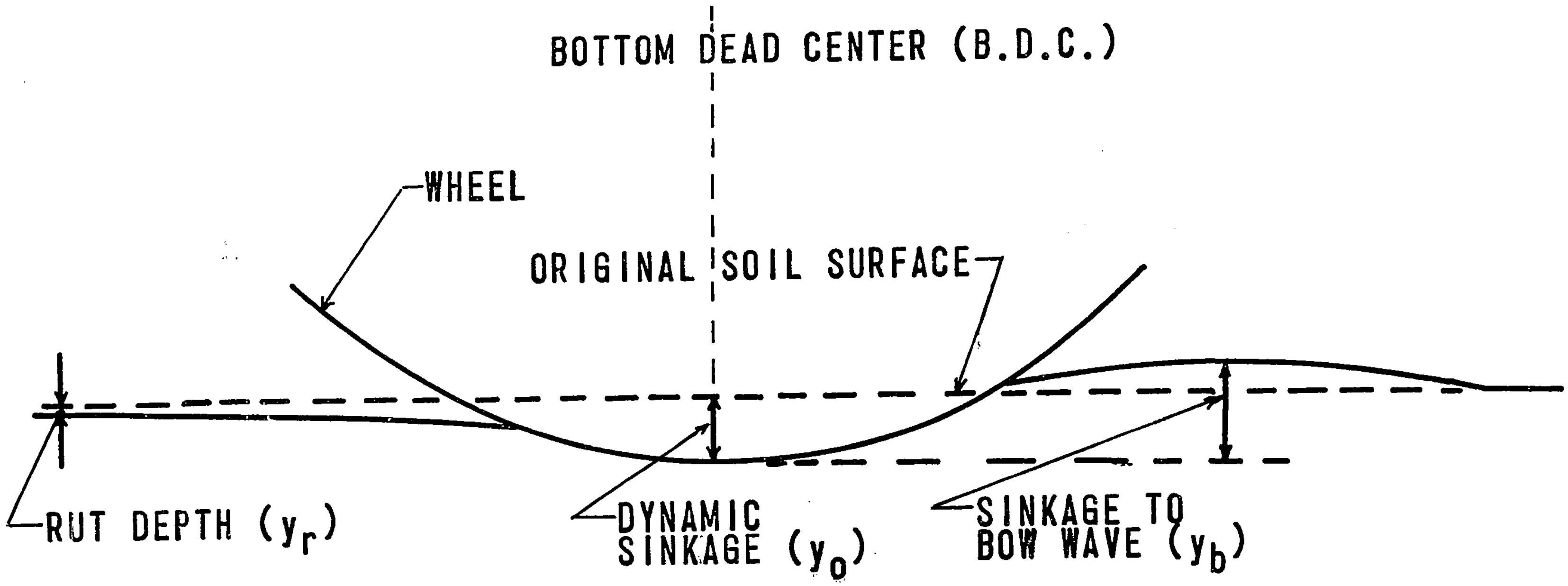

FIGURE 2-1. SINKAGE DEFINITIONS

from the U. V. recorder traces while some are obtained from radiographic data. In some cases explanations for observed behaviour will be given in capsule form since detailed explanations are dependent on the examination of beneath wheel soil behaviour and the energy balance of the entire system. These are discussed in Chapter 5.

Rolling Wheel Sinkage

The sinkage below the original soil surface is measured before recovery for rut formation and is referred to as the dynamic or rolling sinkage y_o. (See Figure 2-1).

The sinkage versus slip curves for the model wheel (23.5 lb.) and the prototype wheel (51 lb.and 79 lb) are shown in Figure 2-2. The following features are noticeable:-

i) λ^2 load scaling between model and prototype produced the same sinkage.

ii) Sinkage, y_o, seems to be independent of slip.

The height and shape of the bow wave is accurately determined by the cine-radiographic technique. The following were evident:-

a) Rut recovery was substantial.

b) The bow wave ahead of the prototype wheel (51 lb) was small and showed a small increase with decreasing slip.

c) The bow wave ahead of the model wheel was larger

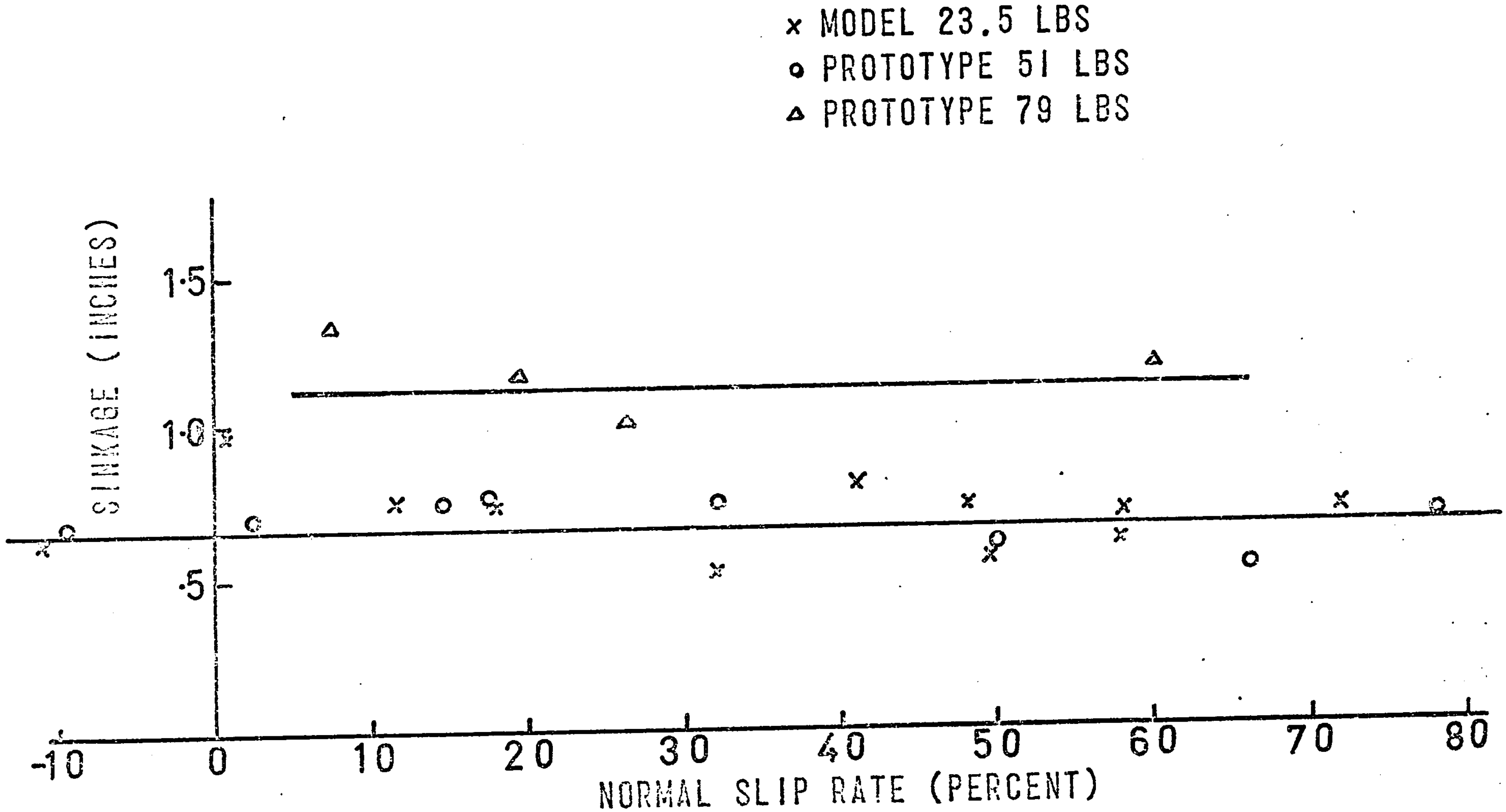

FIGURE 2-2. DYNAMIC SINKAGE VERSUS SLIP RATE (PERCENT)

and showed a larger increase with decreasing slip. From b) and c) above it can be concluded that the sinkage to bow wave increased with decreasing slip.

Slip Sinkage

In Chapter 1 it was stated that soil-vehicle studies carried out on soils (especially sands) show an increase of sinkage with slip. Several explanations have been offered for this phenomena. Reece (1966) shows the velocity distribution beneath a wheel in sand, if continuity relations are to be satisfied for an incompressible medium. For the slipping wheel he shows that the average soil velocity in the deforming region is larger than the initial soil velocity (carriage velocity V_c) and therefore the sinkage can be calculated. Reece was not able to specify the magnitude of these velocities but it may be concluded that the higher the velocity, the greater the sinkage. For the skidding wheel he shows that the velocity at the interface is less than the carriage velocity, while further down the soil velocity is greater than V_c. Reece, however, assumes that the average soil velocity is equal to V_c and postulates that sinkage must be zero. To reinforce this idea he shows a photograph for a skidding wheel where the sinkage is in fact zero. This experiment however, is questionable because "the right shape of bow wave" was placed ahead of

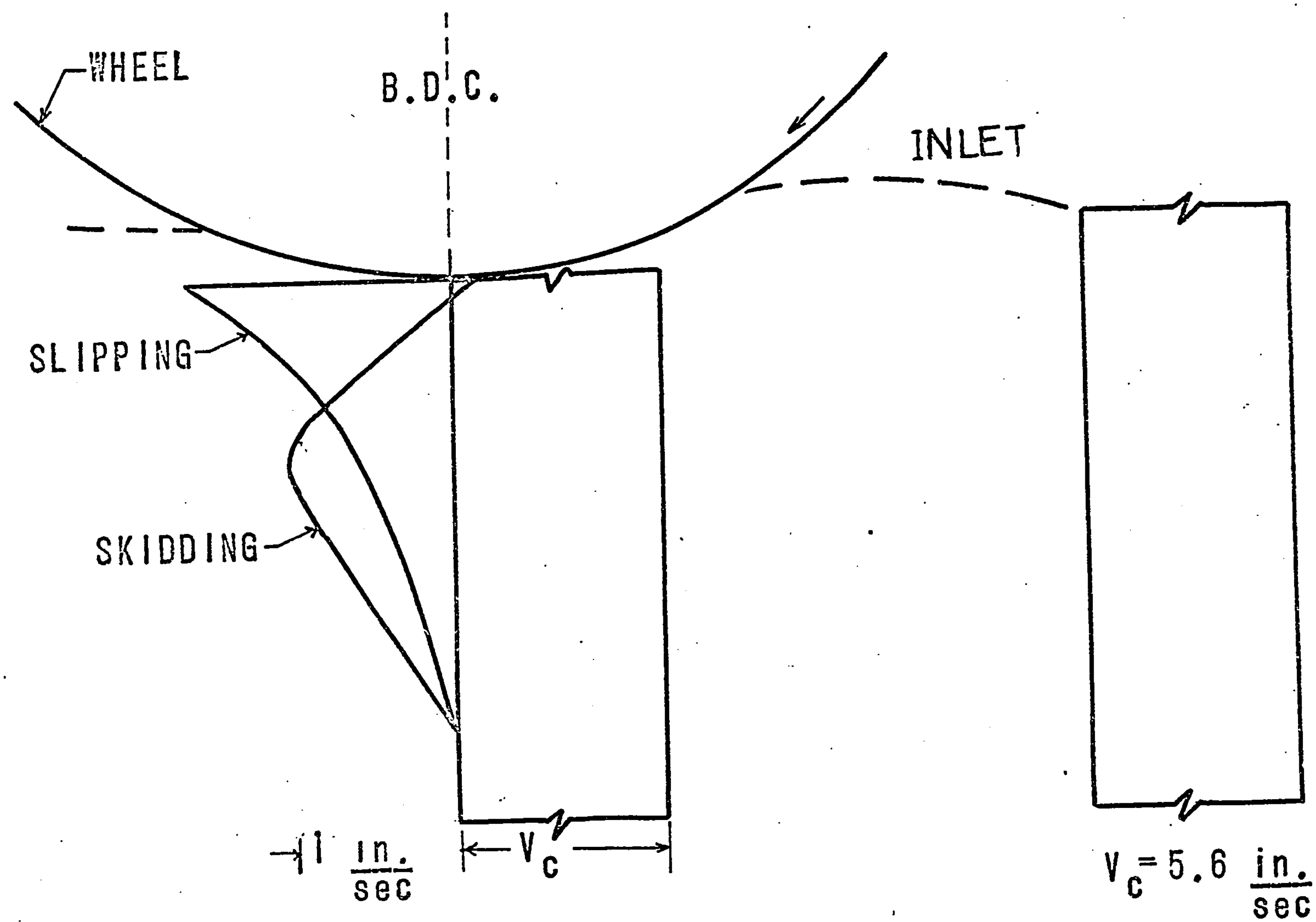

FIGURE 2-3. VELOCITIES AT BOTTOM DEAD CENTER

the wheel to attain equilibrium. Reece's idea for the slipping wheel is correct although the magnitude of the soil velocities were not directly obtainable. However the idea that sinkage must be zero for the skidding wheel is not necessarily true.

Figure 2-3 shows the experimentally obtained X velocities below a skidding wheel (-9% normal slip) and a slipping wheel. At the B. D. C., the Y velocities are close to zero and therefore the X velocities are the flow tube velocities. It will be shown (in Chapter 4) that incompressibility is a reasonable assumption and thus the continuity equation can be applied to the flow tubes from the interface to the bottom of the deformed zone. The instantaneous sinkages calculated in this way are close to the measured dynamic or rolling sinkages. Slip sinkage is negligible because the X velocities do not become excessively large at high slips. This is due to the fact that the wheel soil interface is a discontinuity and the soil work hardens in a narrow region.

For dry sands however, the velocities will be very large in a larger region near the interface since dry sand does not exhibit a substantial strain rate effect. This will produce slip sinkage. The lower post peak stress for dense sand which has been suggested as a reason for slip sinkage will in fact result in higher velocities in the sand at high normal slips. However even if the soil strength is unchanged at high slips, there will be higher velocities at higher slip.

Torque and Drawbar Pull Versus Normal Slip

The torque and drawbar pull versus slip rate for the model wheel are shown in Figure 2-4 and for the prototype wheel in Figure 2-5. The drawbar pull curves show the classical relationship, rising to some peak value and then staying relatively constant. The self propelled points are achieved at relatively high normal slip (around 25 per cent). This feature is also evident in the data review of rigid wheel behaviour by Frietag (1965).

Torque

Figure 2-6 shows the torque ratio between the model and prototype wheels. For the prototype wheel with λ^2 weight scaling, λ^2 torque scaling is obtained over most of the slip range; however λ^3 weight scaling did not provide λ^3 torque scaling. The inability of the λ^3 weight scaling to produce λ^3 torque scaling is due to the limiting shear stress which depends only on slip velocity. The λ^3 scaling produces greater sinkage and greater contact area but the shear stress at the same slip velocity is identical.

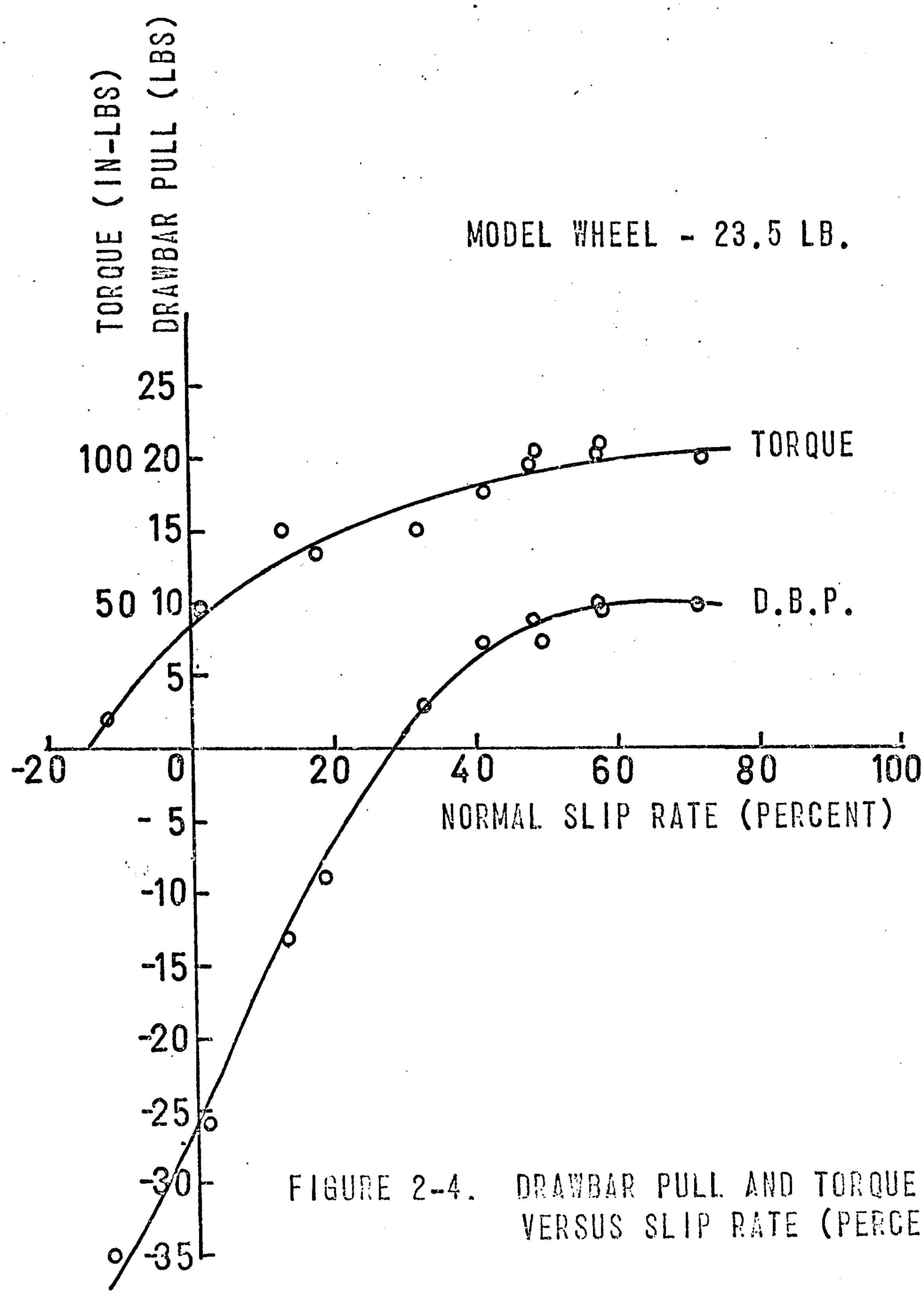

FIGURE 2-4. DRAWBAR PULL AND TORQUE VERSUS SLIP RATE (PERCENT)

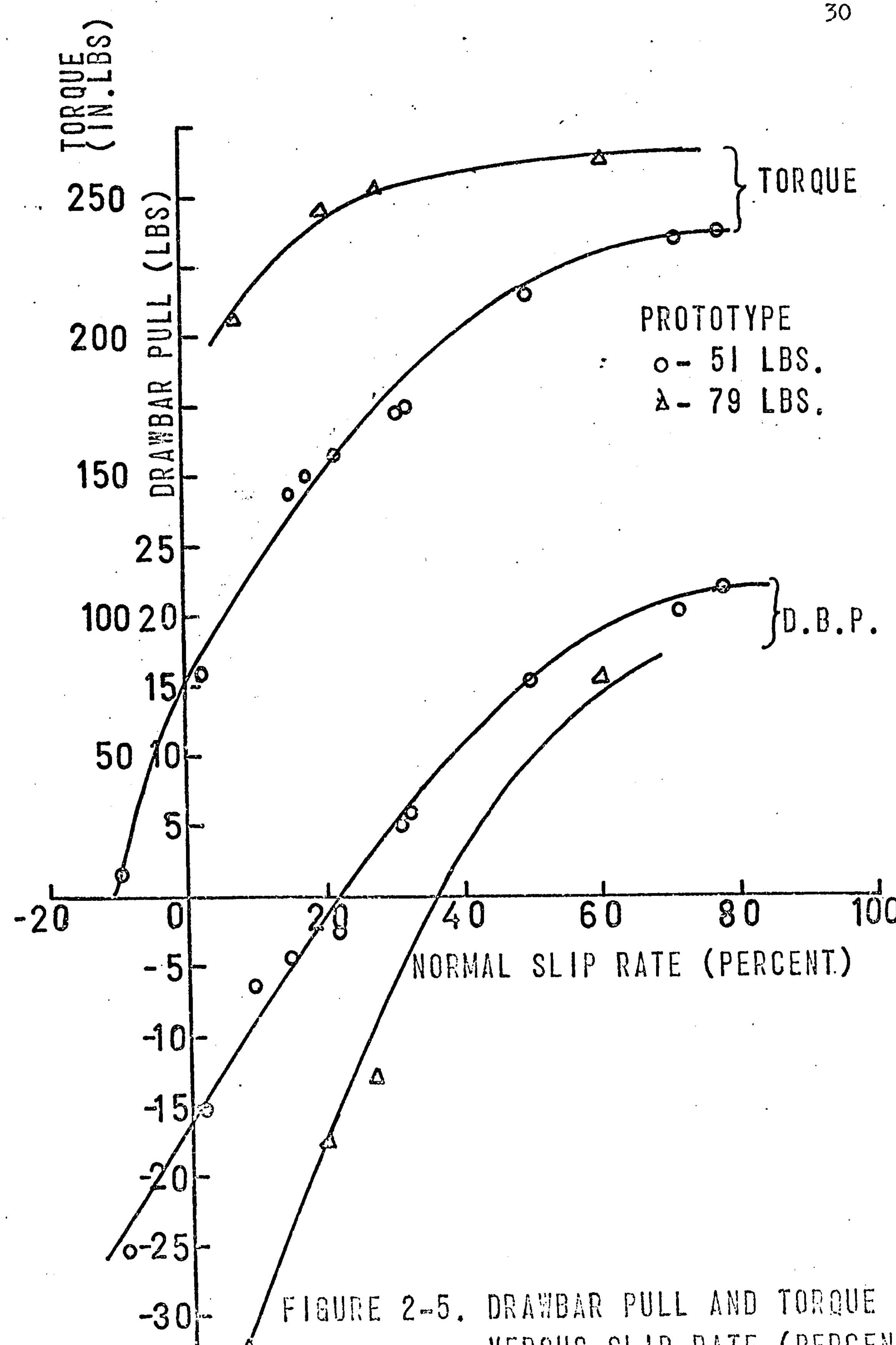

FIGURE 2-5. DRAWBAR PULL AND TORQUE VERSUS SLIP RATE (PERCENT)

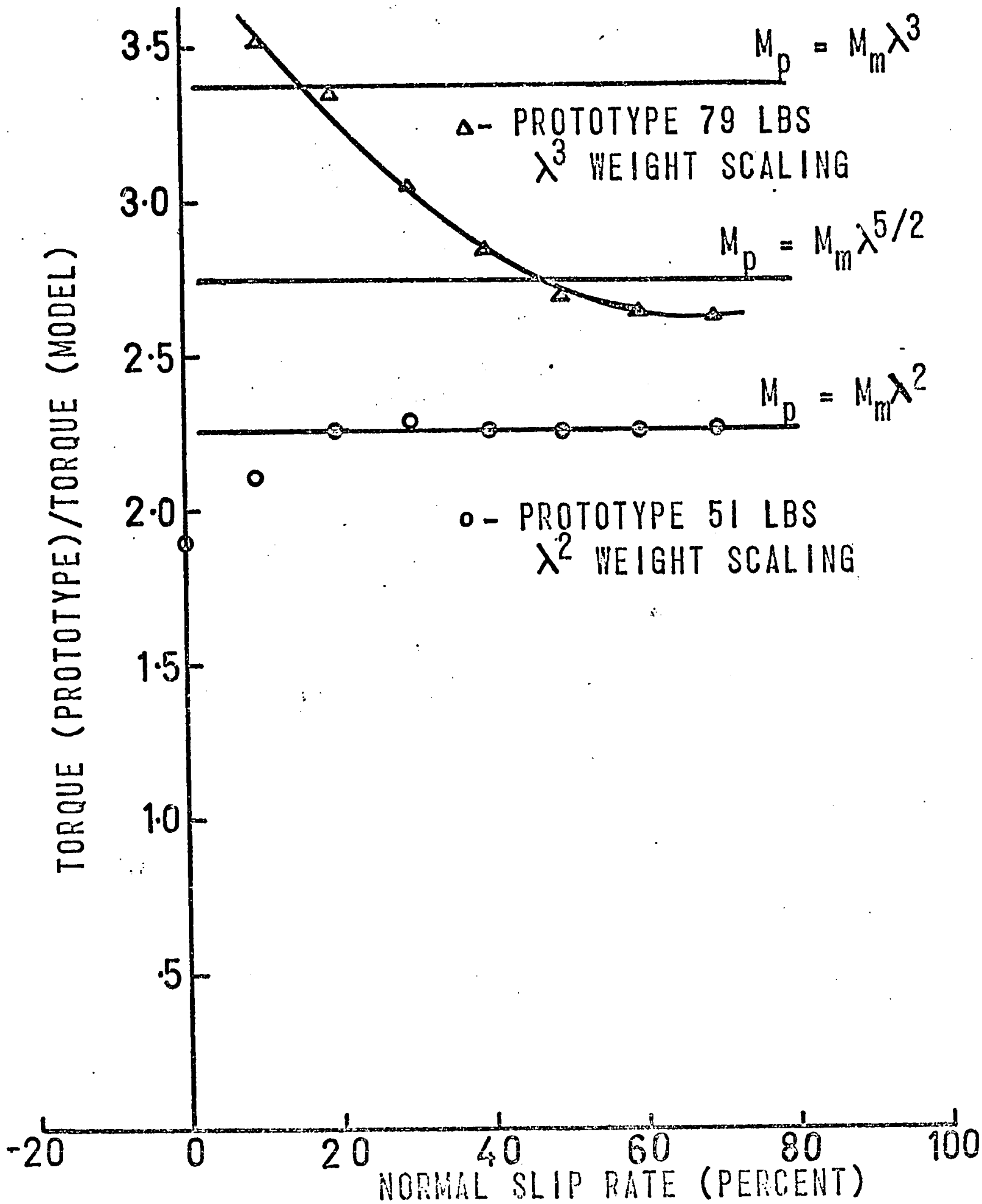

FIGURE 2-6. TORQUE RATIO VERSUS SLIP RATE (PERCENT)

Pull/Weight Versus Slip

The pull/weight versus slip curves for both wheels are shown in Figure 2-7. At slips above the self propelled point the pull/weight relationship for the model wheel and the prototype with λ^2 load scaling are close but not identical. However there is a significant difference in the relationship below the self propelled point. Since λ^2 torque scaling is obtained for λ^2 weight scaling, the torque per unit weight is the same for both wheels. However since $\omega_p = \frac{\omega_m}{\lambda}$ at the same slip (for equal carriage velocities), the input energy per unit weight for the model will be λ times the input energy per unit weight for the prototype wheel. Similarly it will be shown that the interfacial energy for the model wheel is λ times that of the prototype. If the energy balance equation is considered, the λ^2 scaling seems to offer a partial solution to the scaling of rigid wheels on cohesive soils. The deformation energy component however does not follow a specific scaling pattern at low slips and as a result the drawbar pull/weight ratio deviates at low slips. The reasons for the additional deformation energy or "resistance" at low slips for the model wheel is seen to be due to a radically altered strain rate field. This will be discussed in detail in Chapter 5.

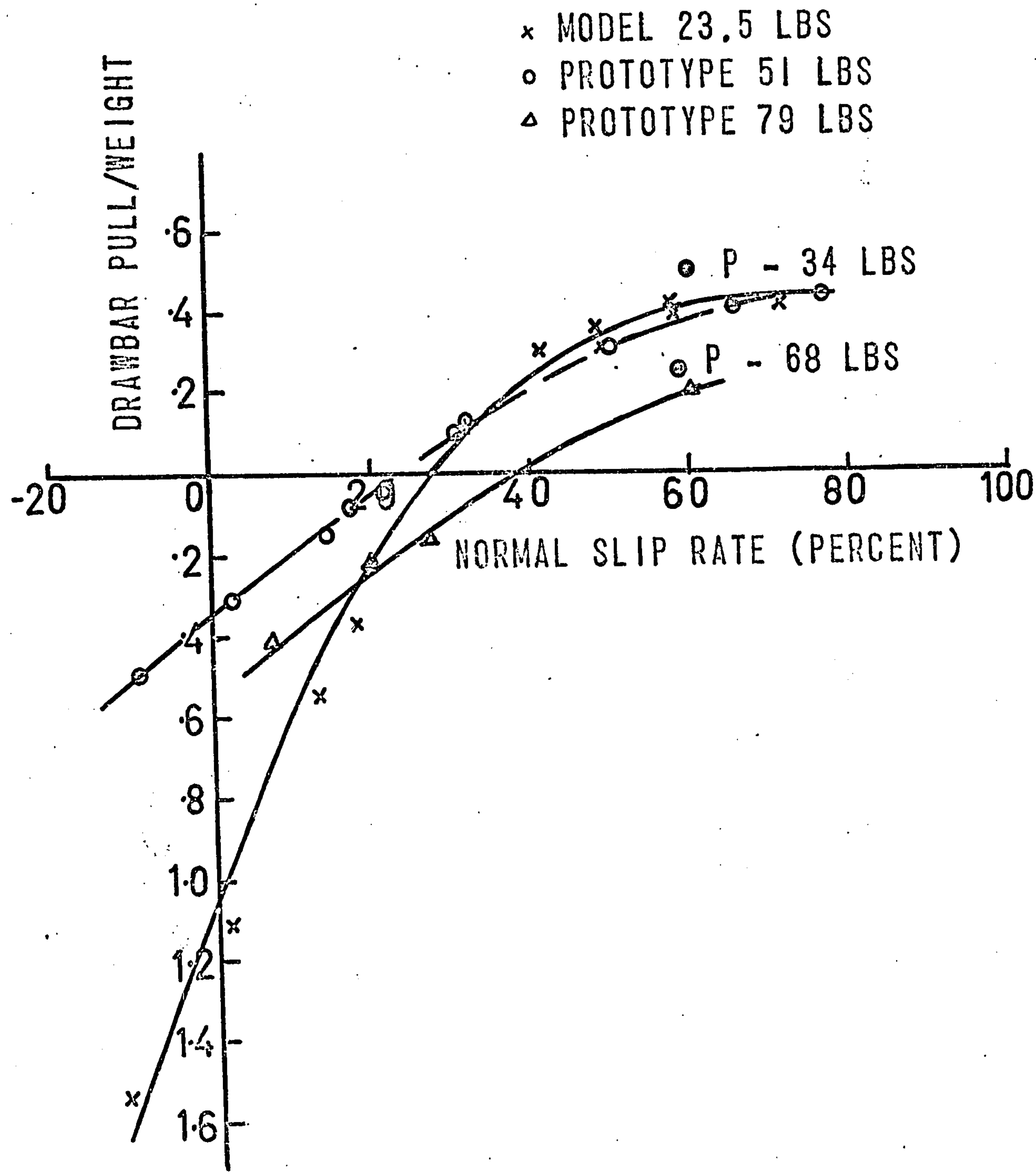

FIG.2-7. DRAWBAR PULL/WEIGHT VERSUS SLIP RATE (PERCENT)

CHAPTER 3

VISIOPLASTICITY AND LAWS OF FRICTION

In this chapter, a review of the visioplasticity method will be given together with a brief discussion of the soil-vehicle interfacial relationships. The governing equations arrived at will be used in the analysis of results shown in Chapter IV.

VISIOPLASTICITY

For a metal forming process such as extrusion a grid spacing as small as 1/10 inch can be scribed on the meridian plane. If a clay box with glass or lucite is used to study the behaviour below a grouser, a grid spacing of 1/2 inch can be used. If the photographic technique is used an original picture of the grid is taken. At successive deformation stages, additional pictures are taken or a continuous record can be obtained with a cine camera. These pictures can then be projected onto a sheet of tracing paper with enlargements several times the original grid size. Using reference markers, the displacements of the node points on the grid can be obtained. From these displacements and distortions, the flow paths can be obtained for the deformation process. The cine-radiographic technique with the marker matrix provides similar information when special data reduction techniques are used.

Velocity computations can then be made either in material or spatial x - y coordinate systems. This is dictated by the type of analysis to be made. Having established the x and y velocity components i.e. u and v respectively, it is then possible to make plots of the following relations:-

u versus x; v versus x; u versus y; v versus y.

Strain Rate Analysis

The rate of plastic deformation of a particle can be expressed in terms of the normal and shear strain-rate components. These strain-rate components can be written as:-

$$\dot{\epsilon}_x = \frac{\partial u}{\partial x} ; \quad \dot{\epsilon}_y = \frac{\partial v}{\partial y} ; \quad \dot{\epsilon}_z = \frac{\partial w}{\partial z} .$$

$$\dot{\gamma}_{xy} = \frac{\partial v}{\partial x} + \frac{\partial u}{\partial y} ; \quad \dot{\gamma}_{yz} = \frac{\partial w}{\partial y} + \frac{\partial v}{\partial z} ; \quad \dot{\gamma}_{zx} = \frac{\partial u}{\partial z} + \frac{\partial w}{\partial x} \qquad 3\text{-}1$$

where u, v, and w are velocities in the x, y and z direction respectively.

The second invariant, I_2, of the strain rate tensor can be expressed as:-

$$I_2 = \frac{(\dot{\epsilon}_x^2 + \dot{\epsilon}_y^2 + \dot{\epsilon}_z^2)}{2} + \frac{(\dot{\gamma}_{yz}^2 + \dot{\gamma}_{zx}^2 + \dot{\gamma}_{xy}^2)}{4} \qquad 3\text{-}2$$

Most definitions of strains and strain rates apply only when there are infinitesimal displacements. The deformation in metal forming processes or soft soil deformation beneath a wheel falls under the heading of unrestricted plastic flow. Prager and Hodge (1951) have shown for a material in which the choice of reference state is arbitrary, (for example, rigid, perfectly plastic or visco-plastic materials in contradistinction to an elastic or elastic plastic solid in which there is one stress free state,) that the instantaneous reference state can be used and that the rate of strain can be obtained with respect to the deformed medium. For the elastic or elastic plastic material, the rate of strain must be defined with respect to the undeformed stress free state. These two definitions of strain rates lead to different results only in the case of finite deformations. Several definitions of finite strain have been advanced, Love (1946) gives the following relationship:-

$$\epsilon_x = \frac{\partial u_x}{\partial x} + \frac{1}{2}\left[\left(\frac{\partial u_x}{\partial x}\right)^2 + \left(\frac{\partial u_y}{\partial x}\right)^2 + \left(\frac{\partial u_z}{\partial x}\right)^2\right] \qquad 3\text{-}3$$

$$\cdots\cdots\cdots\cdots\cdots\cdots$$

$$\gamma_{xy} = \frac{\partial u_y}{\partial x} + \frac{\partial u_x}{\partial y} + \frac{\partial u_x}{\partial x}\frac{\partial u_x}{\partial y} + \frac{\partial u_y}{\partial x}\frac{\partial u_y}{\partial y} + \frac{\partial u_z}{\partial x}\frac{\partial u_z}{\partial y}$$

where u_x, u_y, u_z are displacements.

The components of rate of straining with respect to the undeformed medium are obtained by differentiating Equation (3-3) with respect to time. The resulting equations although linear in velocity components referred to natural coordinates, contain the derivatives of the displacement with respect to these natural coordinates as coefficients.

However the rate of straining defined with respect to the deformed medium (spatial coordinates) is linear in the derivatives of the velocity components computed with respect to the spatial coordinates.

Stress Analysis

The state of stress at a point P in a continuous medium can be defined by the six stress components σ_x, σ_y, σ_z, τ_{yz}, τ_{zx}, τ_{xy}, See Figure 3-1. The normal stress can be decomposed into a spherical part corresponding to the mean normal stress, $s = 1/3\ (\sigma_x + \sigma_y + \sigma_z)$ and a deviatoric part.

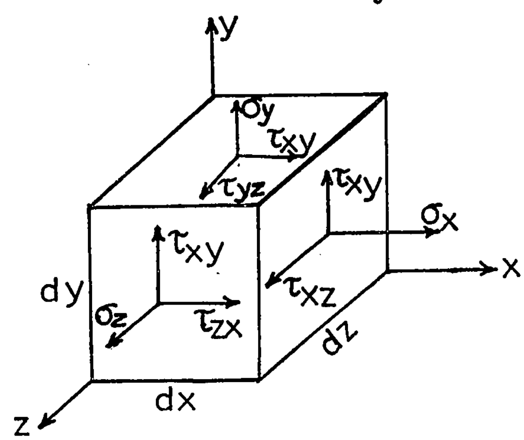

Figure 3-1: General State of Stress at a Point

The stress deviations can then be written as:-

$$\sigma'_x = \sigma_{x-s}$$
$$\sigma'_y = \sigma_{y-s} \qquad 3\text{-}4$$
$$\sigma'_z = \sigma_{z-s}$$

The second invariant, J_2, of the stress deviation can be expressed as:-

$$J_2 = \frac{1}{2}\left(\sigma_x'^2 + \sigma_y'^2 + \sigma_z'^2\right) + \tau_{yz}^2 + \tau_{zx}^2 + \tau_{xy}^2 \qquad 3\text{-}5$$

Instead of the second invariant of the strain rate and stress deviation the following relation can be used:-

i) The effective stress and effective strain rates which are the stress and strain intensities due to Hencky (1924) can be written as:-

Effective Stress:- $\bar{\sigma} = \sqrt{3 J_2}$ 3-6

Effective Strain Rate:- $\bar{\dot{\epsilon}} = \sqrt{\frac{4}{3} I_2}$

ii) The octahedral shear stress and strain rates due to Nadai (1950) can be written as:-

Octahedral Stress : $\tau_{OCT} = \sqrt{\frac{2}{3} J_2}$ 3-7

Octahedral Strain Rate: $\dot{\gamma}_{OCT} = \sqrt{\frac{8}{3} I_2}$

Basic Plasticity Equations

The equations below must be examined when a solution for any problem in plastic flow is sought.

The continuity equation for the plane strain case can be written as:-

$$\frac{\partial \rho}{\partial t} + \frac{\partial \rho u}{\partial x} + \frac{\partial \rho v}{\partial y} = 0 \qquad 3\text{-}8$$

In Equation (3-4), the density of the material at various deformation stages must be examined. The volume change characteristics of soils covers the whole spectrum from dilation (volume increase) in dense sands to small volume decrease in clay soils. The researcher in soil mechanics is therefore faced with a material whose "material" properties can change under varying loading conditions.

The equations of motion of a plastic mass (momentum equations) can be written as:-

$$\frac{\partial \sigma_x}{\partial x} + \frac{\partial \tau_{xy}}{\partial y} + \rho u \frac{\partial u}{\partial x} + \rho v \frac{\partial u}{\partial y} + \rho \frac{\partial u}{\partial t} = X$$

$$\frac{\partial \sigma_y}{\partial y} + \frac{\partial \tau_{xy}}{\partial x} + \rho u \frac{\partial v}{\partial x} + \rho v \frac{\partial v}{\partial y} + \rho \frac{\partial v}{\partial t} = Y \qquad 3\text{-}9$$

The loading of soils by the passage of a wheel is a transient phenomenon which falls between static and dynamic loading. In Equation (3-9) the acceleration or inertial terms must be examined. The third and fourth terms on the right hand side are the convective acceleration terms while the fifth term is the local acceleration. The body forces X and Y represent the matrix and gravitational potential. The changes in the matrix potential resulting from possible density changes during shearing and total effect of matrix potential on soil strength must be specified.

Having satisfied the above relationships, a suitable constitutive equation which links the stresses to the strain-rates must be selected.

The behaviour of soils in the deviatoric plane and the provision of constitutive equations for the behaviour of soils under static loading conditions in cylindrical and triaxial tests have been the object of intense study in the soil mechanics field. The classical Mohr-Coulomb failure criterion has found almost universal acceptance, although the von-Mises, Tresca and Extended Mohr-Coulomb yield theories have been critically examined. (For a literature review see Yong and Warkentin (1966) and Yong and McKyes (1966). Japp (1967) has also investigated the strain rate effects of soil under dynamic compression.) These studies have provided valuable insight into the behaviour of soils under controlled loading conditions. Nevertheless many problems such as volume change effects, directions of principal stress and strain rate increment vectors, work hardening, strain rate and quasi-viscous effects have only been partly answered.

The suitability of these equations for use in soil-vehicle mechanics studies must be examined and if necessary, suitable constitutive equations for beneath wheel soil behaviour must be developed.

A VISIOPLASTIC SOLUTION

For a plane strain plastic flow problem with the following conditions satisfied:-

i) Steady state process

ii) Negligible inertial and body forces

iii) Incompressible flow

iv) Elastic strains small compared to the plastic strains

The continuity relation reduces to:-

$$\dot{\epsilon}_x + \dot{\epsilon}_y = 0 \qquad 3\text{-}10$$

and the momentum equations reduce to:-

$$\frac{\partial \sigma_x}{\partial x} + \frac{\partial \tau_{xy}}{\partial y} = 0 \qquad \text{3-11a}$$

$$\frac{\partial \sigma_y}{\partial y} + \frac{\partial \tau_{xy}}{\partial x} = 0 \qquad \text{3-11b}$$

The Levy-Mises relationship can then be used as a link between the strain-rate and stress. These can be written as:-

$$\dot{\epsilon}_x = \frac{\sqrt{I_2}}{k}\sigma_x' \qquad \text{3-12a}$$

$$\dot{\epsilon}_y = \frac{\sqrt{I_2}}{k}\sigma_y' \qquad \text{3-12b}$$

$$\dot{\gamma}_{xy} = \frac{2\sqrt{I_2}}{k}\tau_{xy} \qquad \text{3-12c}$$

where $k^2 = J_2$ = Second stress Invariant (von-Mises criterion)

k = Yield stress in shear or $1/\sqrt{3}$ yield stress in tension or compression.

To determine the stress from strain rates for extrusion of lead, Thomsen and Lapsley (1954) used the effective strain-rates and effective stress Equation (3-12) instead of the second invariant of the stress and strain-rate tensor.

If $\dot{\epsilon}_y$ is subtracted from $\dot{\epsilon}_x$, the following equation results:-

$$\dot{\epsilon}_x - \dot{\epsilon}_y = \frac{\sqrt{I_2}}{k}\left(\sigma_x - \sigma_y\right) \qquad \text{3-13}$$

Solving for σ_x gives:-

$$\sigma_x = \sigma_y + \frac{k}{\sqrt{I_2}} \left(\dot{\epsilon}_x - \dot{\epsilon}_y\right) \tag{3-14}$$

Differentiating Equation (3-12) with respect to y, gives:-

$$\frac{\partial \sigma_x}{\partial y} = \frac{\partial \sigma_y}{\partial y} + \frac{k}{\sqrt{I_2}} \frac{\partial}{\partial y} \left(\epsilon_x - \epsilon_y\right) \tag{3-15}$$

The term $\frac{\partial \sigma_y}{\partial y}$ in Equation (3-15) can be obtained by the use of Equation (3-11b) and by differentiating Equation (3-12c). The resulting equation is:-

$$\frac{\partial \sigma_y}{\partial y} = -\frac{\partial \tau_{xy}}{\partial y} = -\frac{1}{2} \frac{k}{\sqrt{I_2}} \frac{\partial}{\partial x} \left(\dot{\gamma}_{xy}\right) \tag{3-16}$$

Substituting Equation (3-16) into Equation (3-15) gives:-

$$\frac{\partial \sigma_x}{\partial y} = \frac{k}{\sqrt{I_2}} \frac{\partial}{\partial y} (\dot{\epsilon}_x - \dot{\epsilon}_y) - \frac{1}{2} \frac{k}{\sqrt{I_2}} \frac{\partial}{\partial x} (\dot{\gamma}_{xy}) \tag{3-17}$$

The right hand side of Equation (3-17) can then be evaluated for any point in the flow field where the strain-rates have been determined and for which k is known.

Rate of Doing Plastic Work

The rate at which stresses do work in connection with the change in shape, $\dot{W}$, can be computed when the stresses and rate of strain are known. The quantity can be expressed as:-

$$\dot{W} = \sigma'_x \dot{\epsilon}_x + \sigma'_y \dot{\epsilon}_y + \sigma'_z \dot{\epsilon}_z + \tau_{yz} \dot{\gamma}_{yz} + \tau_{zx} \dot{\gamma}_{zx} + \tau_{xy} \dot{\gamma}_{xy} \tag{3-18}$$

If the soil is compressible, the total rate of doing work on the soil must include the work done as volume changes are accomodated. The total work (Deformation Energy) can then be expressed as:-

$$\text{Deformation Energy} = \int \text{Plastic Work Rate} + \int \text{Work done by producing volume change} \qquad 3\text{-}19$$

<u>Application</u>

For a material which follows the von-Mises criterion, the rate of doing work under plane strain conditions can be expressed as:-

$$\dot{W} = \sigma'_x \dot{\epsilon}_x + \sigma'_y \dot{\epsilon}_y + \tau_{xy} \dot{\gamma}_{xy} \qquad 3\text{-}20$$

Using Equation (3-12, Equation (3-20) becomes:-

$$\dot{W} = \sigma'^2_x \frac{\sqrt{I_2}}{k} + \sigma'^2_y \frac{\sqrt{I_2}}{k} + \tau_{xy} 2 \frac{\sqrt{I_2}}{k} \qquad 3\text{-}21a$$

$$= \frac{\sqrt{I_2}}{k} \left(\sigma'^2_x + \sigma'^2_y + 2\tau^2_{xy} \right) \qquad 3\text{-}21b$$

$$= \frac{\sqrt{I_2}}{k}\; 2J_2 \qquad 3\text{-}21c$$

Since $k^2 = J_2$, Equation (3-21c) becomes:-

$$\dot{W} = 2k\sqrt{I_2} \qquad 3\text{-}22$$

Equation (3-22) shows that it is possible to calculate the rate of doing plastic work without first determining the stresses. If the material is strain-rate dependent, the plastic work can also be obtained without calculating the stresses as long as the rate dependence of the yield stress is available.

It has generally been accepted by workers in sheet rolling theory that when slippage occurs, the external frictional stress at the interface and its relationship with the shear stress of the material must be examined. A deformation theory is incomplete unless interfacial behaviour is included.

INTERFACIAL STRESSES

The interfacial energy, X, is a measure of the work done by the frictional stresses at the wheel soil interface, and energy can be expressed as:-

$$X = \sum_{\substack{\text{Total Area}\\ \text{of Contact}}} \begin{matrix}\text{Frictional}\\ \text{Stress}\end{matrix} \times \begin{matrix}\text{Elemental}\\ \text{Area}\end{matrix} \times \begin{matrix}\text{Elemental}\\ \text{Slip}\\ \text{Velocity}\end{matrix} \qquad 3\text{-}23$$

To define the external frictional stress at the wheel soil interface, the laws of friction must be examined.

Laws of Friction

i) Assume that a constitutive equation of the form $\tau_s(p,I)$ can be postulated for the yield point in shear of the soil at the wheel soil interface. I is the strain-rate invariant and p is the pressure. The frictional stress, τ, can then be defined in the following manner:-

$$|\tau| \leq \tau_s(p,I) \qquad 3\text{-}24$$

This follows because the shear stress of a point in the thin surface layer of soil (or in a layer parallel and close to the surface) is less than on the slipping surface at this point. The equality holds if the surface of contact is a slip surface, that is, the maximum value of the frictional stress is given by the relation:-

$$|\tau| = \tau_s(p, I) \qquad 3\text{-}25$$

Prandtl (1951) has shown for an ideal plastic material moving between rough platens that the flow boundary is a slip plane and that on this slip plane the shearing stresses reach the value $\tau_s = k$, i.e. the shear stress of the material. It is essential however that the normal pressure p on the surface be greater than a certain value p_s. This condition is satisfied when contact pressure is a few times larger than the yield stress of the material.

ii) One of the basic mechanisms of dry surface friction is the plastic deformation of a thin layer. In metals, it is customary to talk about projections on the surface. These projections act independently at small pressure and the effective cross sectional area is the sum of these projections. Since the effective area in shear which determines the capacity of these projections for a shearing stress is directly proportional to the area of the projections, the frictional stress will be directly proportional to the pressure p. This relation is usually expressed as Coulomb's law and can be written as:-

$$|\tau| = \mu p \qquad 3\text{-}26$$

where μ = coefficient of friction.

The frictional stress can have the values given in Equation (3-25) and (3-26) only at points of contact of the surface where there is relative velocity, that is the rim velocity

$(r\omega)$ must be different from the soil velocity (carriage velocity plus instantaneous soil velocity). Points on the contact surface where $V_s = o$ are zones of adhesion and in these zones static friction applies. These zones of adhesion can be looked upon as changes in the sign of τ. Equations (3-25) and (3-26) are the approximate laws of surface friction which can be used in deformation theory.

CHAPTER 4

DEFORMATION AND INTERFACIAL ENERGIES

In this chapter the visioplasticity method as applied to the soil-vehicle problem (Chapter 3) will be used to calculate the deformation energy. This will entail the following:-

1) Determination of flow paths from observed experimental data and velocity computations.
2) Determination of velocity contours and calculation of strain rate invariants.
3) Application of basic plasticity equations and selection of a yield equation.

Special tests to define the interfacial frictional stress and use of these stresses to define the interfacial energy will be described.

The intent here is to provide a means for obtaining quantitative information from soil deformation results (under the moving wheel). With this information (e.g. deformation energy, interfacial energy loss, etc.) it will be possible ideally to predict drawbar pull for any slip condition if torque energy is known. The application of this technique or correlation between predicted and measured deformation will be found in Chapter 5.

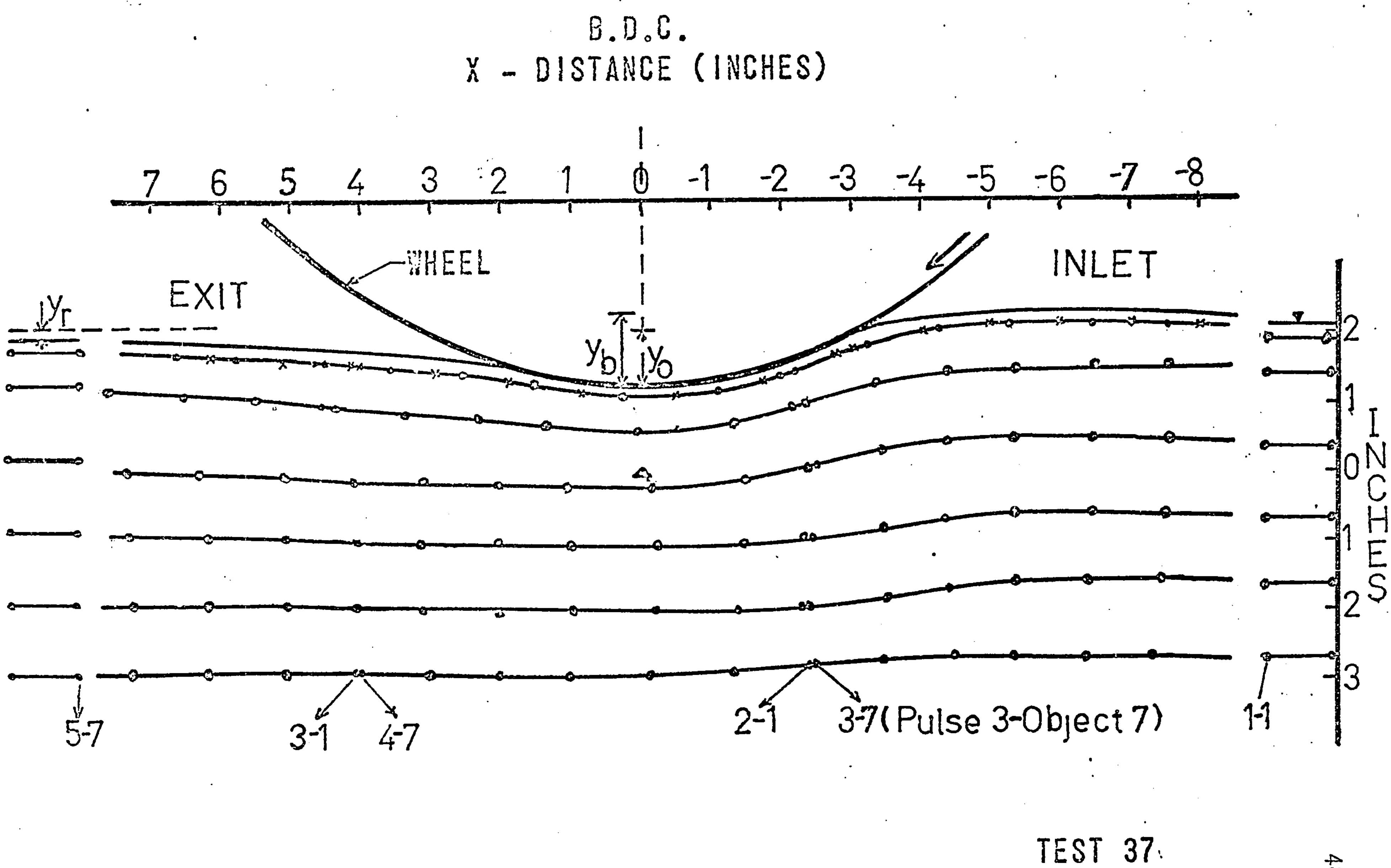

FIGURE 4-1. FLOW PATTERN OF CLAY BENEATH RIGID WHEEL

COMPUTATION OF DEFORMATION ENERGY USING VISIOPLASTICITY

Flow Paths

Figure 4-1 shows the soil flow pattern below the wheel for a typical test (Test 37). These flow patterns are obtained in the following manner.

In program LINDA, described in Appendix III, the X and Y co-ordinates are expressed with respect to the optical centre of the pulser. It is known that the centre line of the wheel is 6.1 inches ahead, exactly over, and 6.1 inches behind the optical centre of the pulser. The wheel can then be considered to be fixed in space, and the tracer object position plotted with respect to the fixed wheel.

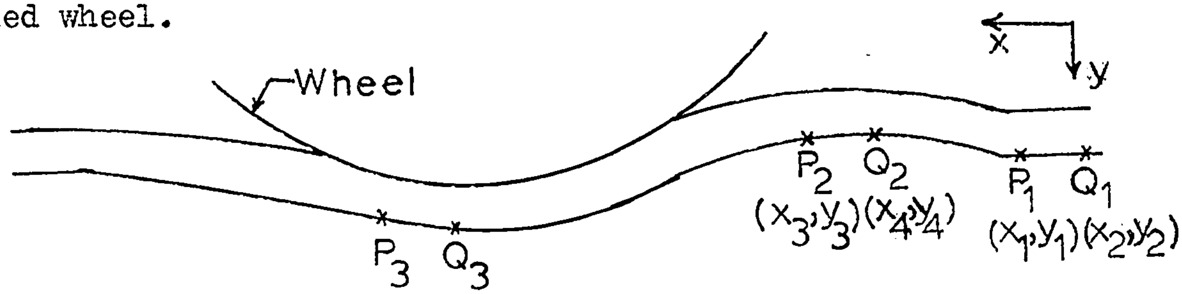

Figure 4-2:- Velocity Computation

Calculation of Velocities (With reference to Figure 4-2)

1) At instant $t = t_1$, tracer object P has spatial co-ordinates P_1 (x_1,y_1) and tracer object Q has co-ordinates Q_2 (x_2,y_2).
2) At instant $t = t_2$, tracer object P has co-ordinates

P_2 (x_3, y_3) and tracer object Q has co-ordinates Q_2 (x_4, y_4).

3) Tracer object P has moved (x_3-x_1) while tracer object Q has moved (x_4-x_2) in X direction.

4) Object P and Q both have an initial velocity V_c. This distance ΔS travelled due to the initial velocity can be expressed as:-

$$\Delta S = (t_2-t_1)V_c \qquad 4\text{-}1$$

5) Distance tracer object has moved, due to an additional instantaneous velocity caused by flow around the wheel, can be expressed as:-

$$\text{For P: Distance} = (x_3-x_1) - \Delta S \qquad 4\text{-}2$$

$$\text{Q: Distance} = (x_4-x_2) - \Delta S \qquad 4\text{-}3$$

6) The difference of the two terms shown above in Equation (4-2) and (4-3) represent the difference in deformation undergone by the two tracer objects P and Q due to instantaneous velocity. This distance Δx can be expressed as:-

$$\Delta x = (x_3-x_1) - \Delta S \; - \; (x_4-x_2) - \Delta S$$

$$\Delta x = (x_3-x_1) - (x_4-x_2) \qquad 4\text{-}4$$

7) An object placed at the same level below the wheel will show the same deformation history. At time $t_1 + \Delta t = \frac{x_1-x_2}{V_c}$ object Q will occupy position P_1. The instantaneous X velocity can therefore be expressed as:-

$$\Delta u = \frac{(x_3-x_1) - (x_4-x_2)}{\Delta t} \qquad 4\text{-}5$$

This instantaneous velocity is assumed to act midway between P_2 and Q_3. Therefore X velocity u can be expressed as:-

$$u = \text{Horizontal Velocity} = \Delta u + V_c \qquad 4\text{-}6$$

8) Similarly:-

$$v = \Delta v = \frac{(y_3-y_1) - y_4-y_2)}{\Delta t} \qquad 4\text{-}7$$

For ease in computation in program JANE, the material co-ordinate (0,0) was assigned to the initial object positions as shown in Figure 4-3.

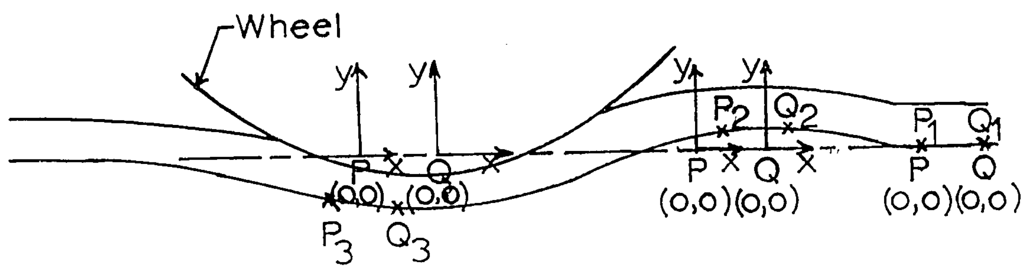

Figure 4-3 :- Velocity Computation

(P_1,Q_1) will coincide with $P_{(0,0)}$ and $Q_{(0,0)}$ and P_2,Q_2 and P_3,Q_3 can be expressed with respect to $P_{(0,0)}$ and $Q_{(0,0)}$.

Δx in Equation (4-4) can be expressed as:-

$$\begin{aligned} \Delta x &= P_2 \text{ wrt } P_{(0,0)} - Q_2 \text{ wrt } Q_{(0,0)} \\ \Delta y &= P_2 \text{ wrt } P_{(0,0)} - Q_2 \text{ wrt } Q_{(0,0)} \end{aligned} \qquad 4\text{-}8$$

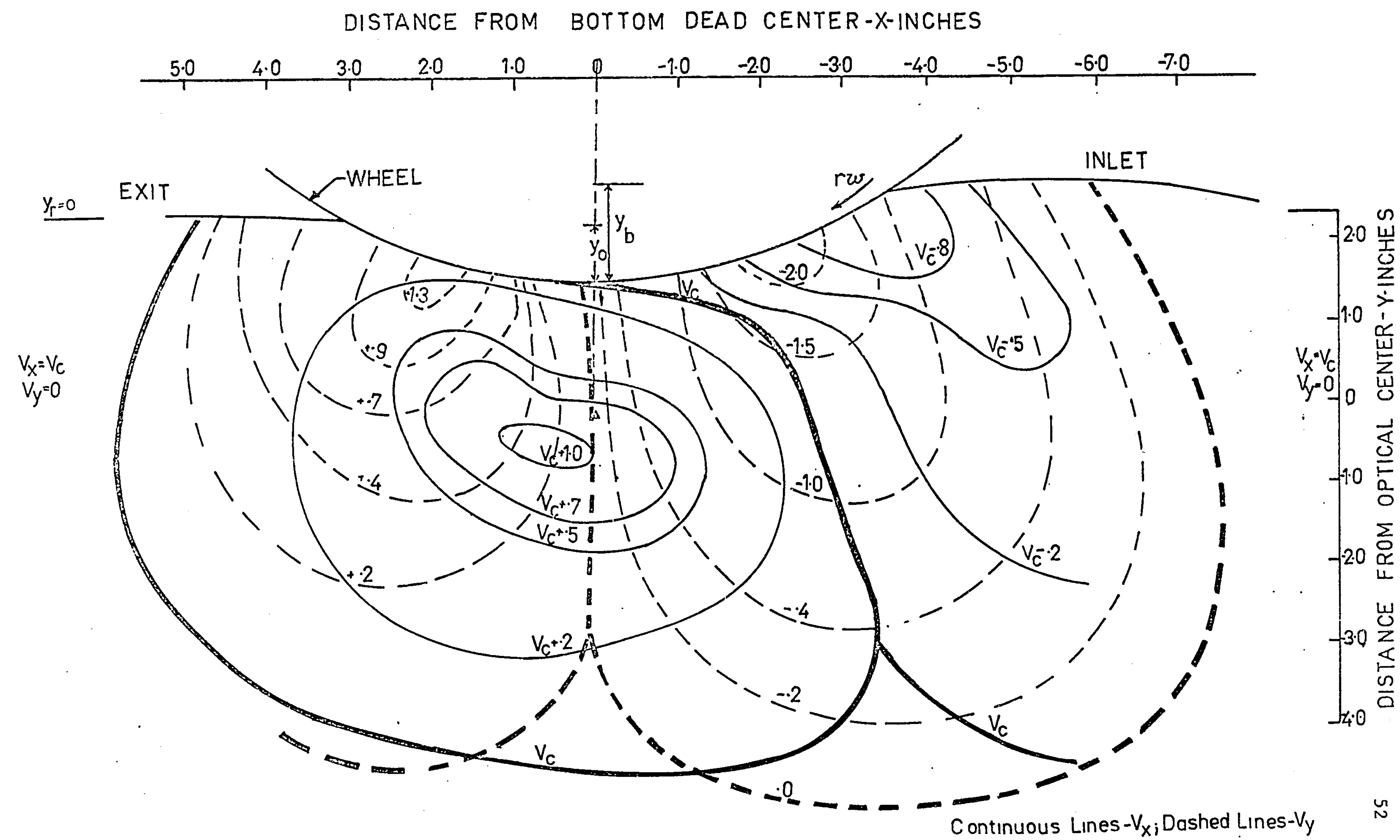

FIGURE 4·4 - VELOCITY CONTOURS - TEST 36. -9% SLIP

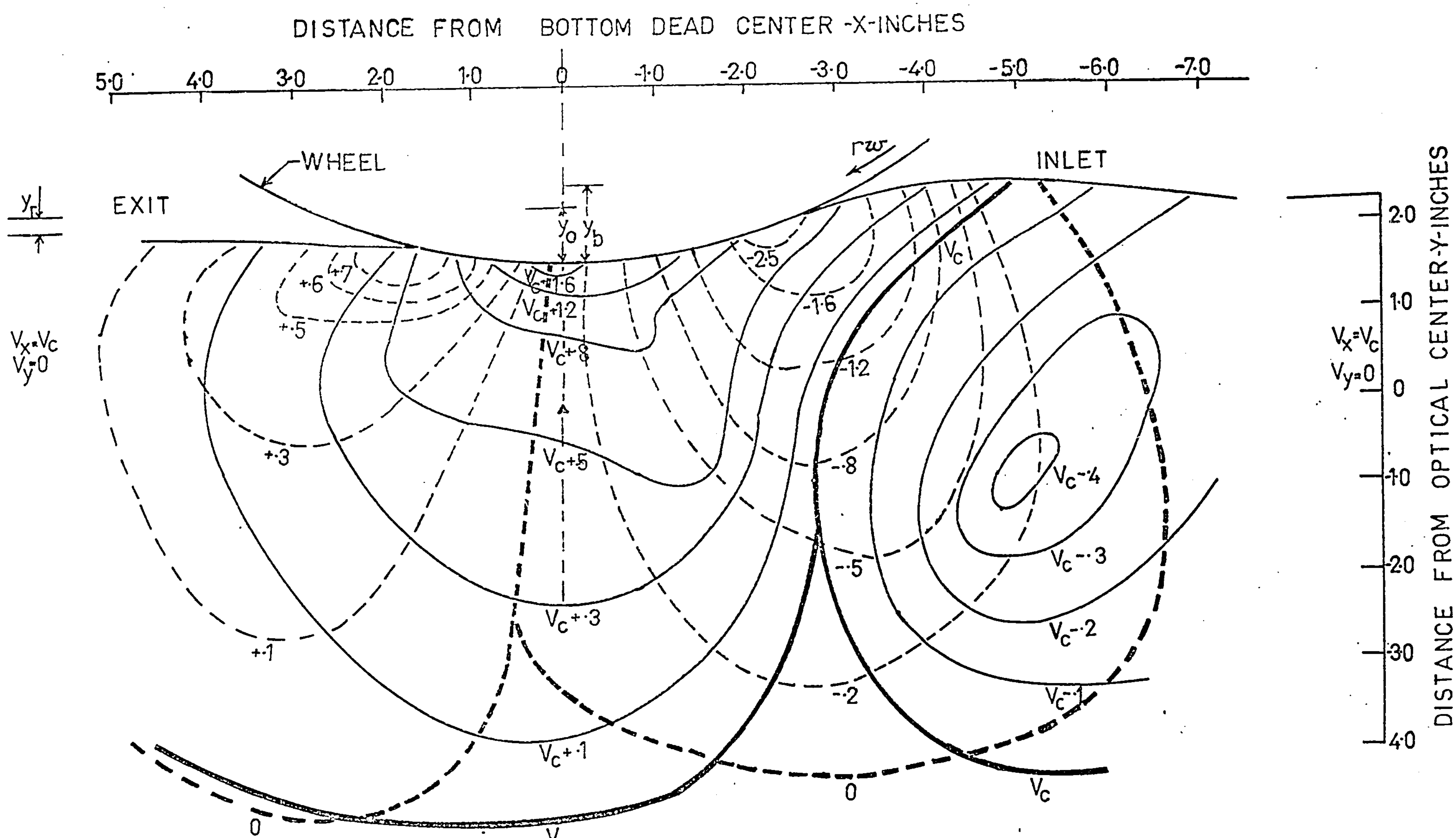

Continuous Lines-V_x; Dashed Lines-V_y.

FIGURE 45 - VELOCITY CONTOURS - TEST 38. 78% SLIP

Iso-Velocity Lines

The instantaneous X and Y velocity components were plotted relative to the wheel fixed in space. Points of equal velocity were joined up as in Figures 4-4 and 4-5 to form velocity contours.

Plots of u and v versus X at constant Y

As shown in Figures 4-6 and 4-7 smooth curves can be drawn by linking the points at which the instantaneous X and Y velocities are known. From these plots, u and v can be specified at 1/2 inch node points.

In obtaining the velocity contours and subsequent plots of u and v, some interpolation is done, resulting in some smoothing of the data. Smoothing of velocities is a necessary feature of the visioplasticity method. The extent of the smoothing necessary is directly related to the grid size and time lag between incremental deformation stages.

Density Check

From Figure 4-8 and using the principle of conservation of matter, we can write:-

$$\rho_1 A_1 V_1 = \rho_2 A_2 V_2 = \rho_3 A_3 V_3 \qquad 4\text{-}9$$

where ρ = Density

A = Area

V = Velocity

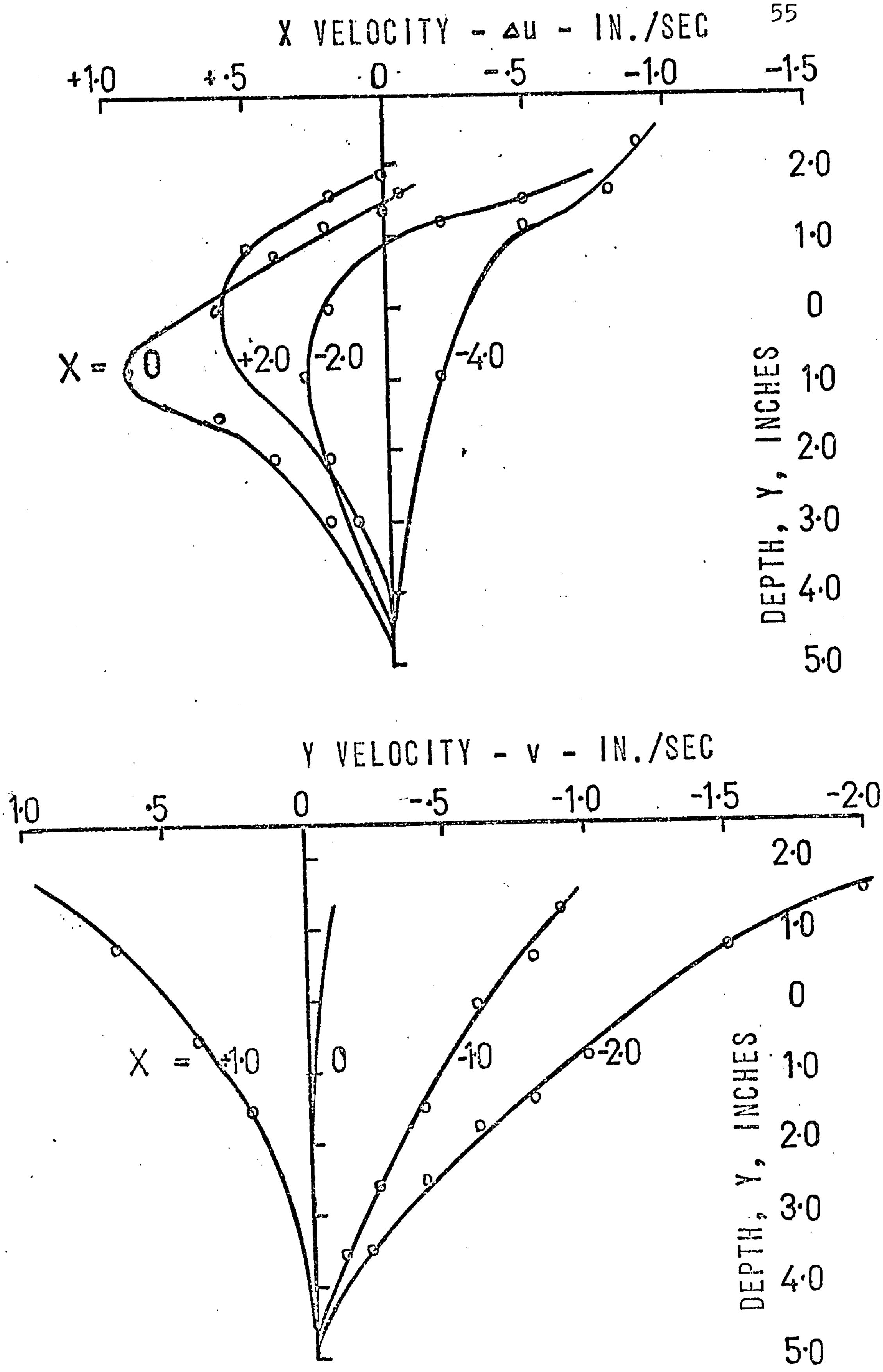

FIG. 4-6. v AND Δu VERSUS Y, AT CONSTANT X
TEST 36 -9% SLIP

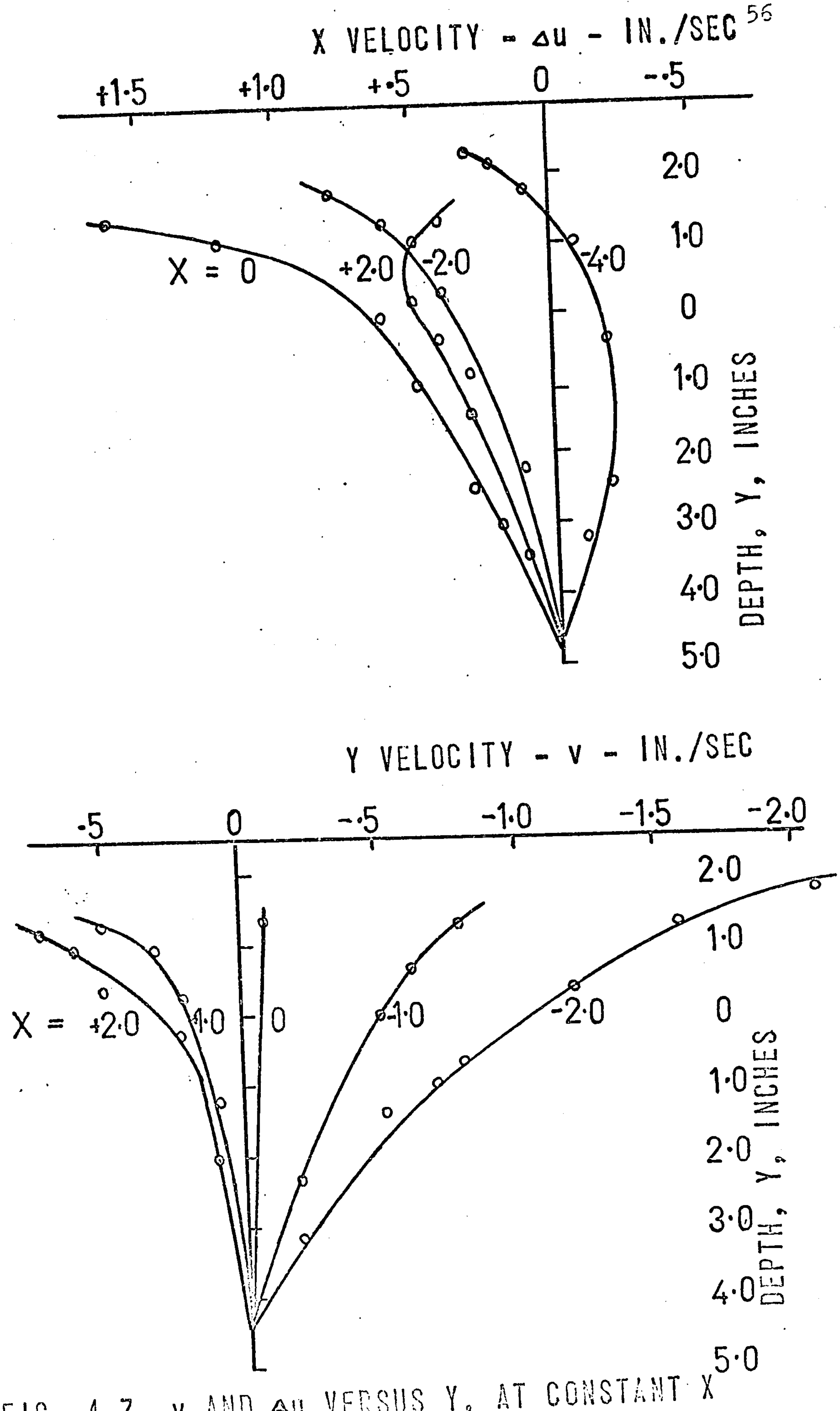

FIG. 4-7. v AND Δu VERSUS Y, AT CONSTANT X
TEST 38 78% SLIP

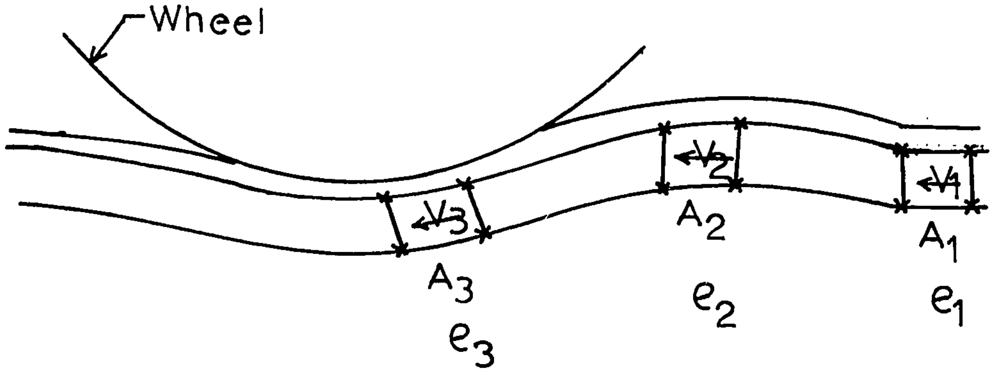

Figure 4-8 :- Flow Tube

Equation (4-9) can be expressed as:-

$$\rho_2 = \rho_1 \frac{A_1 V_1}{A_2 V_2} \quad \text{and} \quad \rho_3 = \rho_1 \frac{A_1 V_1}{A_3 V_3} \qquad 4\text{-}10$$

ρ_1, is given the value 1.00 and by dividing the original area A_1 contained by four neighbouring markers by the area contained by the marker in subsequent deformation stages, the quantities $\rho_2 \frac{V_2}{V_1}$, $\rho_3 \frac{V_3}{V_1}$, $\rho_4 \frac{V_4}{V_1}$, and ρ_5 were calculated. This computation was done in the program JANE shown in Appendix III. Table 4-1 shows the values of these quantities for markers enclosed by the two top rows of markers for a typical test (See No. 40).

The quantities $\frac{V_2}{V_1}$, $\frac{V_3}{V_1}$, $\frac{V_4}{V_1}$ vary slightly from the first quadrilateral to the sixth, and also depend on slip conditions. For Test 40 the following relationship can be calculated from the velocity contours:-

$\frac{V_2}{V_1}$	$\frac{V_3}{V_1}$	$\frac{V_4}{V_1}$	$\frac{V_5}{V_1}$
.98	1.1	.99	1

The values of $\rho_2, \rho_3, \rho_4, \rho_5$, calculated are statistically very close to unity and therefore for the clay soil used, incompressibility is a reasonable assumption. The continuity equation for the plane strain case with the condition $\rho =$ constant is applicable.

TABLE 4-1

$\rho\frac{V_2}{V_1}$	$\rho\frac{V_3}{V_1}$	$\rho\frac{V_4}{V_1}$	ρ_5
.988	1.027	1.011	1.013
.988	.962	.997	1.002
1.001	1.010	1.000	1.014
1.005	1.091	1.054	1.111
1.063	1.100	1.082	1.101
1.042	1.008	1.000	1.040

Check on Equation of Motion of a Plastic Mass

In Equation (3-9) the local acceleration terms $\rho\frac{\partial u}{\partial t}$ and $\rho\frac{\partial v}{\partial t}$ are equal to zero since for steady state flow, the velocity at a point in space is unchanged with time and $\frac{\partial u}{\partial t}$ and $\frac{\partial v}{\partial t}$ which are the local acceleration terms must be zero. The terms $(\rho u\frac{\partial u}{\partial x} + \rho v\frac{\partial u}{\partial y})$ and $(\rho u\frac{\partial v}{\partial x} + \rho v\frac{\partial v}{\partial y})$

represents the inertial terms due to convective acceleration. An estimate of these terms can be made as follows:-

$$\text{Value of } \rho = .000146 \ \frac{\text{lb}}{\text{in}^4}\text{sec}^2$$

$$\text{Maximum Value of } u = 7.5 \text{ in/sec}$$

$$v = 2.8 \text{ in/sec}$$

$$\frac{\partial u}{\partial x} = 0.5 \text{ in/in.sec}$$

$$\frac{\partial u}{\partial y} = .5 \text{ in/in.sec}$$

$$\frac{\partial v}{\partial x} = .5 \text{ in/in.sec}$$

$$\frac{\partial v}{\partial y} = .5 \text{ in/in.sec}$$

These terms are very small compared to the principle and shear stress increment and therefore the work done by inertial forces can be neglected.

The body force X and Y refer to the matrix and gravitational potential. The gravitational force gradient can be expressed as ρg. Using the quoted value of ρ this force will be very small. The changes which occur in the matrix potential X and the total effect on matrix potential has not been completely elucidated. However the matrix potential of the almost saturated soil is small and the short loading time of a few seconds precludes the extrusion of pore air or water and the consequent changes in matrix potential in the greater portion of the deforming medium.

Selection of a Constitutive Equation

The characteristics and properties of the compacted clay are described in Appendix II.

The compacted soil is frictionless and the short loading cycle for a test precludes the extrusion of pore water and the consequent build-up of frictional resistance.

A typical stress strain curve for the compacted clay is shown in Figure 4-9.

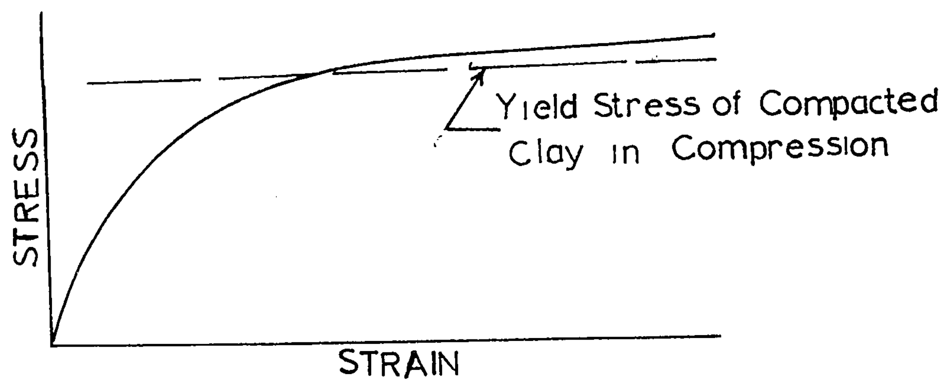

Figure 4-9 :-Typical Stress-Strain Curve

There is an elastic or more correctly a piecewise linear behaviour at small strains after which the material flows at a fairly uniform yield stress. Tests at low strain rates did not produce any significant change in yield behaviour. Strain rates for the soil 1/8 inch below interface to the bottom of the deformed zone did not exceed 100% per second.

The behaviour of kaolin in drained tests or undrained tests with pore-water pressure measurement is under examination by McKyes (1969). If the yield of soil is considered to be piecewise linear, the yield loci at small strains before substantial water build-up or pore water extrusion define concentric circles (See Figure 4-10) following the von-Mises criterion. However as failure strain is reached, the yield locus approaches the Mohr-Coulomb criterion.

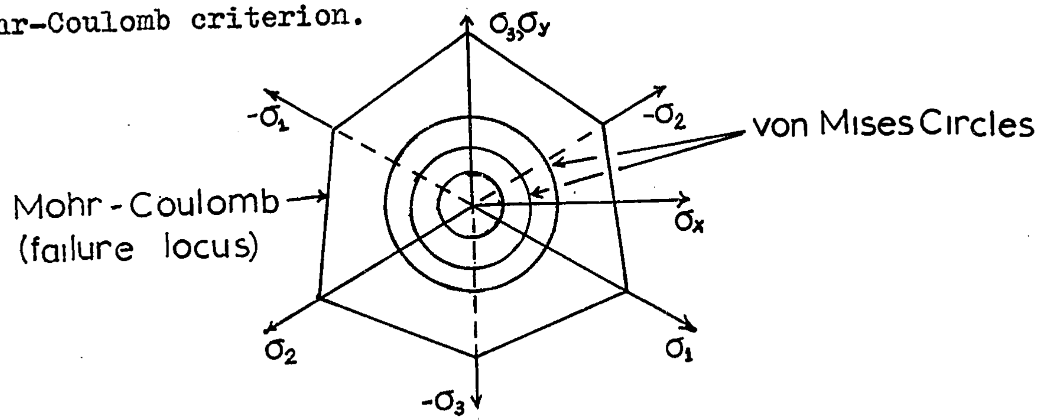

Figure 4-10 :-Yield Loci in Deviatoric Plane

The above suggests that the Mohr-Coulomb theory begins to define shear strength characteristics at large strains when pore-water pressure has dissipated in drained tests or in undrained tests when allowance is made for pore-water pressure. In drained tests the extrusion of pore-water allows the soil to develop frictional or quasi-viscous resistance.

As mentioned before the short loading cycle prevents any substantial pore-water pressure dissipation. At low strains the soil can be considered to be yielding at a stress lower than the ultimate yield stress, however at a large enough strain the ultimate yield stress is reached and because the soil cannot drain (i.e. pore-water does not move sufficiently) this stress is maintained at increasing strains. For the major part of the loading cycle the strains are large enough so that the smaller yield stresses at small strains can be neglected. The compacted clay can then be considered to be a rigid, perfectly-plastic material under the loading conditions, and a value of $k = 0.95$ lbs./in.^{2} will be used.

Effect of Stress Reversals on Yield Stress

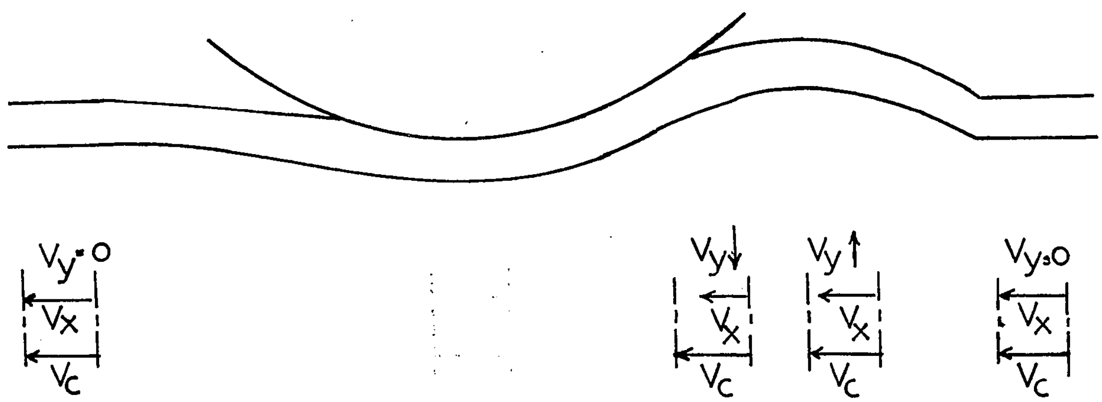

Figure 4-11:- Low Slip - Soil Velocity Changes

At low slips, there is a large upward movement of soil ahead of the wheel. However for the clay soil tested the flow pattern is still continuous. This is a major difference between the surficial behaviour of a cohesive soil and a sand for example. For a wheel on sand if the bow wave is large there will be discontinuities.

Consider the wheel fixed in space and the soil moving with an initial velocity V_x equal to the carriage velocity and V_y equal to zero (Figure 4-11). At low slip, V_x decreases in the bow wave, while V_y has some finite value upwards; as we get nearer the wheel the soil velocity increases from a value lower than V_x to a value equal to V_x at the exit while V_y also changes sign.

In the soil mechanics field, the effect of stress reversals on yield strength has been limited to loading and unloading cycles. The effect of going from compression to extension in one quick cycle has not received any attention because of difficulties involved in testing. This factor must be considered in the determination of a constitutive equation for soil behaviour beneath wheels.

Calculation of Strain Rate Invariants

The X and Y velocities at each 1/2 inch node point are known. Using Figure 4-12 the square root of the strain rate invariant can be calculated as follows:-

$$\sqrt{I_2}(L,K)=\mathrm{SQRT}\left[\frac{\{\text{E Dot X }(L,K)\}^2+\{\text{E DOT Y }(L,K)\}^2}{2} + \frac{\{\text{GAMMA DOT XY }(L,K)\}^2}{4}\right] \qquad 4\text{-}11$$

where E DOT X (L,K) $= u\,(L,K-1)-u(L,K+1)$

E DOT Y (L,K) $= v\,(L-1,K)-v(L+1,K)$

GAMMA DOT XY (L,K) $= \{v(L,K-1)-v(L,K+1)\} + \{u(L-1,K)-u(L+1,K)\}$

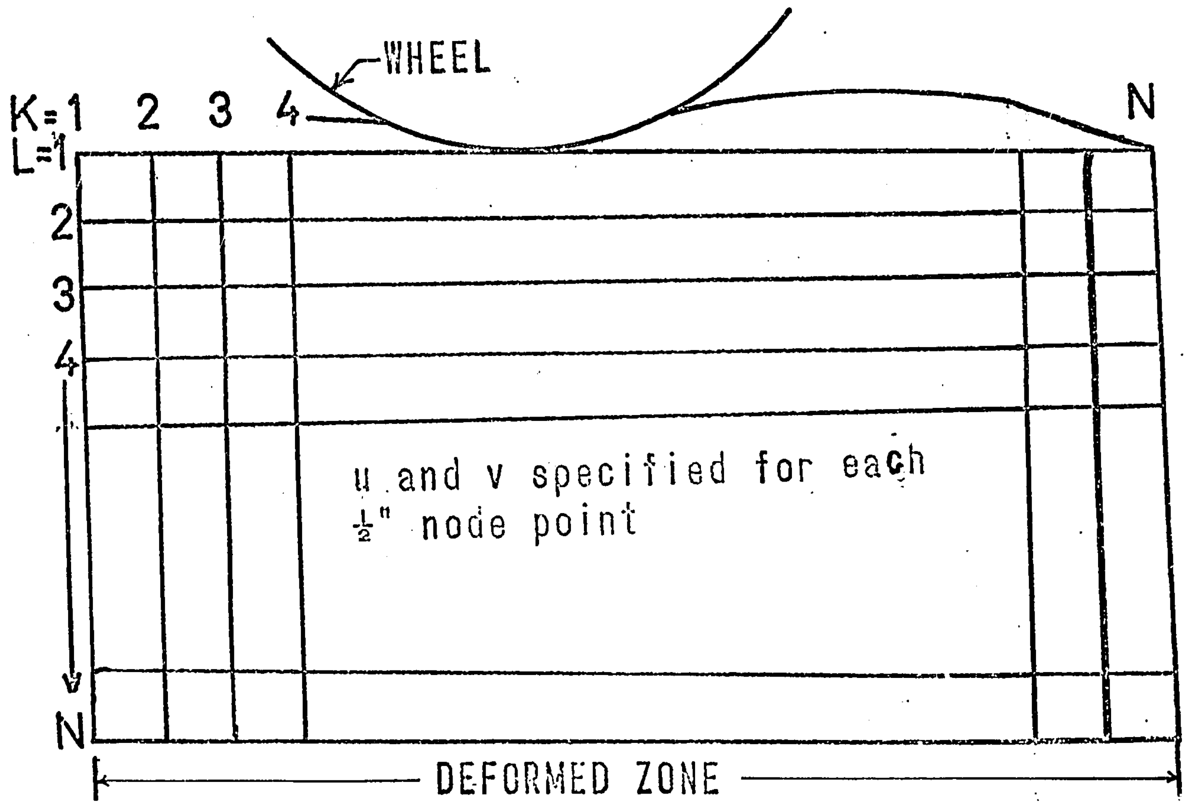

FIG. 4-12. DETERMINATION OF STRAIN RATE INVARIANTS

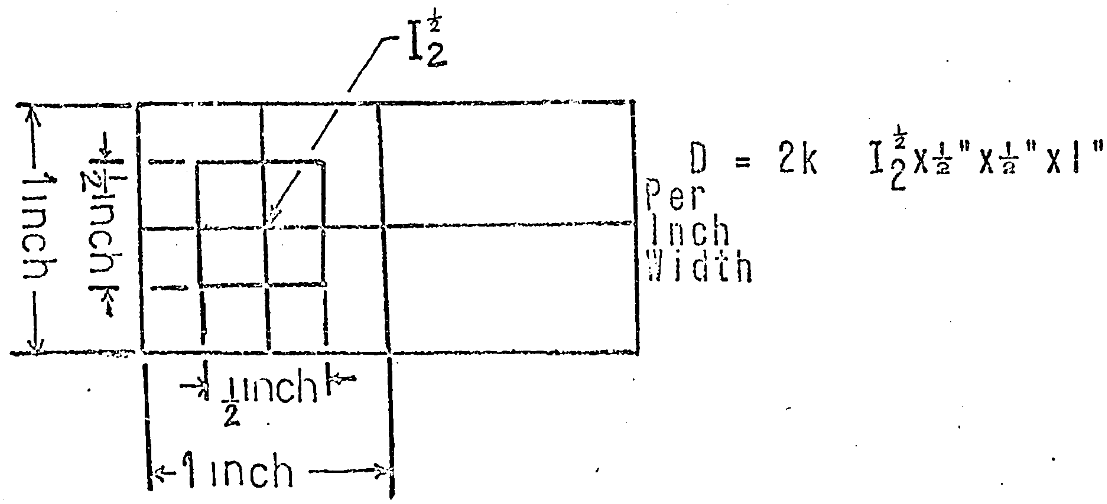

FIGURE 4-12b. DETERMINATION OF DEFORMATION ENERGY

The INVTS subroutine shown in Appendix III is used to calculate the strain rate invariants at 1/2 inch node points.

Calculation of Deformation Energy

The total deformation energy can be expressed as:-

$$D = \int_{\substack{\text{Volume} \\ \text{Deformed}}} 2k \sum I_2^{\frac{1}{2}} \qquad 4\text{-}12$$

Considering a small section (see Figure 4-12b), the deformation energy can be expressed as:-

$$D_{\substack{\text{Per} \\ \text{Inch} \\ \text{Width}}} = 2k\ I_2^{\frac{1}{2}} \times \tfrac{1}{2} \times \tfrac{1}{2} \qquad 4\text{-}13$$

and the total deformation energy as:-

$$D_{\substack{\text{Per} \\ \text{Inch} \\ \text{Width}}} = 2k \sum_{Y} \sum_{X} I_2^{\frac{1}{2}} \times \tfrac{1}{2} \times \tfrac{1}{2} \qquad 4\text{-}14$$

The first summation sign implies summation from the soil surface to the bottom of the deformed zone. The second summation sign implies summation from beginning of deformation to end of deformation in X direction. The calculation of $\sum I_2^{\frac{1}{2}}$ x Depth x Length in X direction in the region above L = 1 is done manually because of the odd shaped area involved. The instantaneous velocities close to the beginning and the end of the deformation process are very small and somewhat erratic. The strain rate invariants are extrapolated from the region where the instantaneous velocity will give consistent strain rate values back to zero at the beginning or end of the deformation region.

Typical curves showing D per inch width with depth are shown in Figures 4-13, 4-14 and 4-15.

DETERMINATION OF FRICTIONAL STRESS AND COMPUTATION OF INTERFACIAL ENERGY

Frictional Stress

As shown in Chapter 1, if the soil-wheel interface is a slip surface the following must be defined:-

1) The strain rate invariants at the wheel soil interface.
2) A constitutive equation which links up this strain rate equation to shear stress so that the frictional stress can be defined.

In the experimental technique velocities were obtained for the soil 1/8 inch - 1/4 inch below the wheel soil interface. Strain rate invariants cannot be calculated from the rim velocity ($r\omega$) and the soil velocities 1/8 inch - 1/4 inch below the surface since velocity discontinuities can occur in the tangential direction across a slip surface.

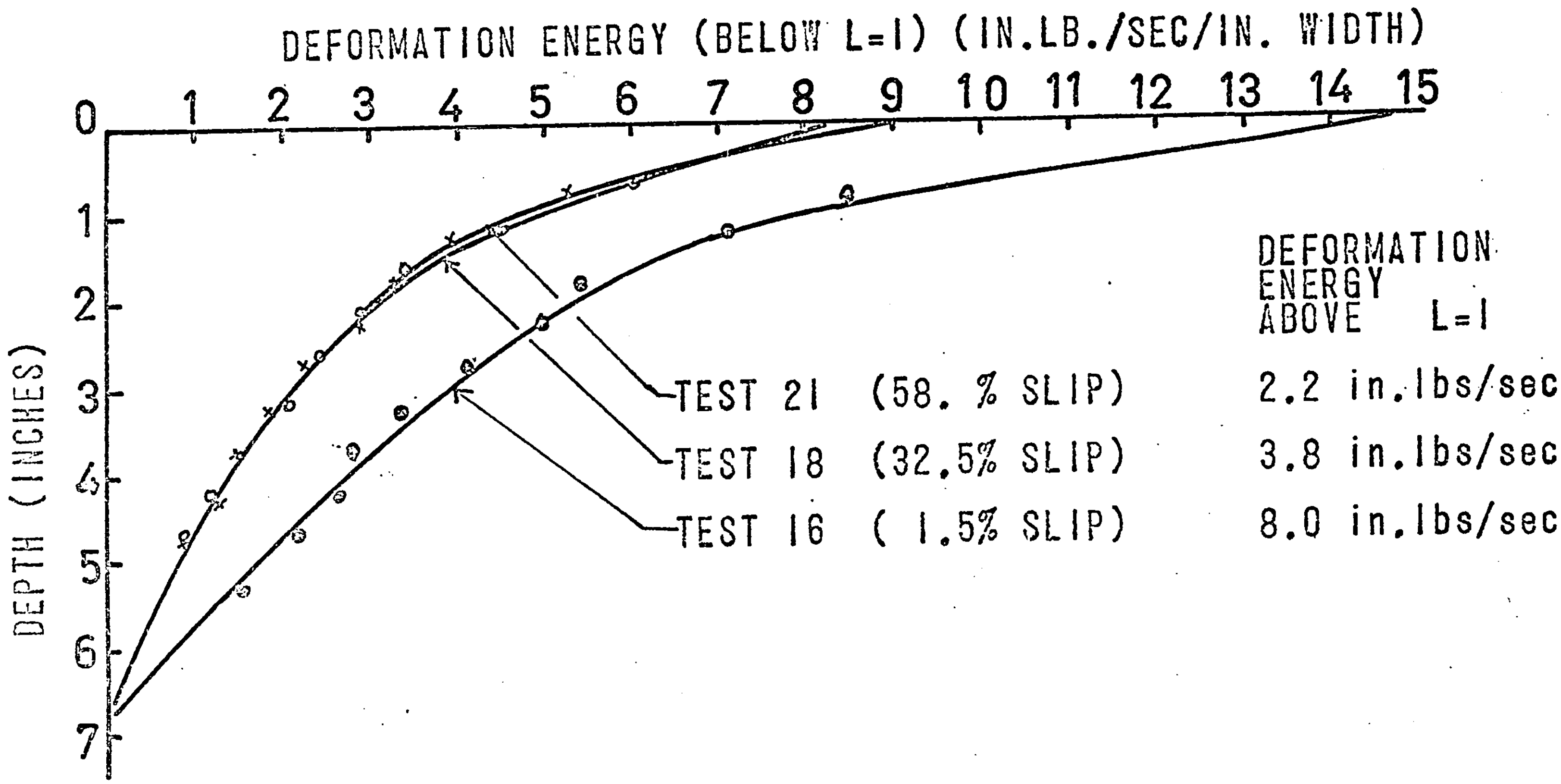

FIGURE 4-13 DEFORMATION ENERGY VERSUS DEPTH
MODEL WHEEL. 23.5 LBS

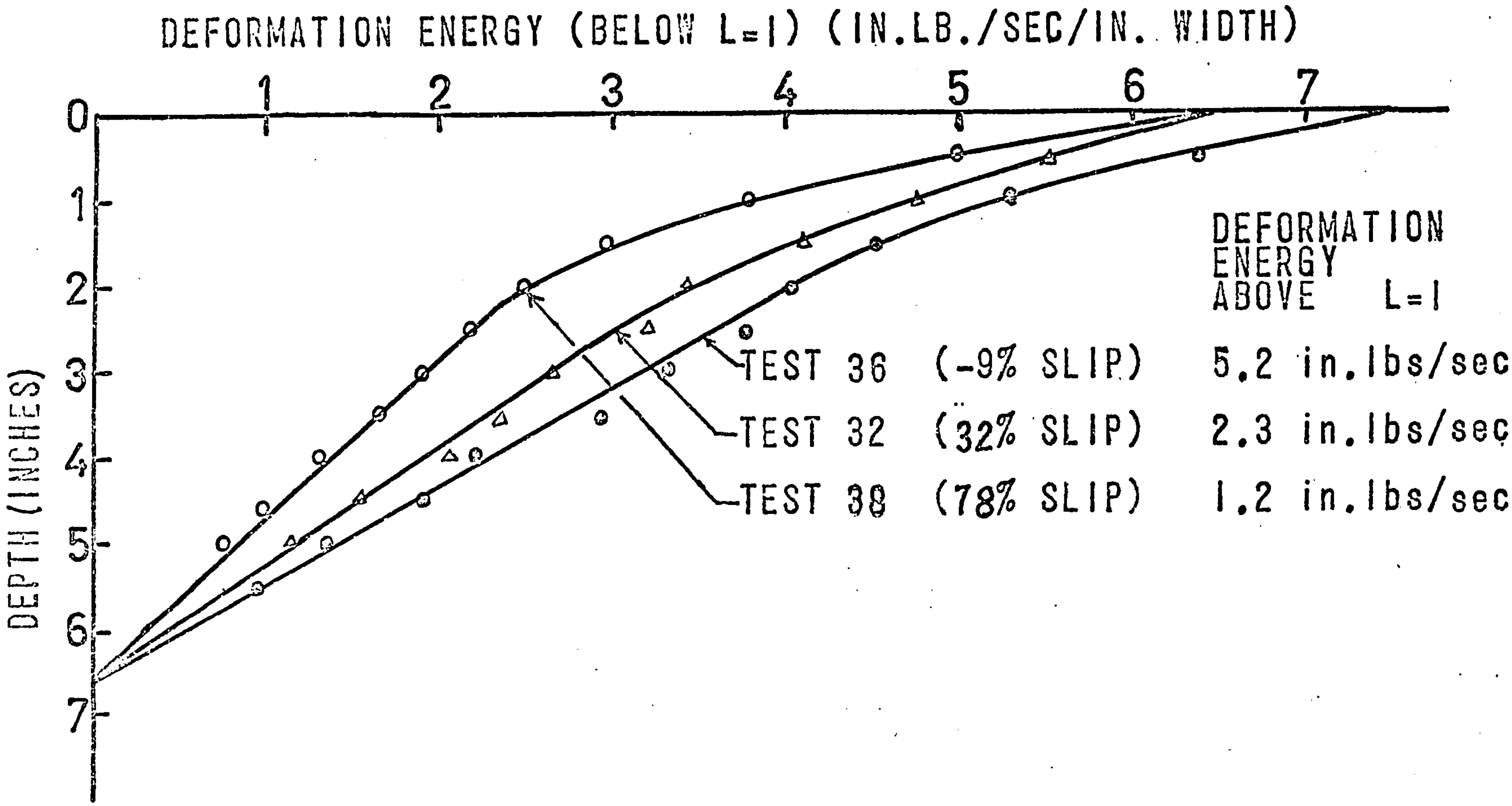

FIGURE 4-14 DEFORMATION ENERGY VERSUS DEPTH
PROTOTYPE, 51 LBS

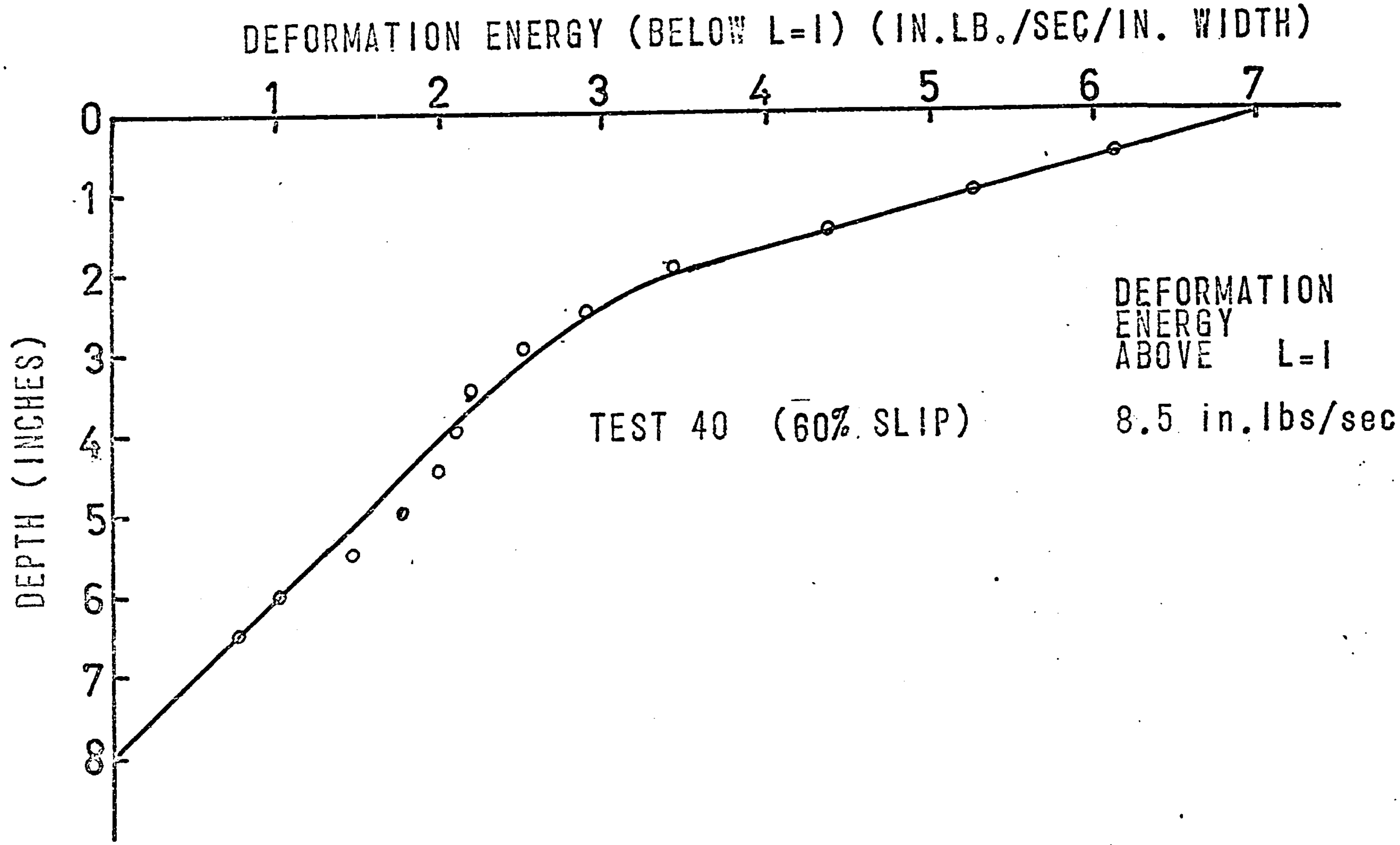

FIGURE 4-15 DEFORMATION ENERGY VERSUS DEPTH
PROTOTYPE. 79 LBS

For non-hardening rigid-plastic bodies, these can be very large and correspond to a small region where the shear strain is very large. For work hardening materials, the degree of transition depends on the rate of work (strain) hardening of the material under consideration.

The strain-rate behaviour of the compacted clay soil was investigated using the dynamic tester of Japp (1967). Figure 4-16 shows that the compacted clay follows a linear stress-log strain rate pattern above 100% per sec.

An attempt was made to simulate the conditions under a slipping wheel by moving an aluminum plate on a compacted soil surface at various speeds. This was achieved by using a high speed horizontal tester, see Sylvester-Williams (1969). Figure 4-17 shows a schematic of the experimental set up. The horizontal force necessary to move the plate over the clay surface was measured by a force transducer. The plate velocity was measured either by a velocity transducer or a displacement transducer with a known time base. The slip velocity was computed from the plate velocity and the soil velocity 1/8 inch below the plate. The soil velocity was obtained from a 1/2 inch square grid placed on the sides of the clay box. As part of this study an attempt was also made to evaluate the strain rate field at the interface. Photographs were taken at the various stages of deformation, however it was not possible to obtain accurate results for the very

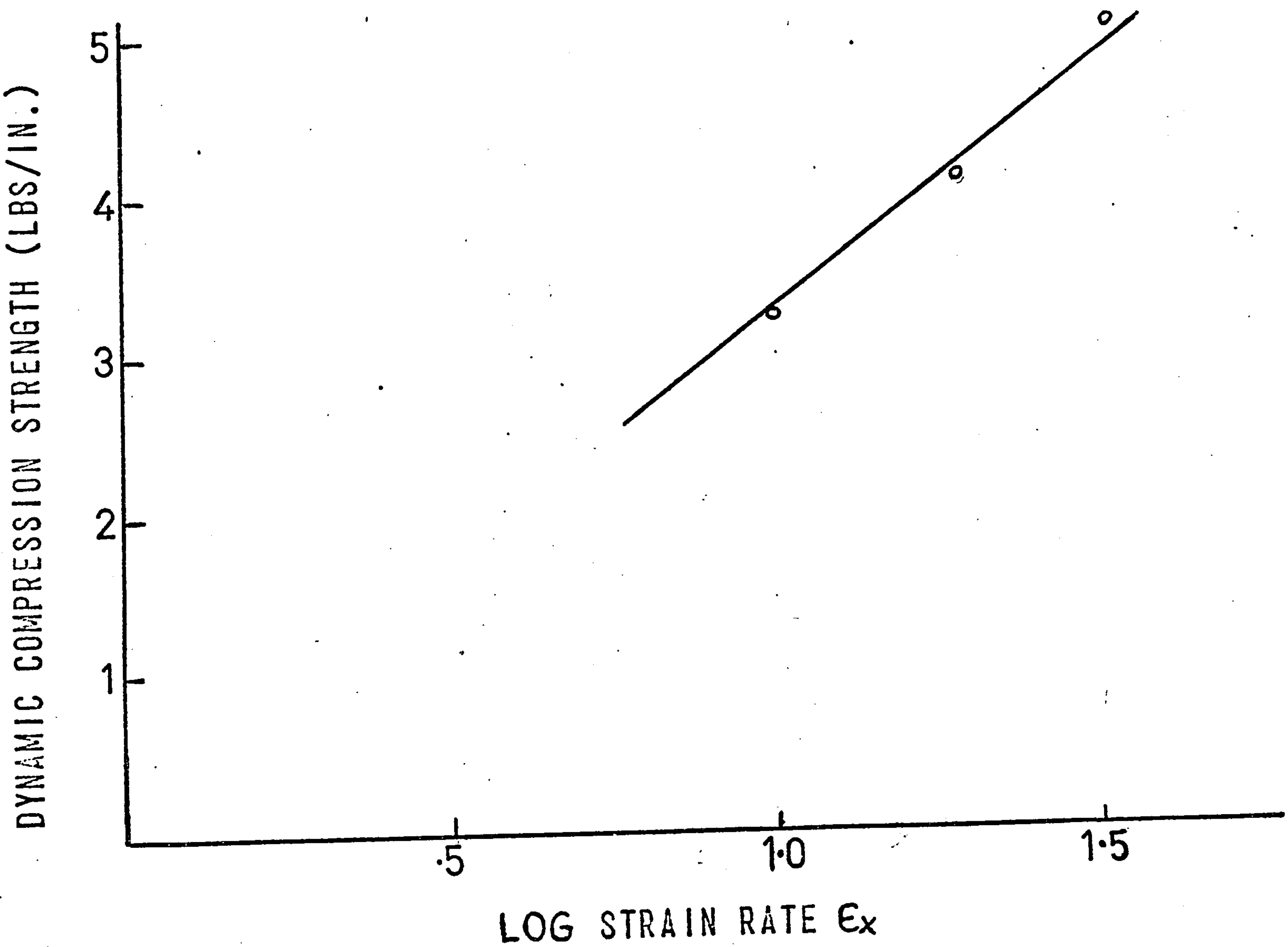

FIGURE 4-16. DYNAMIC COMPRESSION STRENGTH OF COMPACTED CLAY

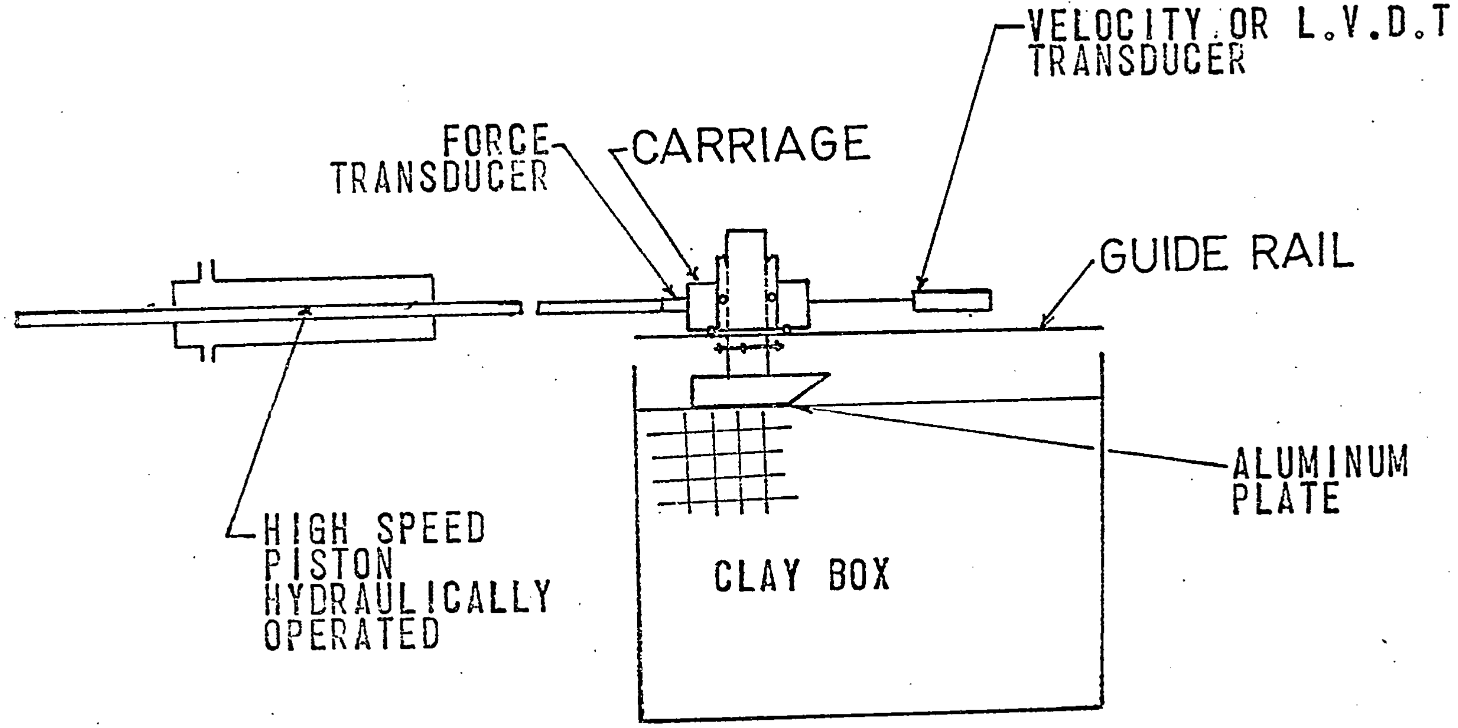

FIGURE 4-17. HIGH SPEED HORIZONTAL TESTER

thin layer under study.

In the absence of a suitable stress-strain rate law for the material at the interface, it was decided that a stress-slip velocity relationship could be used to define the frictional stress. The force measurements which gave the value of the frictional force at various slip velocities showed an increase in frictional stress with an increase in slip velocity. This implies a strain rate dependence of yield stress since the frictional stress is equal to the yield stress of the soil under the conditions of the test.

Figure 4-18 shows a plot of frictional stress versus slip velocity.

For the case where Equation (3-26) applies the classical Coulomb equation can be used. A value of 0.3 was obtained for μ.

Computation of Interfacial Energy

One of the major advantages of the visio-plasticity method is the exact specification of soil velocities. Since rigid wheels are used there is no ambiguity in the definition of radius of the wheel, it is therefore possible to define the slip velocity exactly on each elemental area by the following relation:-

$$\text{Slip Velocity, } V_s = r\omega - (\text{Carriage Velocity } \& \text{ Instantaneous Soil Velocity})$$

The frictional stress corresponding to the slip velocity

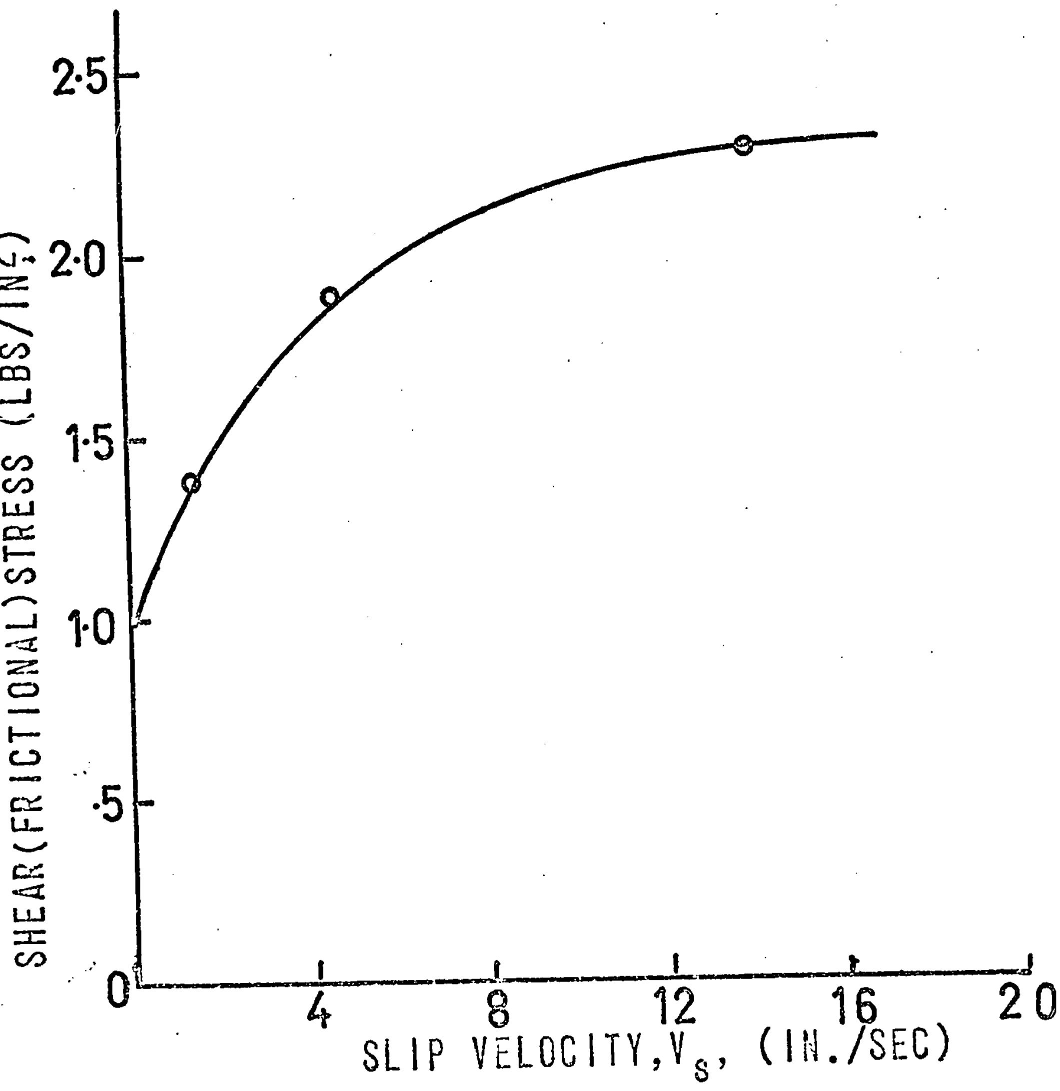

FIGURE 4-18. INTERFACIAL SHEAR STRESS - SLIP VELOCITY RELATIONSHIP

was defined along each segment of the interface. The frictional stress multiplied by the slip velocity was then summed up over the entire area of contact to get the Interfacial Energy X.

Figure 4-19 shows the interfacial energy for a typical test series.

Since the average soil velocity at the interface changes with slip, the zero slip condition exists for different values of $r\omega$. In the range -10% to +10% normal slip, the true slip of the wheel is close to zero. With increasing slip, the soil velocity close to the interface is greater than V_c, the true slip velocity V_s which is ($r\omega$-V) is smaller than the normal slip velocity. The interfacial energy therefore does not increase significantly up to 30% normal slip.

A few simplifications can be invoked for the calculation of Interfacial Energy, these are described in Appendix IV.

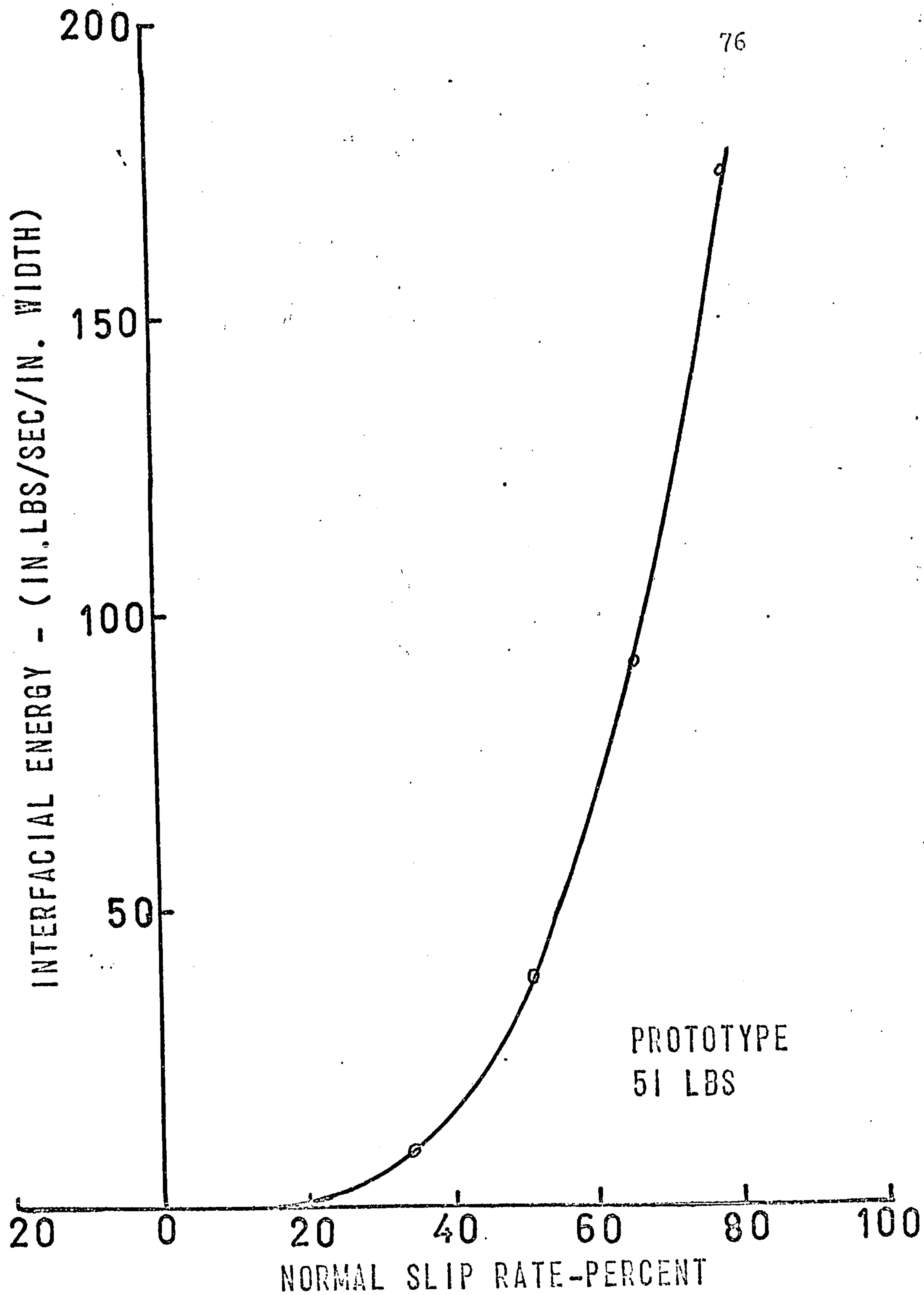

FIGURE 4-19. INTERFACIAL ENERGY VERSUS SLIP RATE-PERCENT

CHAPTER 5

ENERGY BALANCE

The energy quantities computed on the basis of observed soil-vehicle performance (Chapter 2) will now be used to provide the basis for prediction of performance of the mechanical system. In general, drawbar pull will be used as this provides the most meaningful mechanical parameters.

In this chapter, therefore, the computed values of Deformation Energy (See Chapter 4) for representative tests will be substituted into the energy balance equation (Equation 5-1) to determine the validity of the general energy balance equation. This is done by comparing the predicted and measured drawbar pull values.

PREDICTION OF PULL

The energy balance equation can be written as:-

$$M\omega = FV_c + \mathfrak{D} + X \qquad 5\text{-}1$$

The units of terms above are in.lb/second. These quantities were evaluated per inch width of wheel. If Equation (5-1) is divided by V_c (the carriage velocity) the terms will have units of in. lb. per inch of travel and can be expressed as:-

$$F = \frac{M\omega}{V_c} - \frac{\mathfrak{D}}{V_c} - \frac{X}{V_c} \qquad 5\text{-}2$$

TABLE 5-1

ENERGY BALANCE - PREDICTION OF PULL ENERGY

Test	Carriage Velocity in./sec	Angular Velocity rad./sec	Normal Slip Rate %	Torque in.lb.	Per Inch Width of Wheel: Torque Energy in.lb/in	Defor-mation Energy in.lb/in	Inter-facial Energy in.lb/in	Pull Energy: Pre-dicted in.lb/in	Pull Energy: Meas-ured in.lb/in
16-M23.5	5.68	1.257	1.73	47.68	4.31	15.2	0.0	-10.89	-10.47
18-M23.5	5.78	1.885	32.31	76.78	10.09	6.7	1.85	1.54	1.20
21-M23.5	5.63	2.953	57.94	106.07	22.41	6.9	11.50	4.01	3.75
36-P51	5.68	0.754	-9.64	8.39	0.29	7.6	0.0	-7.31	-6.84
32-P51	5.73	1.257	32.14	173.86	10.20	6.6	1.85	1.75	1.54
38-P51	5.78	3.833	77.82	238.47	42.47	6.2	30.10	6.17	5.90
40-P79	5.59	2.236	60.70	263.81	26.55	8.4	14.00	4.15	4.22

LEGEND

Test
16-M23.5 = Test Number 16, Model Wheel, 23.5 lbs.

The deformation energy calculated by the use of the visio-plasticity method, was substituted into Equation (5-2) along with the calculated interfacial energy and the pulls were evaluated. These quantities are shown in Table 5-1.

As can be seen in the Table 5-1, the calculated pulls compare reasonably with the measured pulls, and therefore the validity of the energy balance and the terms contained in it was established.

This represents the first study in which a semi-analytical solution for the soil-vehicle interaction problem has been formulated. The visioplasticity method for the computation of deformation energy uses basic plasticity relations and experimentally obtained velocity fields. These velocity fields are obtained by measurement of the vertical and horizontal soil deformation and they reflect the exact soil behaviour beneath a moving wheel. The biggest problem in soil-vehicle mechanics research has been the inability to properly assess the empirical methods of solution which have been proposed. In these analyses several simplifications have been made, and therefore the true nature of soil-vehicle interaction has not been properly incorporated. The visioplasticity method is a very useful tool and should go a long way towards providing useful relations.

ANALYSIS OF OTHER TESTS

For the remaining tests, the measured pull energy and calculated interfacial energy could be substituted into Equation (5-3) shown below to obtain the deformation energy per inch travel.

$$\frac{D}{V_c} = \frac{M\omega}{V_c} - F - \frac{X}{V_c} \qquad 5\text{-}3$$

The results are shown in Table 5-2.

The deformation energy obtained (see Figure 5-4) confirmed the general pattern which had been established from the calculation of deformation energy using the visioplasticity method. Plots of the components of the energy balance equation are shown in Figures 5-1, 5-2 and 5-3.

DEFORMATION ENERGY

The deformation energy versus normal slip for the model wheel with 23.5 lb. and prototype wheel with λ^2 scaling (51 lb.) and λ^3 scaling (79 lb.) are shown in Figure 5-4. An examination of Figure 5-4 shows that the deformation energy for the 23.5 lb. model is only slightly greater than that of the 51 lb. prototype wheel over 30% normal slip; whereas below 30% slip there is a slight increase in deformation energy for the prototype and a substantial increase in deformation energy for the model wheel. The sinkage to original surface is the same

TABLE 5-2

ENERGY BALANCE - EVALUATION OF DEFORMATION ENERGY

Test No.	Carr. Veloc. in./sec	Ang. Veloc. rad./sec	Normal Slip %	Torque in.lbs.	Energy Per Inch Width			
					Torque (Input)	Pull	Inter-facial	Defor-mation
					in.lbs/in.			
Model Wheel 23.5 lbs.								
15	5.54	2.387	48.39	97.13	16.68	3.35	6.50	6.83
17	5.63	1.445	13.18	74.00	7.57	- 5.18	0.25	12.50
19	5.45	1.508	18.45	67.10	7.41	- 3.59	0.85	10.15
20	5.59	2.953	57.52	102.99	21.54	3.86	10.60	7.08
22	5.73	1.131	-12.71	9.76	.80	-14.30	0.10	15.20
23	5.82	2.575	49.86	102.04	18.06	2.87	7.00	8.10
24	5.82	2.199	41.42	88.00	13.33	2.87	4.00	6.48
25	5.87	4.775	72.81	99.65	32.58	3.83	22.80	5.95
Prototype Wheel 51 lbs.								
30	5.78	1.696	50.18	214.61	17.02	4.07	6.70	6.25
33	5.59	.941	14.52	146.04	6.40	- 1.73	.30	7.93
34	5.73	1.005	17.50	153.99	7.18	- 1.16	.70	7.64
35	5.59	.817	2.37	80.94	3.19	- 4.18	.00	7.37
37	5.78	2.513	66.30	233.99	27.42	5.46	15.80	6.16
39	5.63	1.068	21.91	157.47	7.97	- 0.72	1.20	7.49
43	5.82	1.256	31.02	172.37	9.88	1.32	1.70	6.86
48	8.83	1.958	31.94	188.10	11.10	0.91	3.10	7.09
49	7.28	1.508	29.72	179.83	9.92	0.37	1.70	6.85
50	4.88	1.151	35.95	173.37	10.68	0.62	3.36	6.70
51	3.94	.817	29.43	170.39	9.42	0.68	1.70	7.05

Table 5-2 Cont'd.

Test No.	Carr. Veloc. in./sec	Ang. Veloc. rad./sec	Normal Slip %	Torque in.lbs.	Energy Per Inch Width: Torque (Input)	Pull in.lbs/in.	Inter-facial	Defor-mation
Prototype Wheel 34 lbs.								
28	5.63	2.236	60.37	198.70	19.78	4.65	10.40	4.73
44	5.82	1.257	29.89	148.02	8.35	.84	1.65	5.86
Prototype Wheel 68 lbs.								
31	5.78	2.073	58.57	229.02	21.83	4.46	10.87	6.50
42	5.78	1.257	32.67	189.27	11.11	1.48	2.00	7.63
45	5.78	1.382	36.70	201.69	12.79	2.85	3.08	6.86
Prototype Wheel 79 lbs.								
40	5.59	2.236	60.70	263.81	26.55	4.22	14.70	8.40
41	5.78	0.942	7.82	206.17	8.85	- 8.52	0.16	17.27
46	5.68	1.068	19.75	244.93	12.06	- 4.65	1.28	15.43
47	5.68	1.131	26.78	252.88	13.65	- 3.50	3.08	14.07

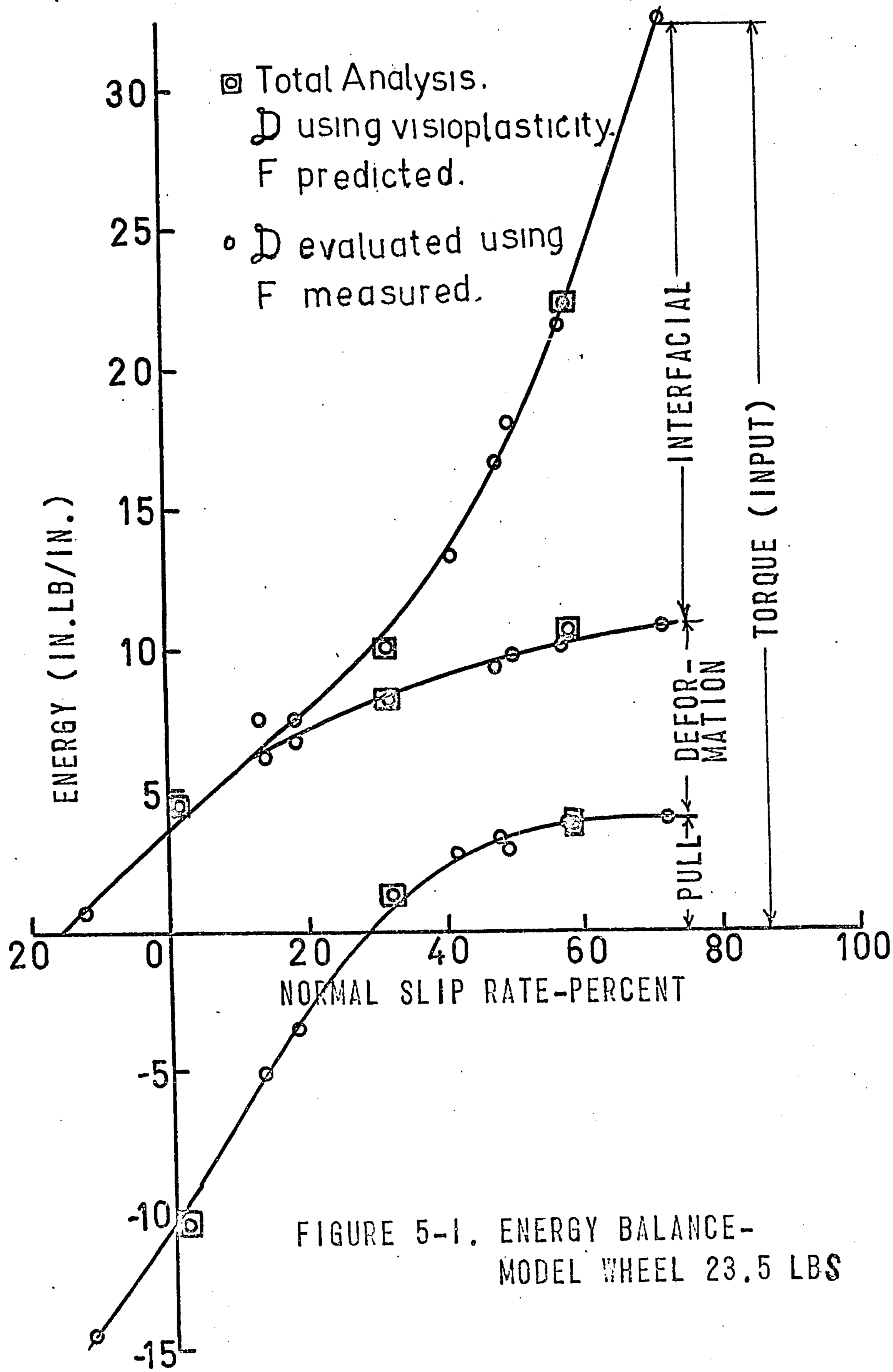

FIGURE 5-1. ENERGY BALANCE-
MODEL WHEEL 23.5 LBS

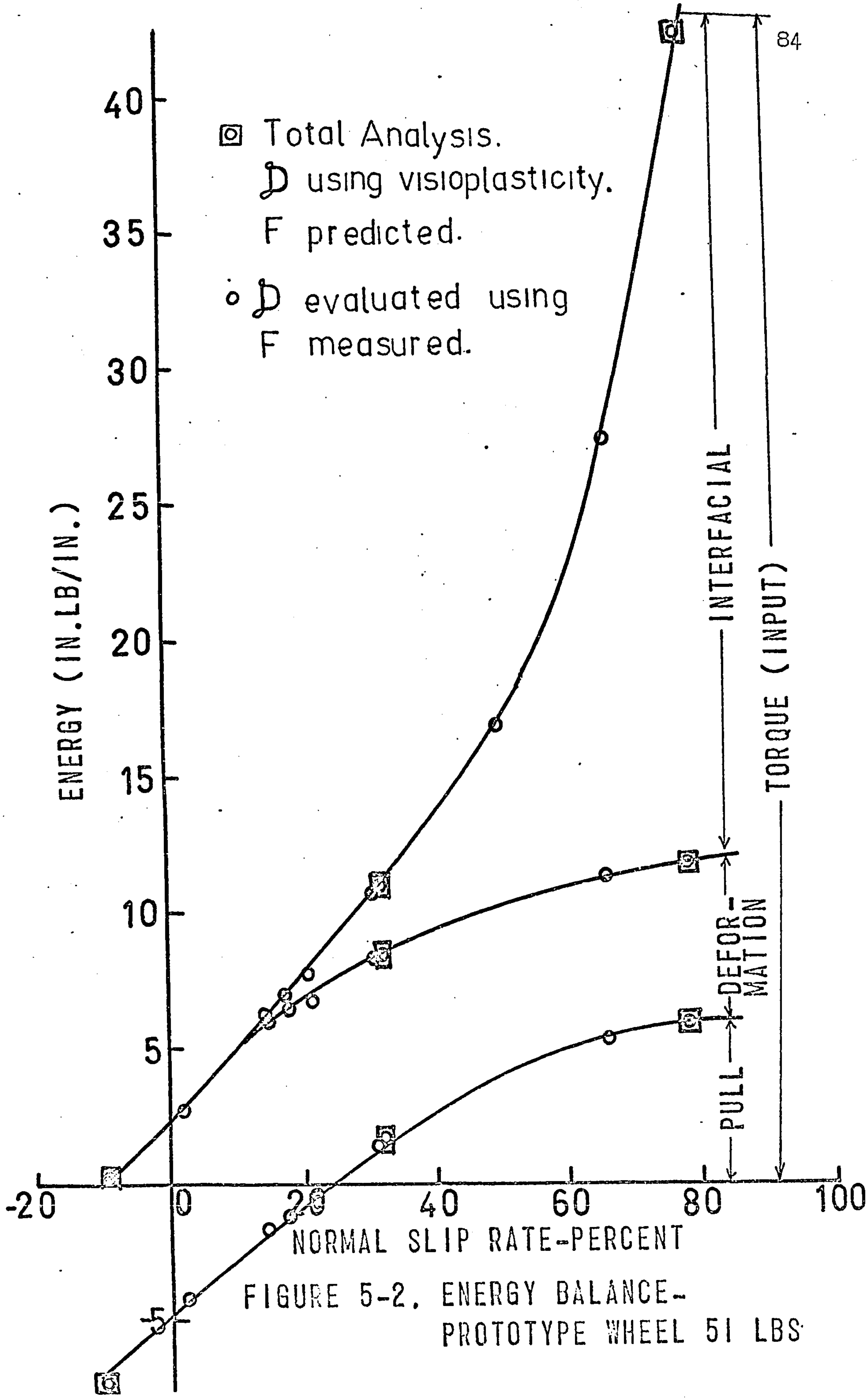

FIGURE 5-2. ENERGY BALANCE-
PROTOTYPE WHEEL 51 LBS

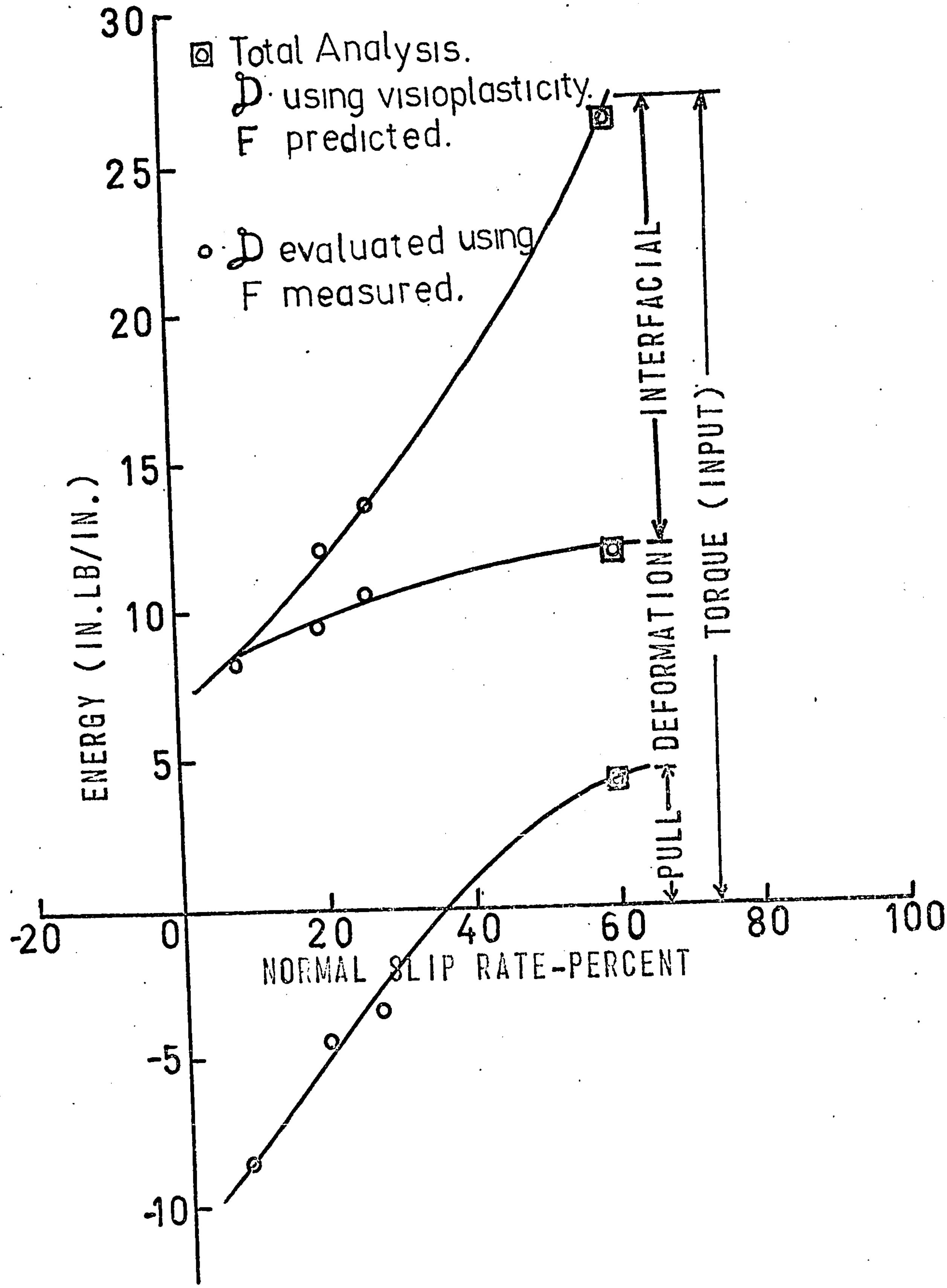

FIG. 5-3 ENERGY BALANCE-PROTOTYPE WHEEL 79 LBS

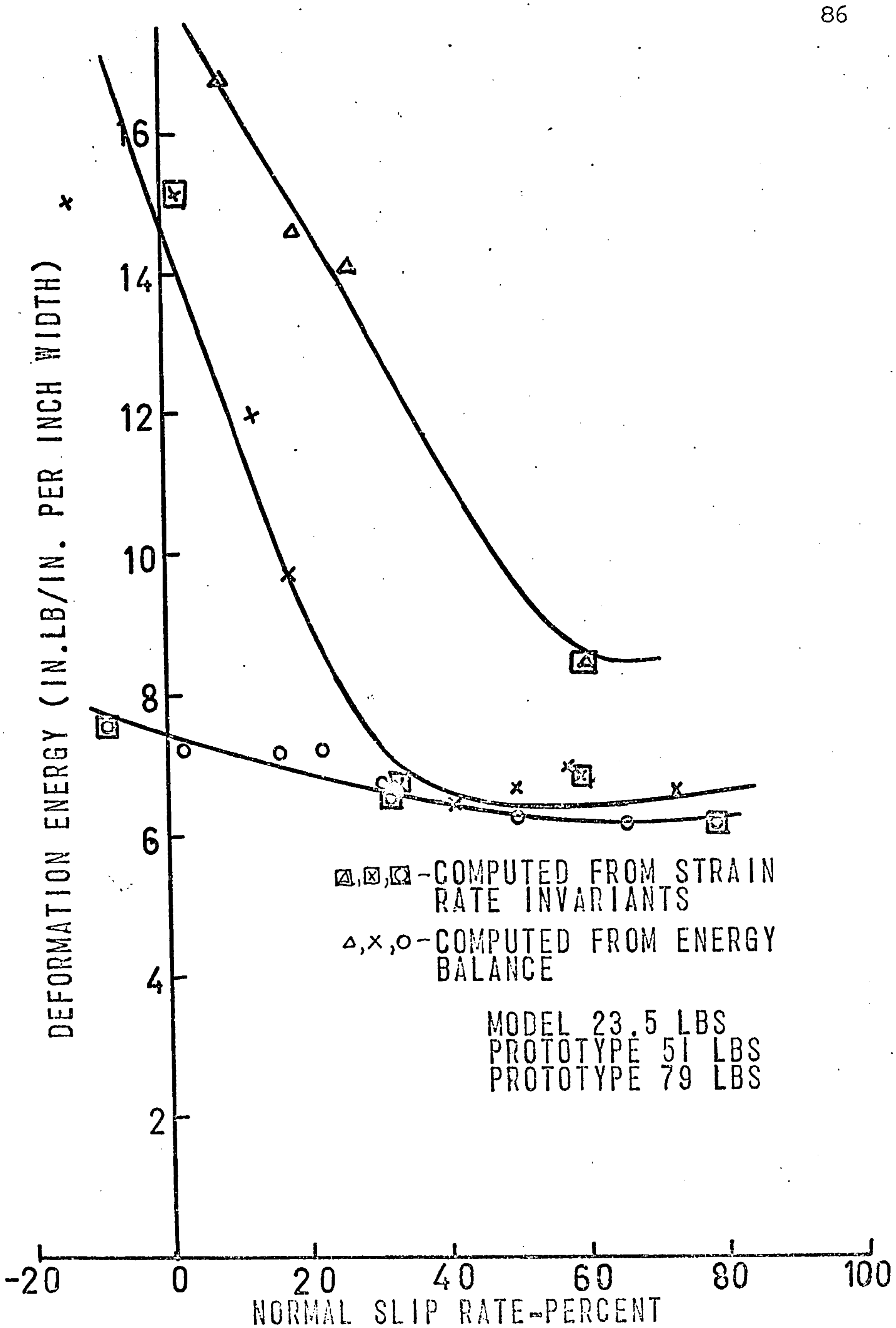

FIG. 5-4. DEFORMATION ENERGY VERSUS NORMAL SLIP RATE

for both wheels and is slip independent.

The following reasons can be advanced for this behaviour. Above 30% slip the entry condition of the soil is slightly different due to the smaller wheel at the same sinkage, but the strain rate field in the remainder of the deformed zone is similar. Below 30% slip the bow wave and the entry conditions are radically different for the smaller wheel at the same sinkage.

The λ^2 load scaling criterion has therefore produced close to dynamic similarity for clay soil response behaviour at high slips. Identical dynamic sinkage was a primary condition, whereas the influence of wheel radius seems to be secondary. At low slips, the deformation energy depends on the slip rate and y_o/D ratio. Scaling of wheels in the low slip range requires a closer examination of strain rate fields.

In soil-vehicle studies changes in rolling resistance are usually ascribed to changes in sinkage. If the deformation energy per unit distance can be equated to a fictitious resisting force, the above results show clearly that for the same rolling sinkage, the deformation energy can be quite different over the entire slip range since the deformation energy is prescribed by the strain rate field which reflects both the vertical and horizontal displacements in the soil beneath the wheel.

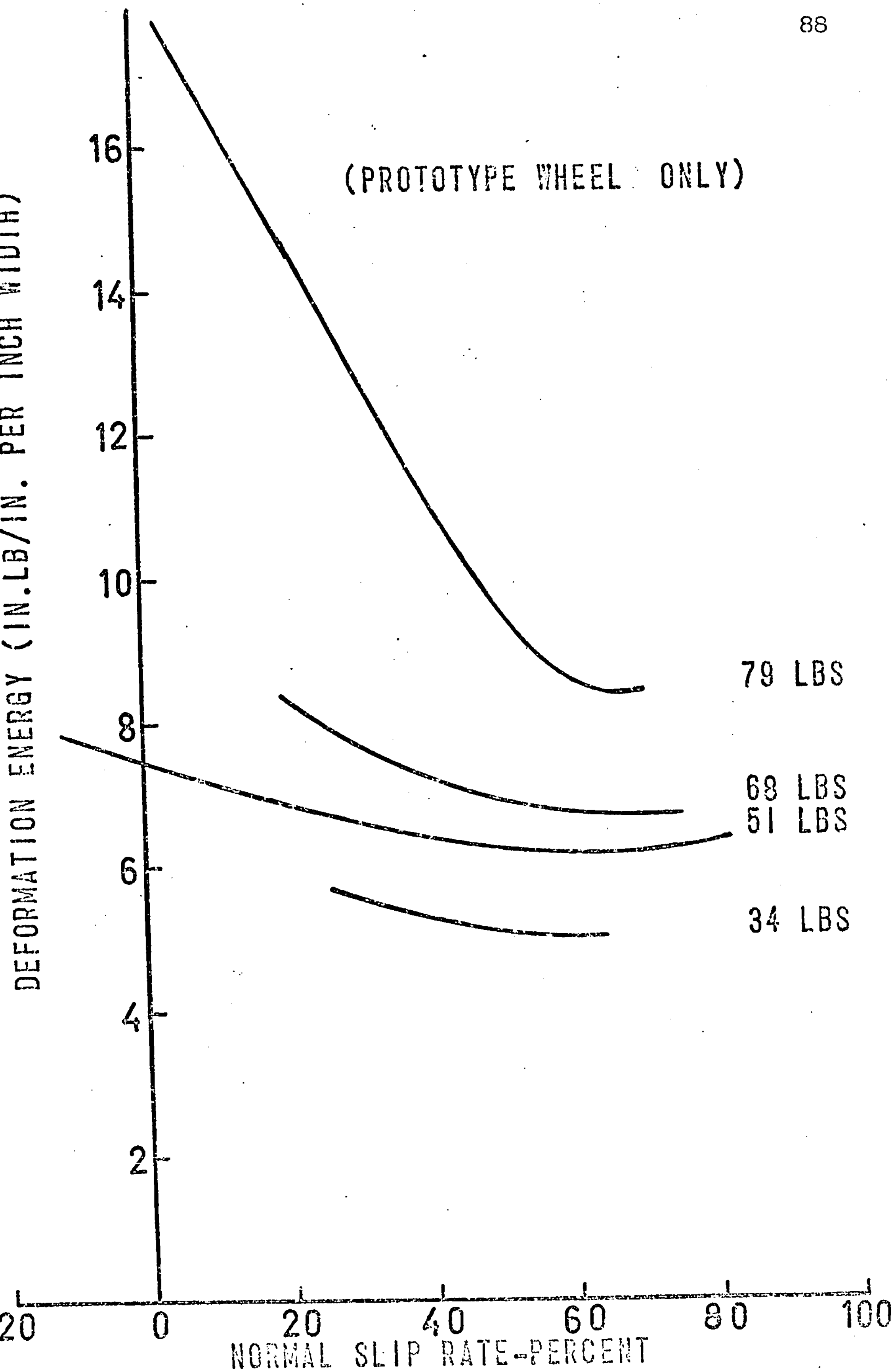

FIG. 5-5. DEFORMATION ENERGY VERSUS NORMAL SLIP RATE

Figure 5-5 shows the deformation energy for the prototype wheel with loads of 34 lbs., 51 lbs., 68 lbs. and 79 lbs. The dimensional sinkage ration y_o/D for the four loads are 0.033, .048, 0.060 and 0.070 respectively. The wheels with loads of 34 lbs. and 51 lbs. show a small increase in deformation energy with decreasing slip because of the slightly changed entry conditions. The 79 lb. wheel shows a substantial increase of deformation energy with decreasing slip which is caused by a large variation in entry conditions.

In can therefore be concluded that y_o/D of .050 defines the small sinkage domain for clay soils and below this value the deformation energy will show only small changes with slip.

Increased Deformation Energy with Decreasing Slip

Figures 5-6 and 5-7 show the X and Y velocities ahead of the wheel centre line for the 79 lb. prototype wheel at 60.7% normal slip (Test 40), and at 19.7% slip (Test 46). The following features are evident:-

1) The X velocities for the test with lower normal slip show a larger variation.
2) There is a greater upward movement of soil ahead of the wheel (caused by increased upward Y velocity). This is reflected in increased sinkage to bow wave. The downward Y velocities

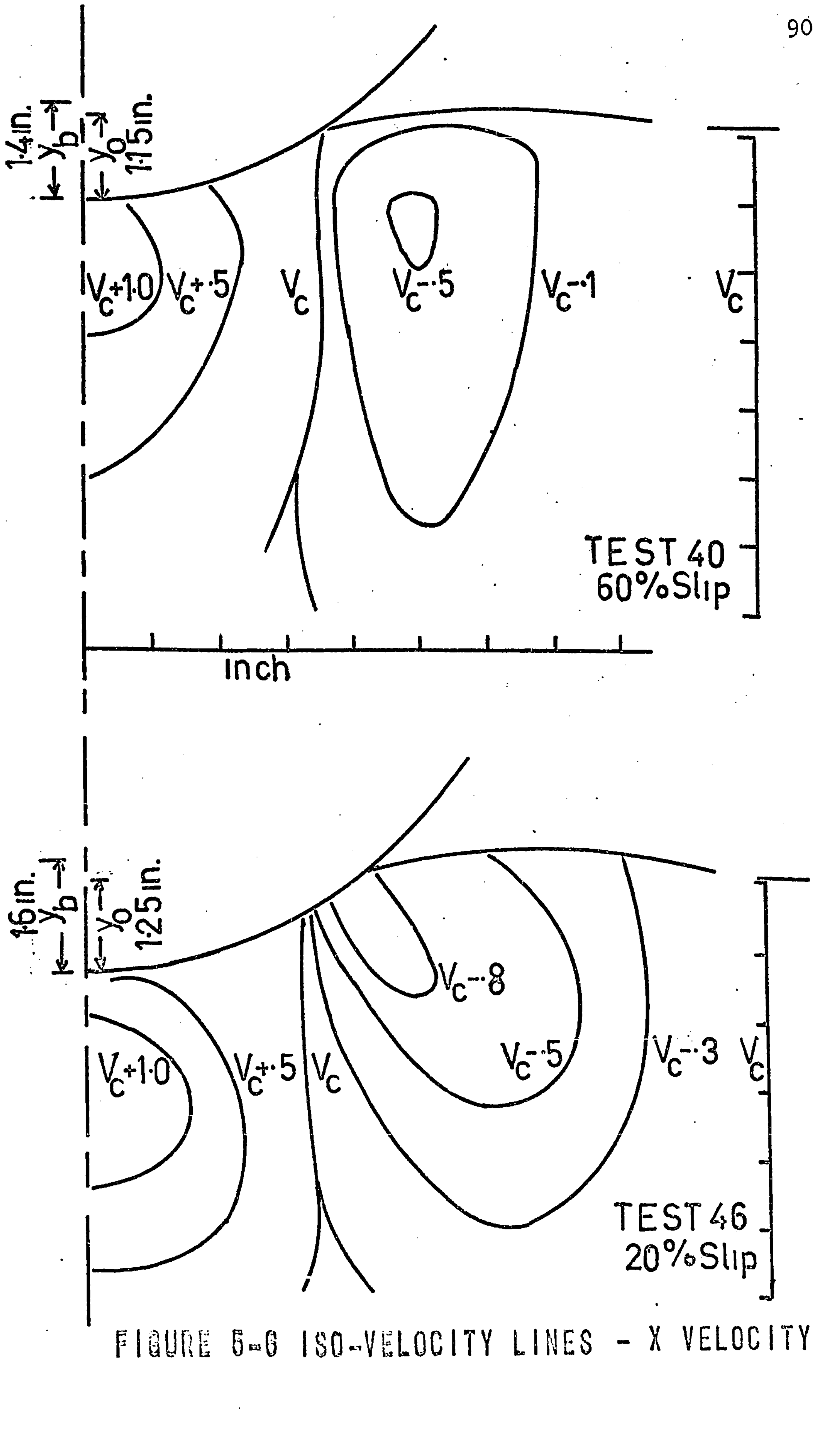

FIGURE 5-6 ISO-VELOCITY LINES - X VELOCITY

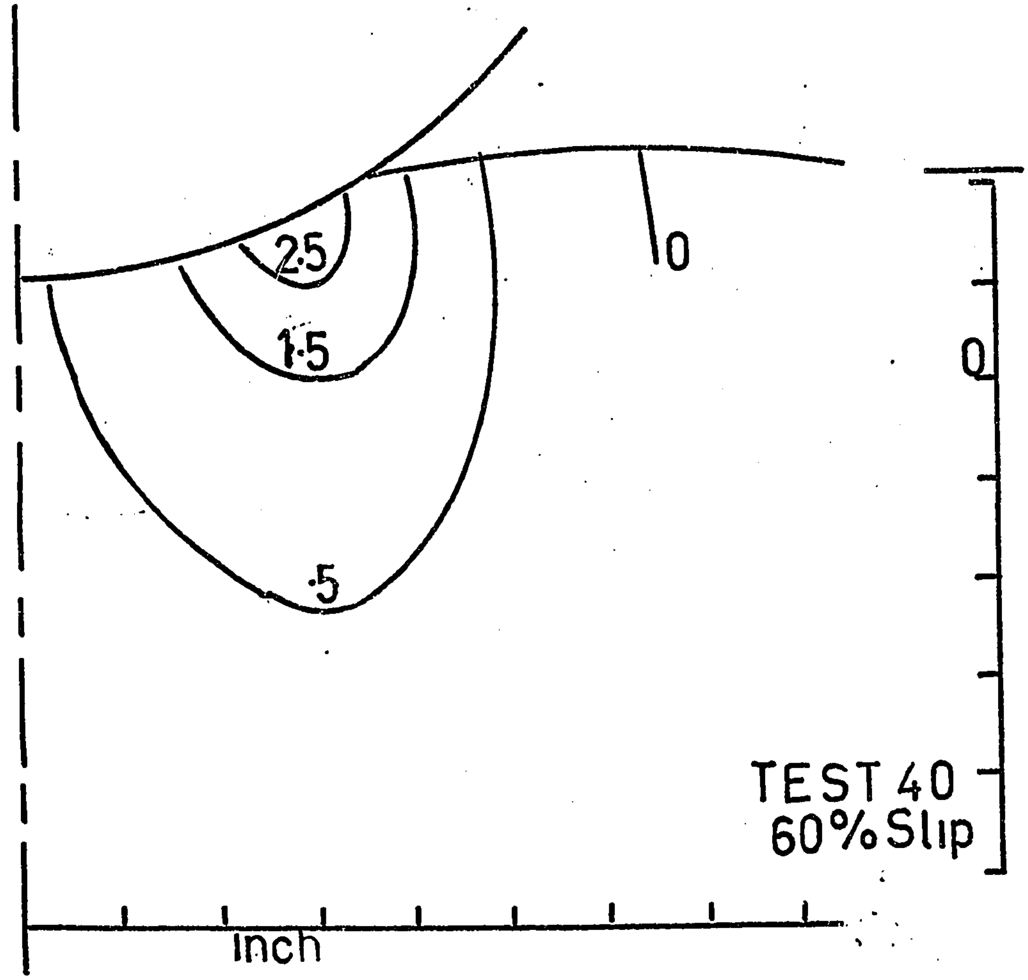

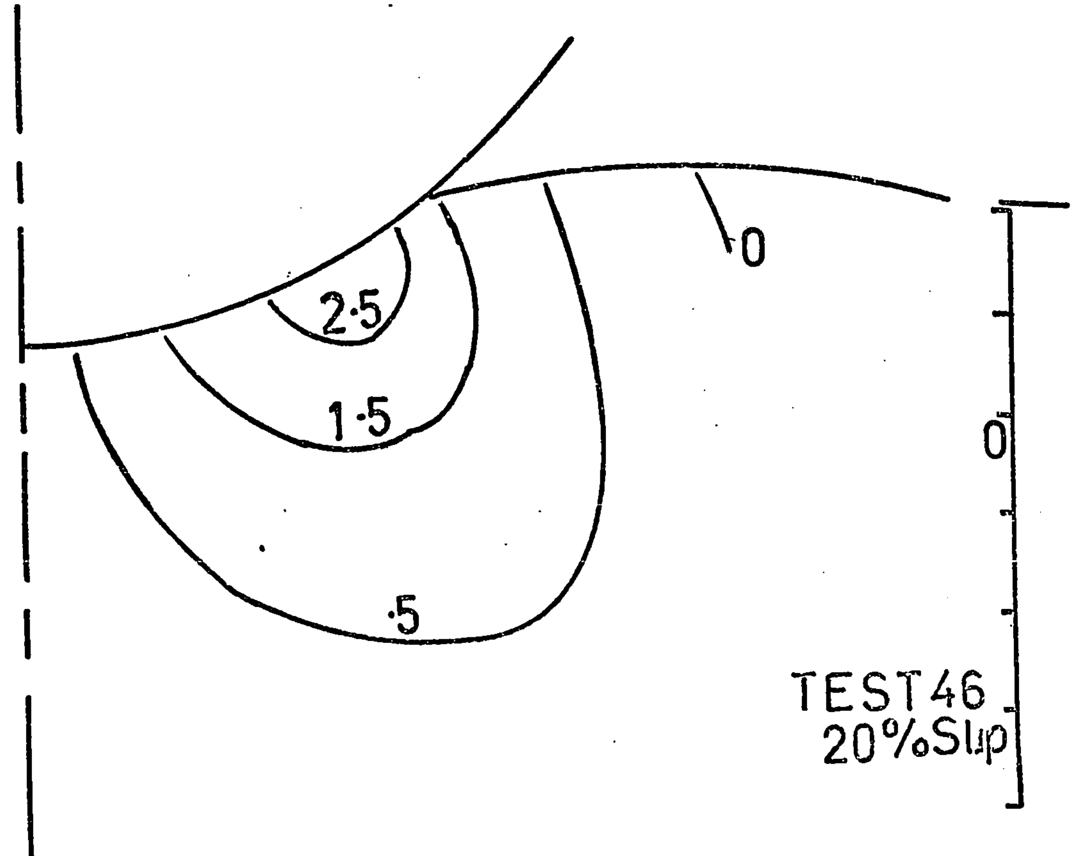

FIGURE 5-7 ISO-VELOCITY LINES - Y VELOCITY

are similar but not identical.

These features mentioned above show clearly why the strain rate invariants and the resultant deformation energy increases with decreasing slip.

Velocity Effects

A few tests were performed to try to evaluate the effect of changing carriage velocities. The main test series were run with constant carriage velocity (V_c approximately 5.6 in. per sec.). For the 51 lb. prototype wheel, tests were performed with carriage velocities between 3.9 in. per sec. and 8.9 in. per sec. Test conditions were so arranged that the normal slip rate was close to 30% normal slip. Within this velocity range it was observed that the energy quantities per unit distance were similar.

DISCUSSION RELATING TO ENERGY QUANTITIES

In the energy balance equation (Equation (5-2)), the energy terms have units of in.lb. per inch travelled. The pull force is the only force whose line of action is specified. The pull energy divided by the carriage velocity V_c gives the pull energy per inch of travel. It is possible to equate this to a force F lb which gives an energy of F in.lb. when the wheel axle has travelled one inch.

The following statements can then be made:-

1) (Input Energy - Interfacial Energy) per unit distance i.e. $\frac{M\omega}{V_c} - \frac{X}{V_c}$ can be equated to the thrust.

2) Although the line of action of the rolling resistance is unknown, it is possible to equate $\frac{D}{V_c}$ lb. to a "fictitious" rolling resistance force which provides energy $\frac{D}{V_c}$ in. lb. per inch of travel.

3) $\frac{D}{V_c}$ lb. can be compared with Bekkers R_c, R_b or the sum of R_c and R_b.

<u>(Input Energy - Interfacial Energy)</u>

Equating the (Input Energy - Interfacial Energy) per unit distance to the thrust is suggested because at high slips, it bears more resemblance to what Bekker considers to be Gross Tractive Effort. However it is possible to think of the Input Energy as a measure of the Gross thrust, and the sum of the Deformation and Interfacial Energy per unit distance as the total resisting force.

At small normal slips the interfacial energy can be neglected and the thrust is equal to the input energy per unit distance $\frac{M\omega}{V_c}$. This can also be expressed as $\frac{Mr\omega}{rV_c}$. For true zero slip $r\omega$ must be equal to V (V_c

plus Instantaneous Soil Velocity) which is not necessarily V_c, that is, $r\omega$ can have slightly different values at true zero slip since V changes. However it can be assumed that the input energy reduces to $\frac{M}{r}$. The quantity $\frac{M}{r}$ gives an estimate of the average shearing force which produces the torque. Schuring (1966) has suggested that $\frac{M}{r}$ should be used as the gross tractive effort. Wismer (1965) has also used $\frac{M}{r}$ as a measure of the thrust developed.

At high slips the difference of Input and Interfacial Energy per unit distance can be expressed as:-

$$\frac{M\omega}{V_c} - \frac{M}{r}\frac{V_s}{V_c} \qquad 5\text{-}4$$

In Appendix IV it is shown that $\frac{M}{r}\frac{V_s}{V_c}$ gives a good estimate of Interfacial Energy.

Equation (5-4) can be written as:-

$$\frac{Mr\omega}{rV_c} - \frac{M}{r}\left(\frac{r\omega - V_s}{V_c}\right) \qquad 5\text{-}5$$

which reduces to:-

$$\frac{M}{r}\ \frac{V}{V_c} \qquad 5\text{-}6$$

At high slips $\frac{V}{V_c}$ is greater than 1 and therefore $\frac{M}{r}$ underestimates the gross tractive effort since it does not allow for instantaneous soil velocity.

<u>Comparison of $\frac{M}{r}\frac{V}{V_c}$ with Coulomb's Shearing Resistance, AC</u>

At the towed point where the torque is zero,

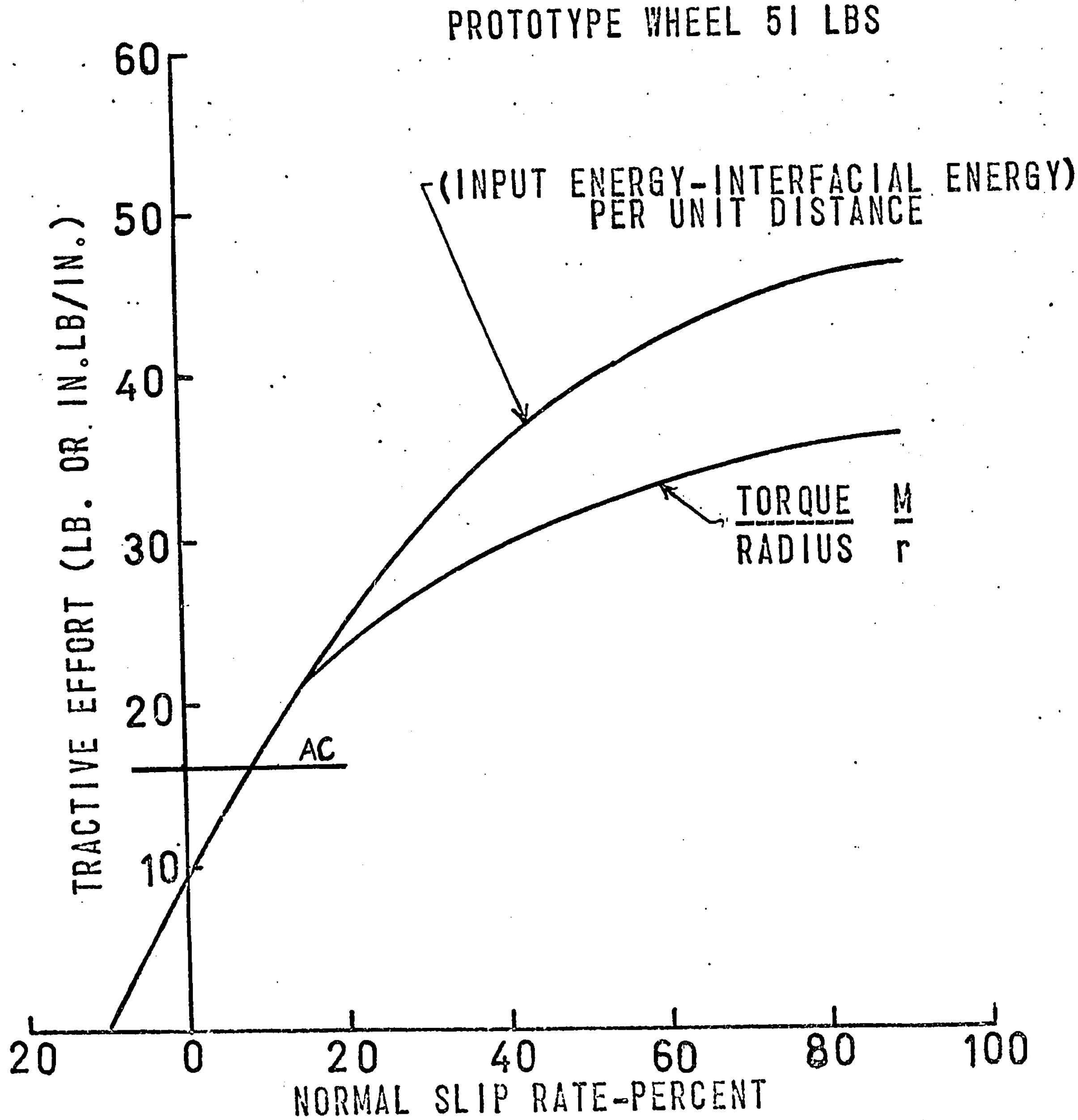

FIG. 5-8. TRACTIVE EFFORT VERSUS NORMAL SLIP RATE

the thrust is also zero. This follows because the resultant shear force on the interface is zero. This is caused by a change in sign of the shear stresses which become negative over a portion of the area contact. The torque M is defined by the following relation:-

$$M = \int_{\theta_1}^{\theta_2} \tau r d\theta \qquad 5\text{-}7$$

where τ = Elemental Shear Stress

r = Radius

$\theta_1 - \theta_2$ Defines Area of Contact.

The torque is zero when the moment of the positive shear stress is equal to the moment of the negative shear stress, i.e. the resultant shear force (traction force) is zero.

Mohr-Coulomb's theory using the entire area of contact will only apply if the slip velocity is sufficiently high that positive shear stress exist over the entire interface, then an average cohesion value determined from a stress-displacement, stress strain rate or stress slip velocity law can be used.

Figure 5-8 shows the three quantities discussed above. The quantities were calculated for the entire wheel width for the prototype 51 lb. wheel. It shows that around zero normal slip the Mohr-Coulomb theory using (AC) will over estimate the thrust. The area of contact was obtained from the third radiographic pulse.

Deformation Energy and Rolling Resistance

It has been suggested that the term "rolling resistance" has no meaning and should be replaced by energy dissipated per unit distance travelled. It is true that in considering the equilibrium of forces on a wheel that the line of action of the rolling resistance is not defined and Bekker has prescribed a "fictitious" line of action for the force. His method suggested for finding this rolling resistance force might be open to some question, but his idea is still basically sound.

To examine statements 2) and 3) above, two dimensional footing tests on the clay used in the experiment were performed and showed that a pressure-sinkage equation of the form below could be used, namely:-

$$p = 5.43z^{\frac{1}{2}} \qquad 5\text{-}8$$

Uffelmann's simple plastic theory uses the following equation:-

$$p = 5.7C \qquad 5\text{-}9$$

These two theories assume that the compaction resistance can be equated to the work in deforming the soil vertically and the dynamic sinkage is used as the rut depth. This work can be expressed as:-

$$\begin{aligned} R_c &= \int_0^z \text{pressure x width x dz} \qquad 5\text{-}10 \\ &= pbz \end{aligned}$$

Using Equation (5-10) the average dynamic sinkage

y_o, a test series was used to calculate the compaction resistance. These dynamic sinkages were measured by the L.V.D.T. and were verified from the radiographic information obtained in the third pulse and by the use of continuity relations.

These compaction resistances for the prototype wheel (51 lb. and 79 lb.) using Uffelmann's and Bekker's pressure equation were much less than the computed deformation energy per unit distance as can be seen in Figure 5-9.

In Bekker's bulldozing resistance formula (Equation (1-8)), for a purely cohesive soil $\frac{\sin(\alpha + \phi)}{\sin\alpha \cos\phi}$ is equal to 1, i.e. the angle of attack drops out of the formula and R_b gives the resistance behind a plate b inches wide and z inches deep (z is sinkage) which is pushed horizontally. The formula then reduces to $R_b = bzCN_c$. Using the dynamic sinkage y_o, bulldozing resistance equal to the compaction resistance will be obtained. These values seem to be quite high, especially for the high slip condition where the velocity field ahead of the wheel shows that bulldozing is small.

Since the sinkage to bow wave y_b (obtained by radiographic information) represents the true downward soil deformation, these values were then used to calculate compaction resistances. It is evident in Figure 5-9 that these values are somewhat closer to the measured

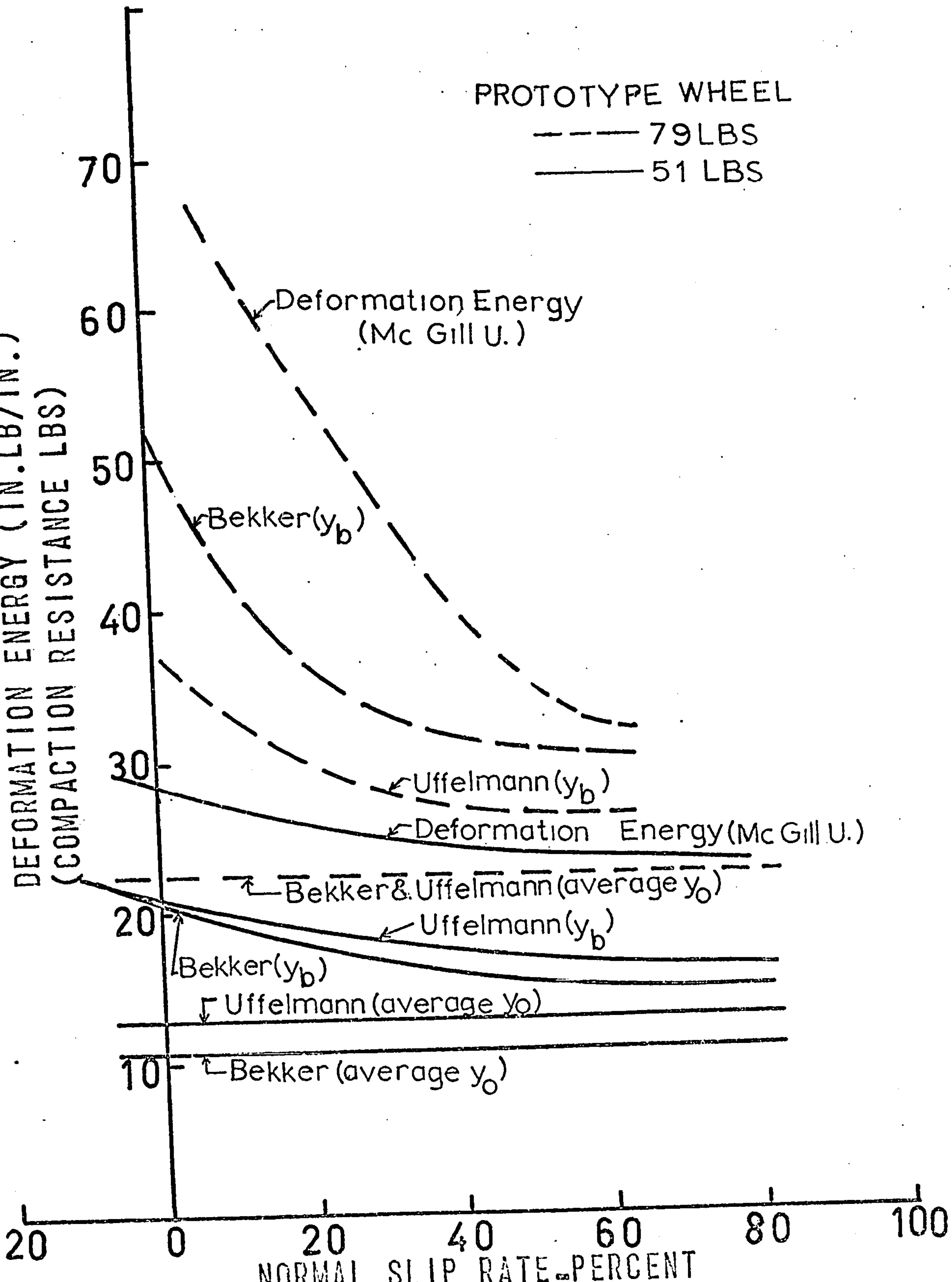

FIGURE 5-9. DEFORMATION ENERGY (COMPACTION RESISTANCE) VERSUS SLIP RATE

deformation energy.

For the 51 lb. prototype wheel the bow wave is small at high slips (.15 in.) and increases slightly with decreasing slip. The difference between the computed deformation energy and the compaction resistance by both methods stays relatively constant over the entire slip range and the difference between the deformation energy and the compaction resistances using y_b can be attributed to the small upward movement of the soil ahead of the wheel.

For the 79 lb. prototype wheel, the compaction resistances computed by both methods are close to the deformation values at high slips. With decreasing slips, the values using Bekker's pressure sinkage equations show a larger increase than the values from the Uffelmann method. This is expected since Uffelmann's simple plastic theory covers the small sinkage domain, whereas the Bekker's pressure sinkage equation was obtained for a larger range of sinkages. However the calculated compaction resistances are still much lower than the computed deformation energy. This is evidence of increased bulldozing resistance with decreasing slip.

The analysis above shows that equating the rolling resistance to the work used in making a vertical soil deformation is a good approximation when the true vertical soil deformation is used and when the entry conditions are such that the energy dissipated ahead of the wheel is small. As pointed out by Bekker the splitting of rolling resistance into compaction and bulldozing resistance by empirical methods is a difficult exercise, however the visioplasticity method seems to offer a means of assessing existing formulas.

CHAPTER 6

SUMMARY AND CONCLUSIONS

SUMMARY

A fundamental prerequisite for soil-vehicle interaction analysis is the exact specification of response behaviour of the soil under vehicular loading.

The behaviour of a clay soil beneath moving rigid wheels was obtained through the use of a cine-radiographic technique. This technique provides the exact nature of the soil response to vehicular loading. The information obtained highlighted the inaccuracies in assumptions invoked in existing empirical formulations and provided a means of properly incorporating the beneath wheel component of soil-vehicle interaction into a more rational overall theory which takes into account the conventional surficial and above ground parameters.

The application of the visioplasticity method to analyse the deformation behaviour represents the first application of a semi-analytical method to the soil-vehicle problem. In this analysis use was made of the velocity fields obtained from the cine-radiographic data, and basic plasticity relations. It was then possible to evaluate the work (Deformation Energy) dissipated in deforming the soil vertically and horizontally.

Considerations of the energy balance of the system making use of the computed deformation energy and the measured input parameters showed that reasonable predictions of the usually accepted soil-vehicle criterion - Drawbar Pull - were obtained.

CONCLUSIONS

Characteristics of Flow of Clay Soil Beneath a Rigid Wheel

The observed behaviour of a clay soil beneath a loaded spinning wheel represents a wheel-soil interaction problem, therefore explanations and analyses must be approached from this basic premise. The yield characteristics of the soil, under the action of the wheel, prescribes the soil behaviour. The following general statements can then be made if the wheel is considered to be fixed in space and rotating, and the soil is moving.

(1) At high normal slips, there is a discontinuity close to the wheel-soil interface where the soil work hardens. The soil velocity, a small distance below the interface at the bottom, dead centre of the wheel is much smaller than the rim velocity, but larger than the carriage velocity. The velocity decreases sharply at shallow depths and then decreases gradually.

(2) At low normal slips the soil velocity is less than the carriage velocity just below the interface. It increases with depth to some value above the carriage

velocity and then decreases gradually with depth.

(3) The upward movement of the soil ahead of the wheel increases with decreasing slip. At higher sinkages the velocity conditions ahead of the wheel are radically altered resulting in velocities much lower than the initial soil velocity (carriage velocity).

(4) There is substantial recovery of soil at the rear of the wheel.

Slip Sinkage

The two dimensional test on a cohesive soil showed that dynamic or rolling sinkage was slip independent. The conditions under which slip sinkage occurs has been the object of speculation in the vehicle mechanics field. The following guide lines can be proposed:-

(1) Slip sinkage can be specified by the soil velocity conditions existing at the bottom dead centre. These velocity conditions are dependent on the yield characteristics of the medium and its interaction with the powered wheel. For a cohesive soil which shows a discontinuity at the wheel soil interface the velocities a small distance below the interface although different from the low slip condition do not become large. The average soil velocities under all slip conditions are similar and there is no slip sinkage.

(2) On the other extreme, for a dry frictional

material which does not work harden, there will be much higher velocities over a greater portion of the deformed region at high slip producing slip sinkage.

(3) For a material with both cohesive and frictional properties the extent of the slip sinkage depends on the yield characteristics of the material under the action of the spinning wheel and will take on a value between cohesive and frictional behaviour.

Energy Balance

Maximum efficiency for the soil-wheel system was attained around the self propelled point (circa 30% normal slip). The efficiency then decreases with increasing slip.

Deformation Energy

The deformation energy under varying conditions reflects the changes in the strain rate fields computed from the velocity values. For a cohesive material, the deformation energy increases with decreasing slip. This is caused by varying entry conditions of the soil with decreasing slip. The entry conditions are radically altered when a y_0/D ratio of .050 is exceeded.

λ^2 weight scaling produced equal sinkage and dynamic similarity at high normal slips, resulting in equal deformation energy. This can be quite useful in the extension of model behaviour to prototype behaviour. At low slips velocity fields are dependent on y_0/D ratio and scaling is more difficult.

Torque Energy

The magnitude of the torque, M, developed by the wheel is prescribed by the shear stresses at the interface. This shear stress is defined by the yield characteristics of the material at the interface. The measured torque can be obtained if the moment of the elemental stresses multiplied by the radius of the wheel are summed up over the area of contact obtained by the radiographic technique. It is therefore possible to define the torque if the expected yield properties can be specified.

λ^2 weight scaling produced λ^2 torque scaling since equivalent sinkage was obtained and the rate dependent shear stresses are equal at the same slip velocity.

Interfacial Energy

For a cohesive material it has been demonstrated that the external frictional stress at high normal slips does not follow Coulomb's Law, when the normal pressure exceeds a certain value. Under these conditions the frictional stress is equal to the shear stress which is rate dependent. This points up the error in certain dissipative coefficients which are weight dependent.

CLAIM TO ORIGINAL WORK

The use of the visioplasticity method to analyse the beneath wheel component of a clay soil-rigid wheel interaction represents the first semi-analytical method that has been applied to the soil-vehicle interaction problem.

The validity of this theory was established by considering the energy balance of the entire system. The separation of the energy dissipated to the soil into deformation energy and the interfacial energy was obtained for the first time by considering the true interaction between wheel and soil.

Implications and Utility of this Study in the General Soil-Vehicle Field

Although this study has been confined to the study of clay behaviour under rigid wheels it is possible to prescribe certain features which will cover a wide range of material.

Explanations for the slip-sinkage phenomena for materials other than cohesive soils have been given before. The components of the energy balance have been prescribed for clay soils, however estimates of the magnitude of these components for other soil-vehicle systems can be anticipated from the expected soil-vehicle interaction.

In clay soils, because of the discontinuity at the interface, the deformation energy stays relatively constant at high slips while the interfacial energy increases rapidly. For a dry frictional material which does not work harden there will be high velocities in a greater portion of the deformed zone as mentioned before. The soil velocities will actually approach the rim velocity, and the true slip velocity will be quite low in spite of high normal slips. As a consequence of this a dry frictional material will show rapidly increasing deformation energy at high normal slips with small interfacial energies.

The behaviour of a material with frictional and cohesive properties will fall somewhere in between.

CHAPTER 7

RECOMMENDATIONS FOR FURTHER STUDY

The visioplasticity analysis represents a significant advance in the soil-vehicle interaction field. It can therefore be used to investigate several aspects of the soil-wheel problem. These include additional tests on sands, clays, and soil with both cohesive and frictional properties, under varying input conditions and with varying wheel sizes.

In this study it was observed that at high slips dynamic similarity was achieved with λ^2 scaling, however for low slips a more detailed examination of velocity fields ahead of the wheel is necessary to define the scaling criterion. Particular attention should be focussed on the behaviour when the dimensionless sinkage ratio y_o/D is greater than .050, the point at which Deformation Energy increases rapidly with decreasing slip.

The capability of the existing pulser sets certain limitations on the wheel width that can be accomodated. A higher kilovoltage pulser and modifications to the existing facility is necessary before the study can be extended to the three dimensional case.

The developement of a constitutive equation which defines the yield behaviour is necessary in all analyses. Special tests which simulate the action of a slipping wheel to a greater degree than conventional strength tests should be investigated.

APPENDIX I

SOIL-VEHICLE EXPERIMENTAL FACILITY

Test Facility

The facility has been described by Yong et al (1965) and Yong et al (1967). Figure I-1 shows a schematic of the soil-bin, the dynamometer carriage and the hydraulic drive mechanism. The bin is 32 feet long by 4 feet deep. The 6 foot width will allow future studies on model vehicles.

The dynamometer carriage which supports the wheel carriage assembly, the wheel drive mechanism and an instrument box is pulled along Z rails located on either side of the bin by endless double-link chains which are driven hydraulically through two worm and wheel reducers. Carriage velocities up to 35 inches per second can be achieved. These velocities are measeured by a tachometer mounted on the main drive shaft.

Wheel Carriage Assembly

The wheel carriage shown in Figure I-2 consists of a frame attached to the dynamometer by two flexures. For wheels of varying diameters the wheel carriage assembly can be attached at various levels so that the flexure frame remains level. Strain gauges mounted on these flexures and connected to a resistance bridge network provide

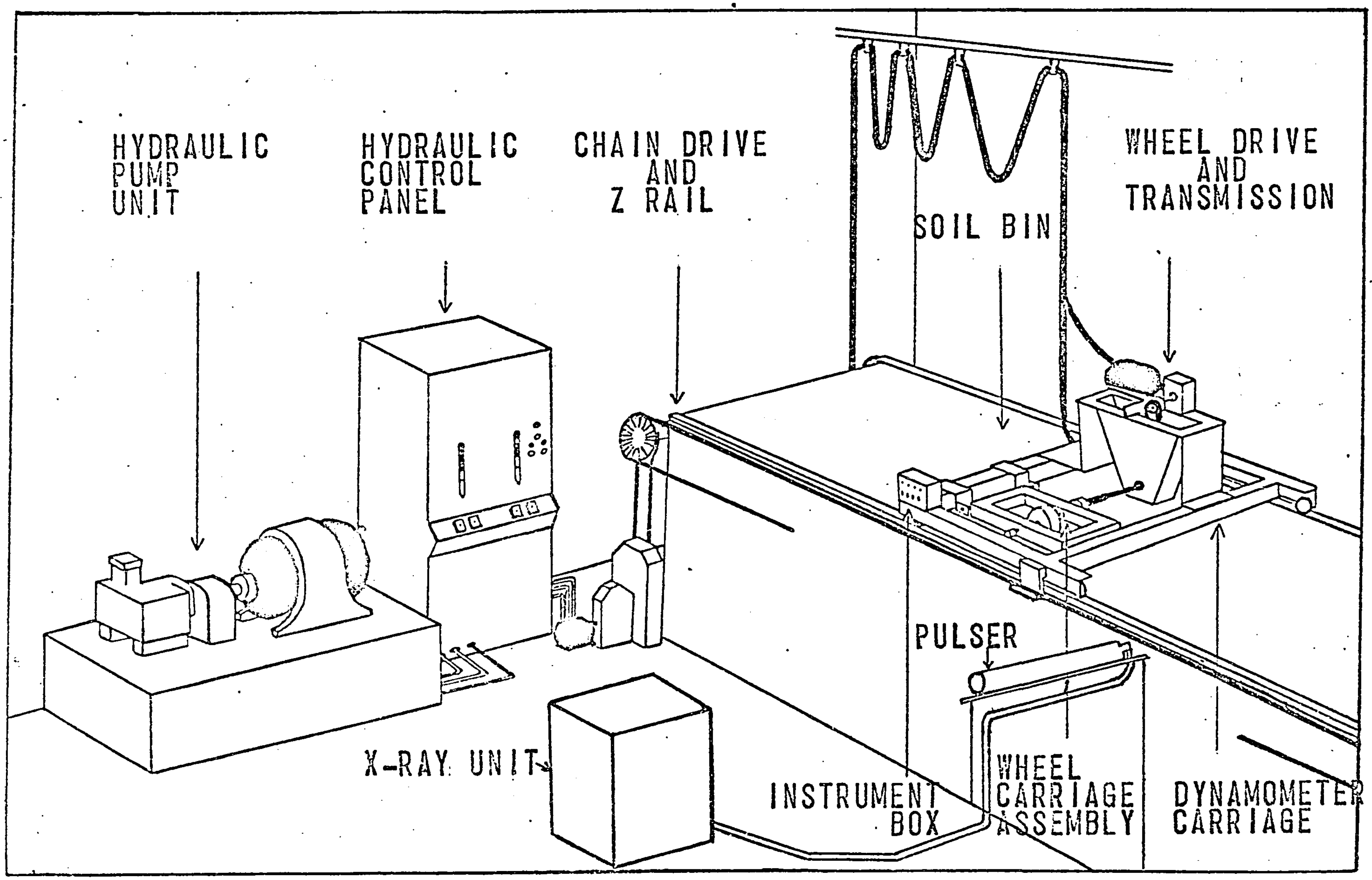

FIGURE I-1. SOIL VEHICLE TEST FACILITY

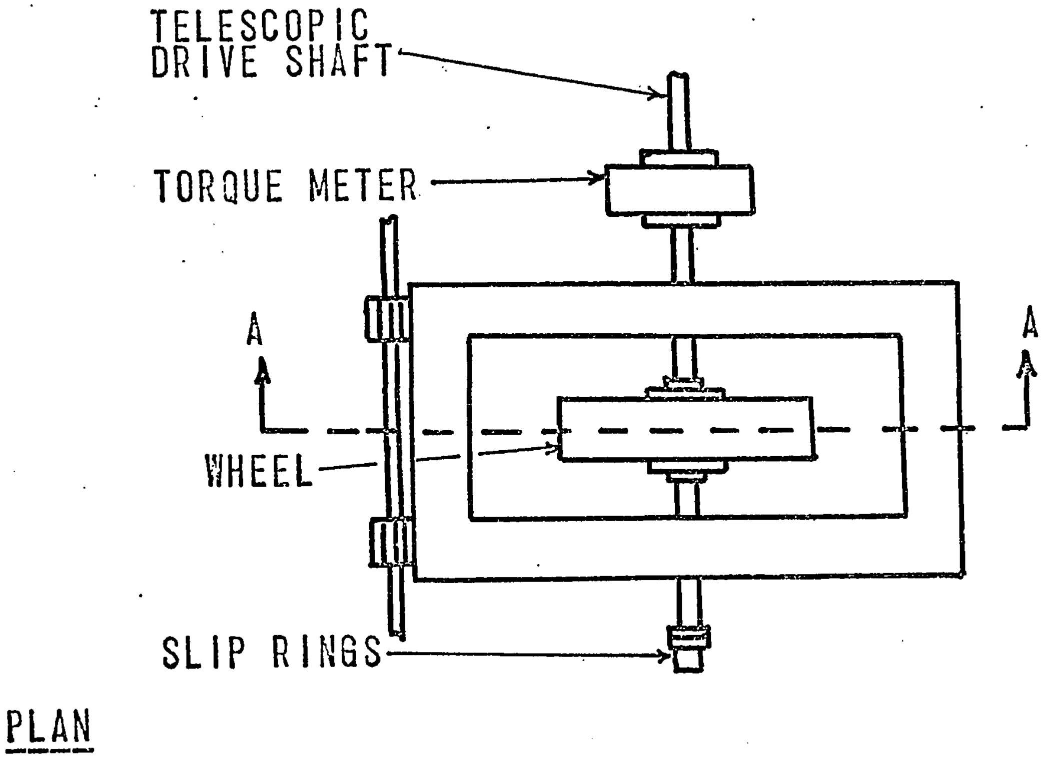

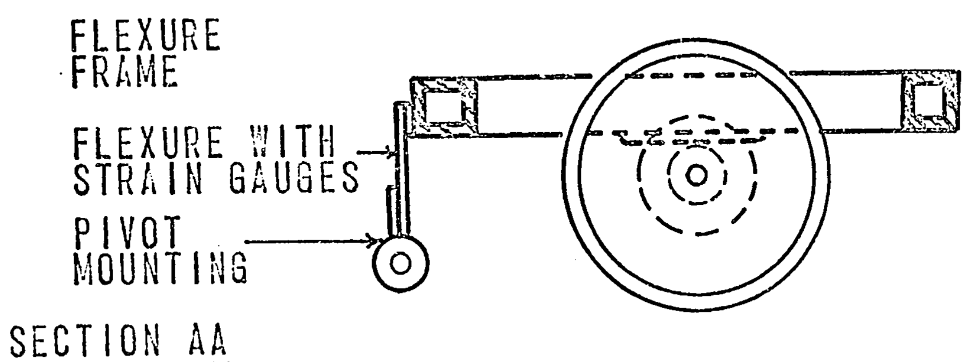

FIGURE I-2. THE WHEEL CARRIAGE ASSEMBLY

a measure of the drawbar pull.

The test wheel is attached to an axle connected to the flexure frame by bearings. One end of the axle is connected via a torque measuring device and a telescopic drive shaft to a variable-speed constant torque, shunt wound 1/2 horse power D. C. motor with a 29:4 reduction ratio. A tachometer mounted on this motor gives the angular velocity ω of the wheel. The torque is measured through a resistance bridge network of four strain gauges. The other end of the axle is connected to a set of slip rings which allow the connection of leads from the torque strain gauges to the instrument box. Experiments have shown that the torque necessary to overcome internal resistance was very small (a few inch-ounces) and therefore an exact measure of the driving torque to the wheel is obtained.

The sinkage of the wheel is obtained from a linear voltage displacement transducer fastened to the dynamometer carriage and resting on the flexure frame.

Accessories

The power supply, switches and resistors for the strain gauge and transducer circuits are incorporated into the instrument box. Power leads to the D. C. motor and the output leads from measuring devices are supported by runners suspended from a guiding track on the ceiling.

The D. C. motor leads are connected to a controlling rheostat while the voltage outputs from the strain gauges, transducers and tachometer are amplified and recorded on a six channel ultra-violet light recorder. The conversion of the signal voltages back to the measured quantities is achieved by the "black box" technique. Calibration details and electric circuitry are described at the end of this appendix.

Flash X-Ray System

The flash x-ray train components were supplied by Field Emission Corp., McMinnville, Oregon. A schematic of the Cine-Radiographic system is shown in Figure I-3.

Mode of Operation

The high voltage power supply charges the pulser rapidly to a prescribed charging voltage of 300 kv. The pulser remains charged at this voltage until a trigger signal from the limit switches arrives at the multipulse trigger generator which, with the trigger amplifier, commands the pulser to fire. The pulser fires and if the multipulse trigger generator has been set for more than one pulse, is recharged again to the charging voltage. A spring loaded arm on the dynamometer carriage activates the limit switches. The process is then repeated until the predetermined number of pulses programmed on the

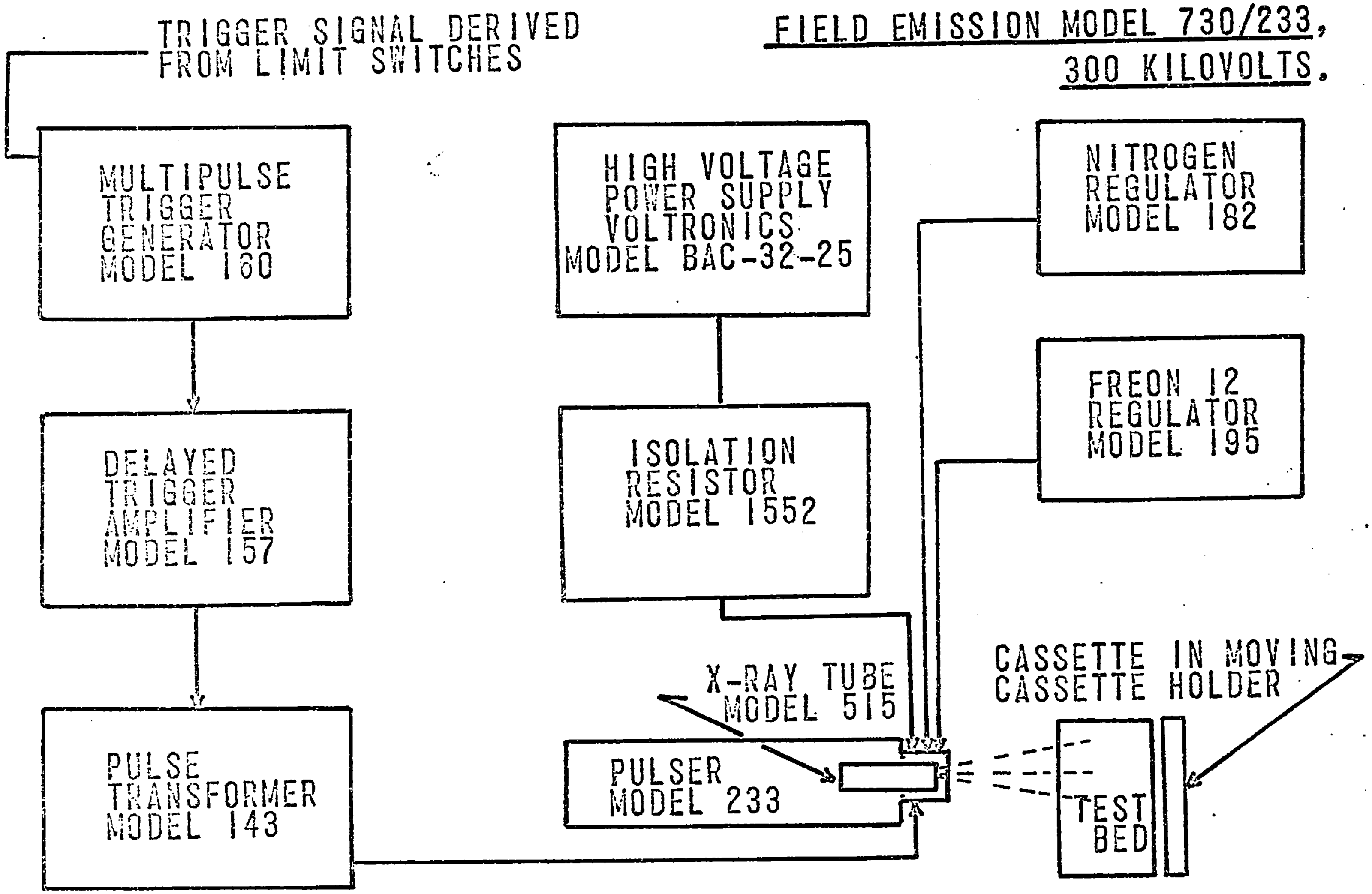

FIGURE I-3. SCHEMATIC OF CINE-RADIOGRAPHIC SYSTEM trigger generator has been completed.

The flash x-ray tubes use a cold cathode electron source resulting in high current densities and very large information rates. A successive train of up to ten exposures at a maximum rate of two pulses per second can be produced by the system.

Specifications of the essential features of the McGill Unit are shown in Table I-1 below:-

TABLE I-1

Essential Specifications of Flash X-Ray Unit

Model Number	730/233
Output Voltage (Kilovolts)	300
Output Current (Amps.)	1400
Output Impedance (Ohms)	215
Pulse Width (Microseconds)	0.1
Peak Power (Megawatts)	420
Source Size (mm.)	6.0
Dose Rate at Tube Face (r/sec)	1×10^8
Penetration of Aluminum (Inches)	6.0 (at 1 ft. S.F.D.)

CALIBRATION PROCEDURES AND ELECTRIC CIRCUITRY

The wheel parameters are measured continuously during a test by electric methods. The calibration procedure for each circuit is given below.

The equations of the calibration curves are, in all cases, obtained using the least squares criterion for the best estimate.

Drawbar Pull at Each Flexure

The wheel is placed on an aluminum plate so that the wheel carriage is level. One flexure is disconnected and the other is loaded symmetrically via a spring balance. Deflections of the ultra-violet light recorder trace are recorded against known loads imparted by the spring balance. The procedure is then repeated for the other flexure. The calibration curves and the electric circuit diagram are shown in Figure I-4.

Torque Applied to Wheel Axle

The wheel is placed on an aluminum plate so that the wheel carriage is level. A certain torque is applied by the D. C. drive motor and the wheel is loaded vertically to a point where the wheel-plate friction prevents rotation of the wheel. The deflections of the three ultra-violet light recorder traces corresponding to the torque and the two drawbar pull flexures are recorded. The total drawbar pull is evaluated using the calibrations obtained above and the torque calculated using the equation:-

Torque = Frictional Force x Wheel Radius

= Total Drawbar Pull x Wheel Radius

The procedure is repeated for several values of torque. It was necessary to repeat the calibration on changing the wheel sizes as a different amplification was required to accommodate the larger torques encountered with the larger wheel. The calibration curves and the electric circuit diagram are shown in Figure I-5.

Sinkage

A pair of vernier calipers is attached to the linear motion transducer and ultra-violet light recorder trace deflections are recorded against known transducer extensions. The calibration curve and electric circuit diagram are shown in Figure I-6.

Angular Velocity

The wheel drive motor rheostat is adjusted to a constant setting to ensure uniform rotation of the wheel. The angular velocity is computed from the time, (measured on a stop-watch), required for the wheel to complete ten revolutions and then compared with the corresponding ultra-violet light recorder trace deflection. The procedure is repeated for several rheostat settings. The calibration curve and electric circuit diagram are shown in Figure I-7.

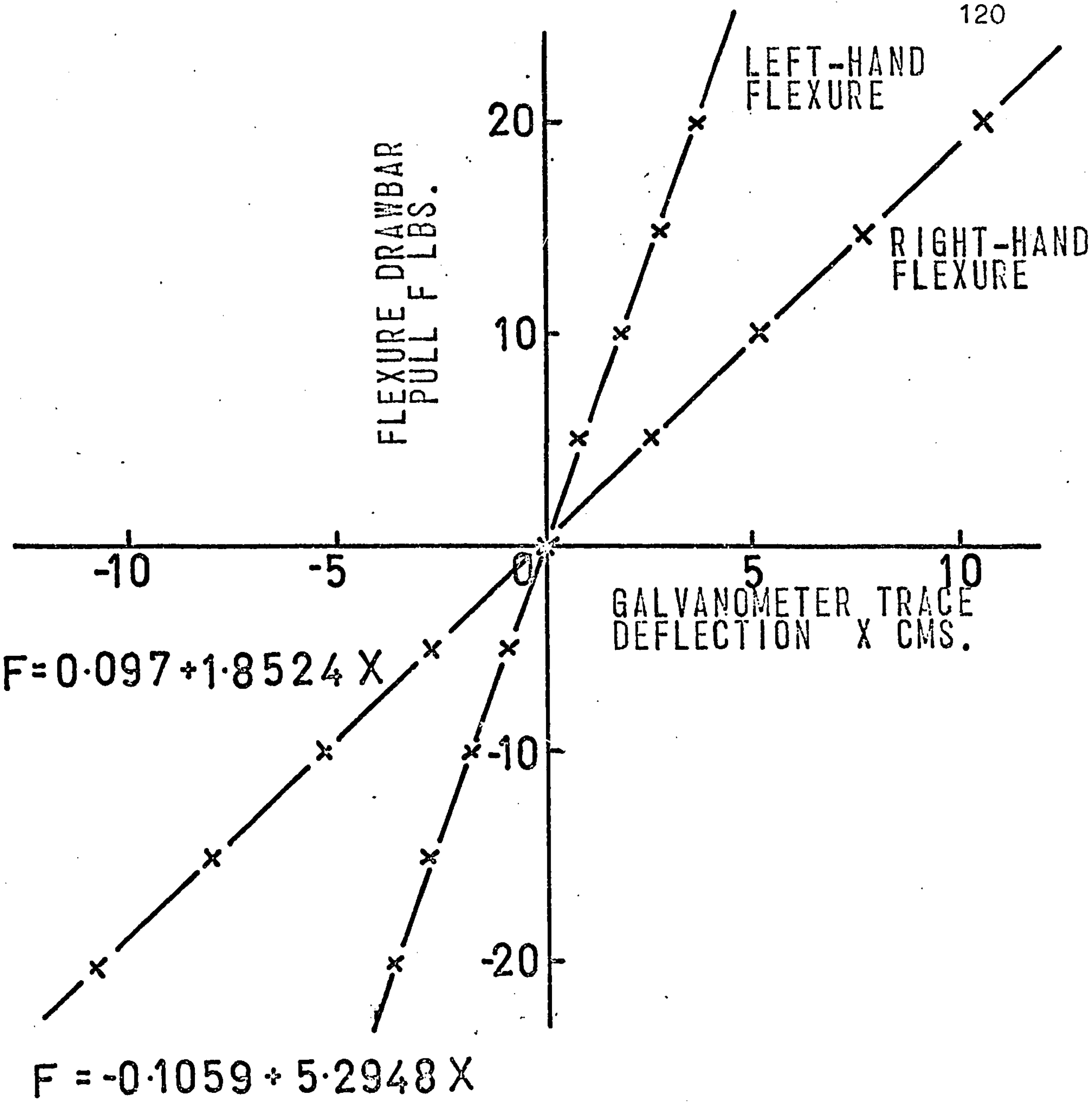

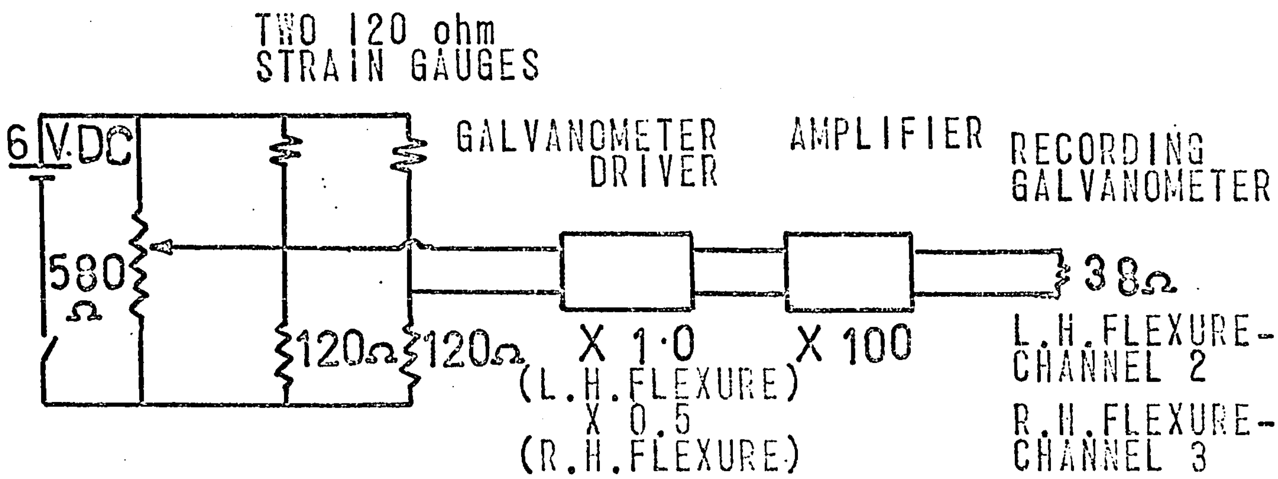

FIG. I-4. CALIBRATION AND CIRCUIT DIAGRAM FOR DRAWBAR PULLS

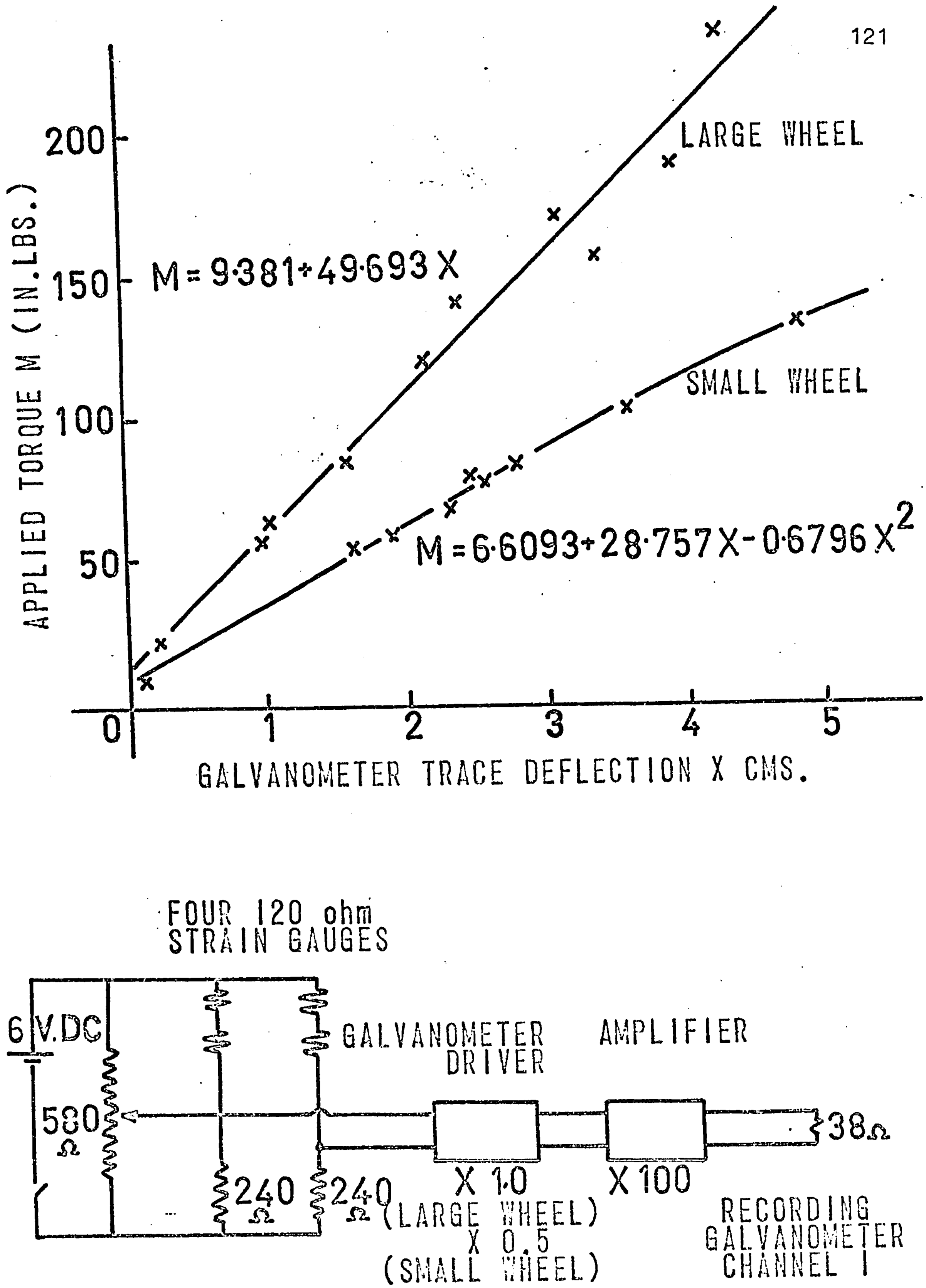

FIGURE I-5. CALIBRATION AND CIRCUIT DIAGRAM FOR TORQUE

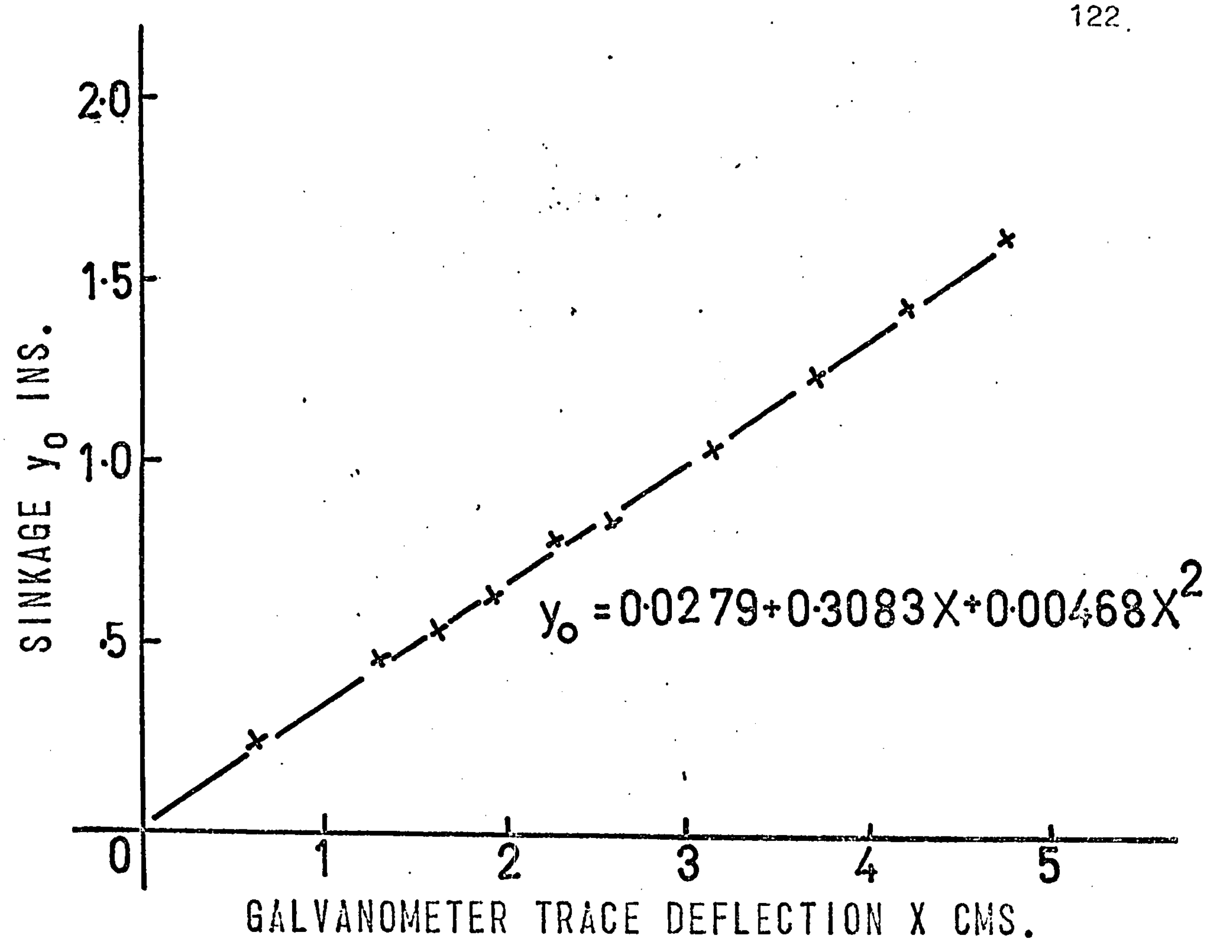

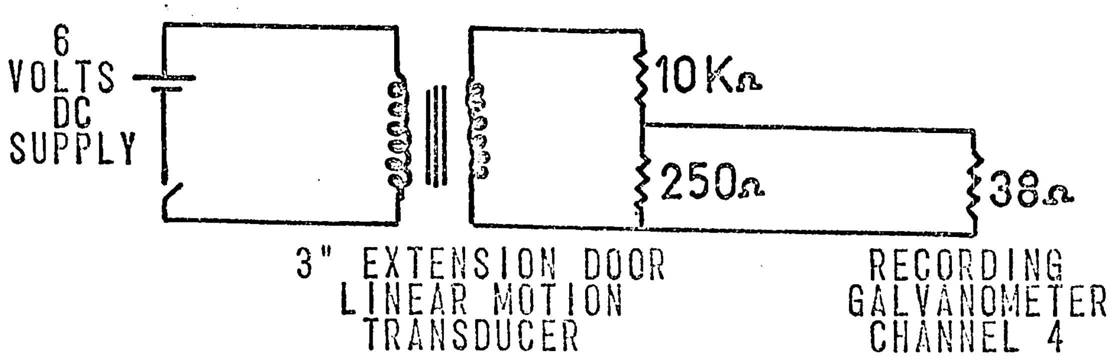

FIGURE I-6. CALIBRATION AND CIRCUIT DIAGRAM FOR SINKAGE

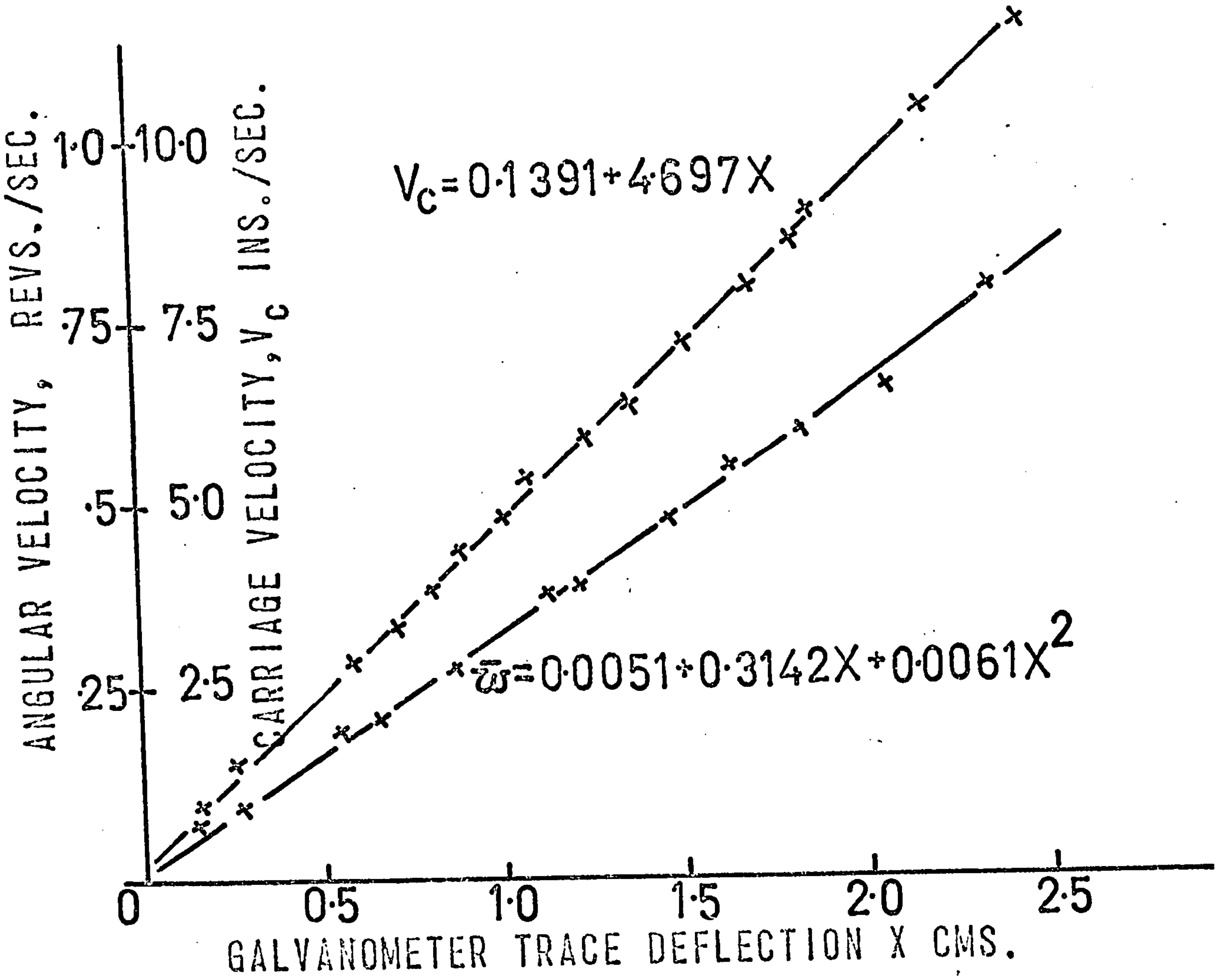

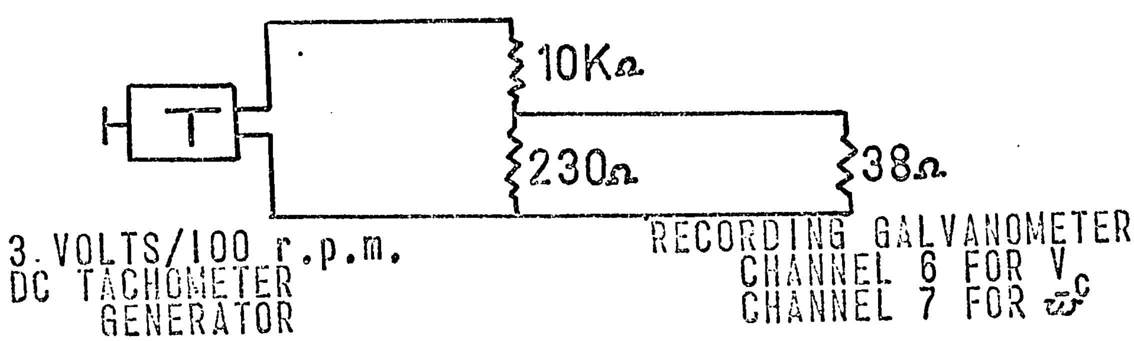

FIG. I-7. CALIBRATIONS AND CIRCUIT DIAGRAMS FOR LINEAR AND CARRIAGE VELOCITIES

Carriage Velocity

The hydraulic flow control valves are adjusted to a constant setting to ensure uniform motion of the carriage. The carriage velocity is computed from the time (measured on a stop-watch), required for the carriage to travel twenty feet and then compared with the ultra-violet light recorder trace deflection. The procedure is repeated for several settings of the hydraulic flow control valves. The calibration curve and electric circuit diagram are shown in Figure I-7.

APPENDIX II

EXPERIMENTATION

In this appendix certain preliminary considerations and modifications to the existing facilites to accomodate the testing of rigid wheels on clay soil are discussed. The following are described:-

i) Construction of a moving cassette holder to obtain additional deformation history.

ii) Preparation, compaction and control techniques used to ensure a uniform test bed.

iii) Selection of system parameters and testing schedule.

RADIOGRAPHIC CONSIDERATIONS

X-rays are a form of electromagnetic radiation having wavelengths in the region 10^{-10} to 10^{-7} cm. The two usual forms of x-ray generation are by thermionic emission and by field emission.

Thermionic Emission

The emission of electrons across the boundary surface that separates a heated electronic conduction from an otherwise non-conducting space is known as thermionic emission.

Field Emission

The emission of electrons from the surface of a conductor into a vacuum under the influence of a high electric field is known as field emission.

ATTENUATION OF X-RADIATION

X-rays are absorbed or scattered in their passage through matter. A complete description of the mechanisms involved will not be given here; for detailed analysis see McMaster (1959) and Fano et al (1959). The predominant interactions which can be summarized as follows are taken from McMaster (loc. cit.).

Photoelectric Effect:- A process in which a photon of energy transfers its total energy to an electron into the shell of an atom.

Compton Incoherent Scattering:- A photon colliding with an electron, instead of giving up all its energy, shares a portion of it with the struck electron.

Rayleigh Process:- Here the photon does not experience an energy shift upon being scattered by an atom and the process is said to be coherent. The electrons are set into motion by absorption of the incident photon. They then emit a photon of the same frequency as the incident photon.

Pair Production:- Very high energy photons are absorbed in matter by a process in which a photon is converted into the electrical field of a nucleus into an electron and a positron.

Secondary Radiation Effects:- An electron, because of its small mass, can experience a large deceleration in the electrical field of a nucleus, resulting in the emission of radiation. This radiation or Bremsstrahlung is the dominant influence in the energy loss of fast electrons.

NARROW BEAM ATTENUATION

A narrow beam of x-ray exhibits an exponential absorption in its passage through matter. To calculate the absorption of mono-energetic x-rays passing through a given material, the following equation can be used:-

$$I_T = I_o \exp\left(- \frac{\mu}{\bar{\rho}} \; r \right)$$

where I_T is the exit intensity

I_o is the incident intensity

$\frac{\mu}{\bar{\rho}}$ is the mass absorption coefficient

$\bar{\rho}$ is the density of the body (lb/in.^{3})

r is the thickness

To calculate the mass absorption coefficients $\frac{\mu}{\bar{\rho}}$ for a material, the values of $\frac{\mu}{\bar{\rho}}$ for the elements contained in that material can be combined by the following formula:-

$$\left(\frac{\mu}{\bar{\rho}}\right)_{\text{material}} = \sum_N R_N \left(\frac{\mu}{\bar{\rho}}\right)_N$$

where $(\frac{\mu}{\rho})_N$ is mass absorption coefficient of element 'N'

R_N is the ratio of the atomic weight of element 'N' to the atomic weight of the material

As an example of this consider the kaolinite used in this study being radiographed with 300 kv. x-rays. Neglecting traces of Fe_2O_3, TiO_2, MgO, CaO, K_2O and Na_2O shown in the analysis the formula can be written as $2H_2O.Al_2O_3.SiO_2$. The value of $\frac{\mu}{\rho}$ for kaolinite can be computed as follows:-

$$\frac{\mu}{\rho} = (\frac{\mu}{\rho})_H R_H + (\frac{\mu}{\rho})_O R_O + (\frac{\mu}{\rho})_{Al} R_{Al} + (\frac{\mu}{\rho})_{Si} R_{Si}$$

From Table II-1

$$\frac{\mu}{\rho} = .212 \times .0202 + .107 \times .5657 + .104 \times .2727 + .108 \times 1.414$$

Therefore $\frac{\mu}{\rho}$ for kaolinite is equal to .1085. The $\frac{\mu}{\rho}$ values have been evaluated by Victoreen (1949). The values used in the calculation pertain to the minimum wavelength of $0.0413^{o}A$ which depend only on the applied voltage. The maximum wavelengths in the field emission units is dictated by the wavelength filters covering the x-ray tubes and an upper wavelength value of $.20^{o}A$ has been suggested. In this wavelength range however, the variation of attenuation coefficients is small.

TABLE II-1

Mass Absorption Coefficient of Kaolinite

X-ray Source = 300 kv. Wave Length = .042^{o}A

Element	Number of Atoms	Atomic Weight	Atomic Weight in Material	R	Mass Absorption Coefficient	$R\frac{\mu}{\rho}$
Hydrogen	4	1	4	.0202	.212	.0043
Oxygen	7	16	112	.5657	.107	.0605
Aluminum	2	27	54	.2727	.004	.0284
Silicon	1	28	28	.1414	.108	.0153

Atomic Wt. of Kaolinite = 198 1.000 $(\frac{\mu}{\rho})$Kaolinite = .1085

Consider the compacted clay mixture used in this study being irradiated with x-rays. The gravimetric moisture content of 54% at 100 pounds per cubic foot wet density gives a volumetric moisture content of 56%. The small quantities of air in the mixture can be incorporated into the exponential absorption law but will be neglected. The soil can be considered as being irradiated with x-rays at S.F.D. of 16.5 inches (see Figure II-1) and the following relationship can be established:-

$$I_T=I_0e^{-\mu(air)r(air)-\mu(kaol)r(kaol)-\mu(H_2O)r(H_2O)}$$

where $r(air) = 16.5 -$ Clay Thickness, x.

$r(kaol.) = r($kaolinite particles$) = .44x$.

$r(H_2O) = r($water$) = .56x$.

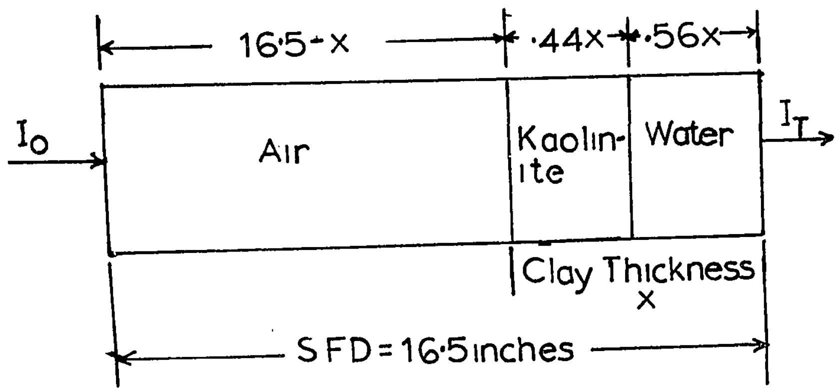

Figure II-1 Attenuation of X-rays

This type of analysis is very useful in evaluating a given source even if the x-ray emitter has a wide beam geometry. However the final criterion is dependent on film quality which in turn depends on type of film, screens, type of chemicals and method of developement.

Film Radiography

X-rays passing through the soil are absorbed more by the small lead markers than the soil itself. The variation in the x-ray beam is recorded on film by allowing the photons to interact with film emulsion. After exposure and development of the film, variation in intensity of the x-rays are recorded as variations of density. Since exposure time is in the nano-second range, calcium tungstate intensifying screens are used. These screens become flourescent in the presence of x-rays, therefore both the x-ray photons and the visible light photons produced by the calcium tungstate act on the film, consequently the x-ray intensity to produce a radiograph of given density is less than that required by the film alone.

APPLICATION TO SOIL INTERACTION STUDIES

Roscoe et al (1963) used a thermionic x-ray emitter to study deformations occuring in sand behind a retaining wall under plane strain conditions. Wilson and Krzywicki (1965) used a low voltage emitter to measure deformations that occured in organic peat when a rigid wheel was driven over. This is the first radiographic application to the soil vehicle problem. Bloedow (1962) examined various radiographic techniques to determine their feasibility for the study of dynamic soil behaviour. High voltage, short pulse duration field emission units were used.

At McGill University, a 300 kv. field emission unit has been previously used for a soil-vehicle interaction study on sand and is described in Appendix I. As shown earlier in this appendix theoretical calculations can be used to get a measure of the effectiveness of a given x-ray system in penetrating a specific thickness of material, however the final decision cannot be made until actual testing is performed. The x-ray beam geometry of 30 degrees along with a S.F.D. of 16.5 inches restrict the area that can be radiographed to 7 inches by 7 inches, and tests showed that good radiographs could be obtained with the existing 300 kv. Field Emission unit with a six inch thickness of wet kaolin clay. The case for two dimensional testing was supported by the following reasons. First, there is some sideways movement of soil in the three dimensional and it was possible that this sideways movement could not be accomodated within the allowable six inches when the 2 1/2 and 3 3/4 inch wide wheels were used. Second, considerable modification and extension of the existing equipment is necessary before quantitative measurements of sideways heave could be obtained.

In previous work on sand, four pulses were fired, one before the test, two intermediate shots registering on the same cassette and a final shot after the test. It was realized that an attempt should be made to obtain as much information of the deformation process consistent with the capabilities of the pulser. The fixed cassette holder was removed and replaced by a moving cassette holder and an additional intermediate radiograph could be obtained.

<u>Moving Cassette Holder</u>

Figure II-2 shows a schematic of the moving cassette holder. It consists of an aluminum frame attached

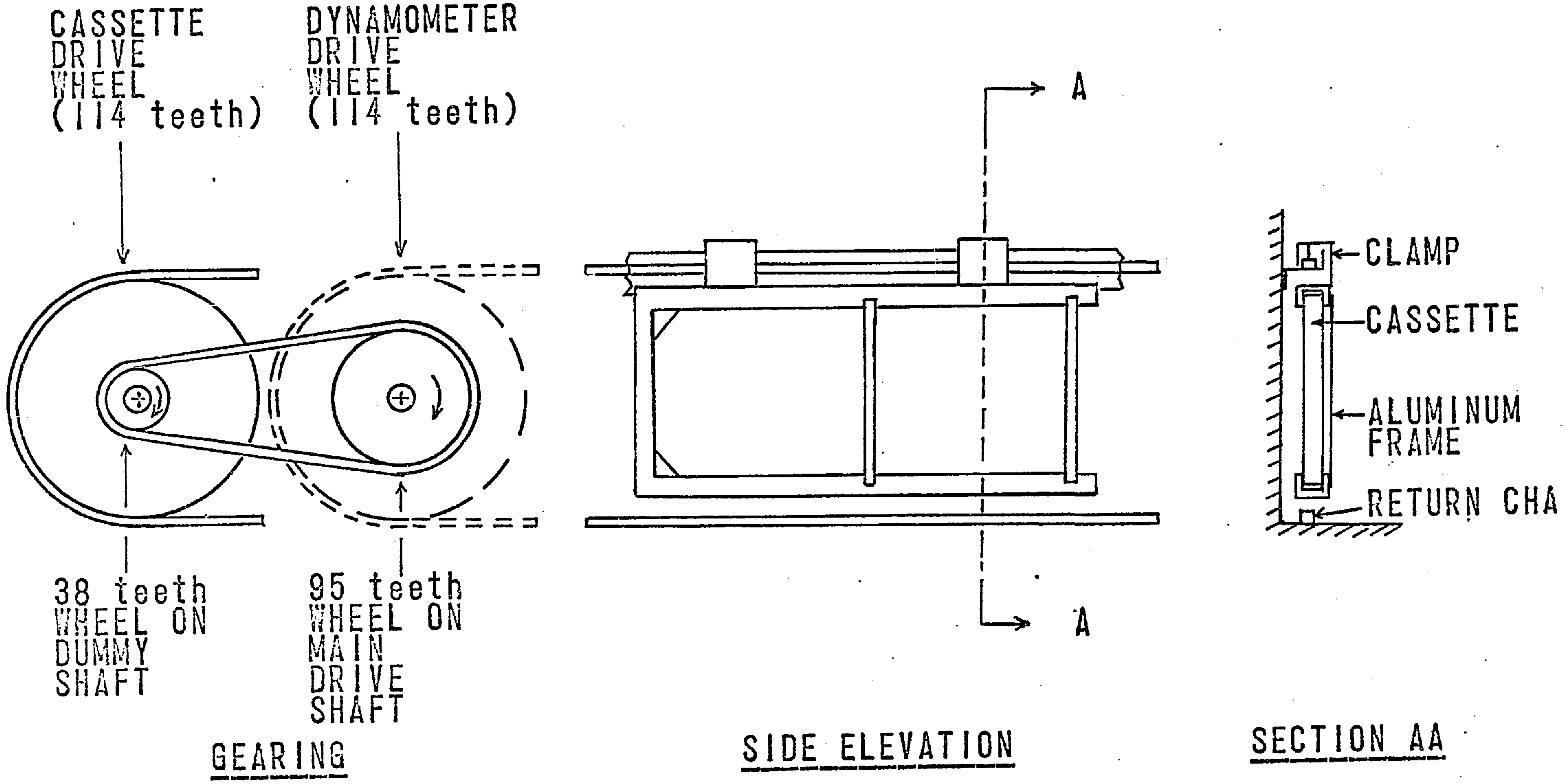

FIGURE II-2. THE MOVING CASSETTE HOLDER AND CHAIN DRIVE to a single link chain which runs on a Z rail attached to the rear of the test bed container. The gearing was chosen such that the cassette holder moves two and a half times as fast as the dynamometer carriage. Using 13 inch long cassettes, a minimum distance of 5.2 inches between pulses could be achieved so that one cassette would be out of place and a fresh cassette in position for the next x-ray pulse. This minimum distance is compatible with the pulser charging times for the carriage velocities used in the experiment. It also allowed some overlap between shots. To accomodate the moving cassette holder a plywood trough 18 inches deep and 6 inches wide was constructed along the entire length of the test bin. The return portion of the endless link chain was supported on the bottom of the trough.

An aluminum plate with a lead reference marker coinciding with the optical centre of the x-ray beam and four other reference markers was inserted behind the test bed in line with the pulser. These markers are used to correlate the information from the five radiographs. Lead screening 1/8 inch thick was affixed to the rest of the far side of the test bed container to shield the moving cassetts from x-radiation when they are not in position for their own particular pulse.

The delay time from triggering to firing is in the order of 10^{-6} seconds, while the duration of the x-ray flash is 10^{-7} seconds. Since this is very much faster than the loading time of the wheel, all motions within the soil may be considered as "stationary" for the instant of the flash. For the same reason the moving cassette holder can also be considered to be "stationary" for the duration of the pulse.

Information collected from the previous work on sand was utilized (See Yong et al (1967)). A S.F.D. of 16.5 inches was maintained for all testing. The use of tracer objects made of 94% lead and 6% antimony was continued. Kodak Royal Blue Medical Film, Du Pont Calcium Tungstate intensifying screens and General Electrix Supermix Chemicals were used with development times for the two penetrations varied to achieve best radiograph quality.

<u>Preselection of Wheel Position for Pulsing, Superposition and Overlap</u>

If the wheel loading of the soil achieves a steady state condition and the soil medium is homogeneous, one tracer-object will describe the same material path, or considering the deformation in spatial co-ordinates, a particle will occupy the same position in the flow path as another particle placed at the same depth initially. If seven tracer-objects are placed in each row, it can then be assumed that 35 image locations are obtained along the material path or flow path. To check this principle of superposition, the wheel positions when the intermediate radiographs are taken should be chosen so that the material co-ordinates from two separate shots overlap or are close to each other. This was achieved by taking the intermediate pulses 6.1 inches ahead, exactly over, and 6.1 inches behind the optical centre of the x-ray pulser.

CLAY PREPARATION AND COMPACTION, TEST BED GEOMETRY

Clay Preparation

A pure kaolin clay with the properties listed below was used in all experiments. The clay - S 187 English Clay - was supplied through the courtesy of Domtar Ltd. The chemical analysis of the clay is shown below:-

SiO_2	47.39%
Al_2O_3	37.94
Fe_2O_3	0.36
TiO_2	0.05
MgO	0.18
CaO	0.32
K_2O	1.17
Na_2O	0.07
Loss on Ignition	13.02
	100.50

Particle Size

% Residue on 300 Mesh	less than 0.05
% Above 100 microns	0.5 max
% Below 2 microns	77.83

Consistency Limits

Liquid Limit	=	54.5%
Plastic Limit	=	37.5%

The preparation and compaction of the large quantities of clay required for the study presents several problems. A moisture content just below the liquid limit was decided upon since reasonable deformations were obtained by the passage of the lightest wheel; also the unconfined compression strength of the compacted clay was sensibly constant in the range of 52% - 56%.

The dry powdered clay was spread out in a thin layer in a large aluminum lined box with a capacity of 500 lb. of wet clay. Sufficient water was sprinkled to achieve the necessary water content. Another thin layer of clay was spread above the wet layer and the process was repeated. The clay was left to equilibrate in the covered box for about a week. It was then removed and placed in 50 lb. polythene bags where it was allowed to equilibrate for another three or four days. The above procedure resulted in a mixture with very uniform moisture conditions in the range of 53.5% $\pm$ 1%.

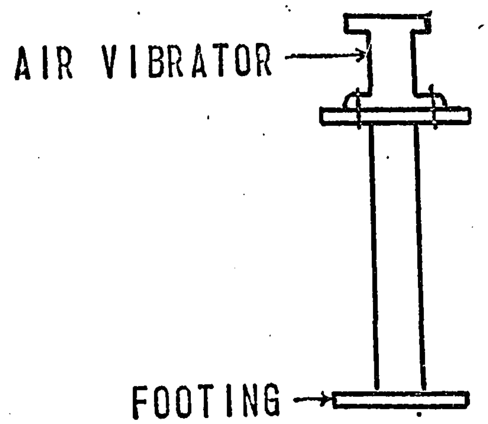

FIGURE II-3a. SOIL COMPACTOR

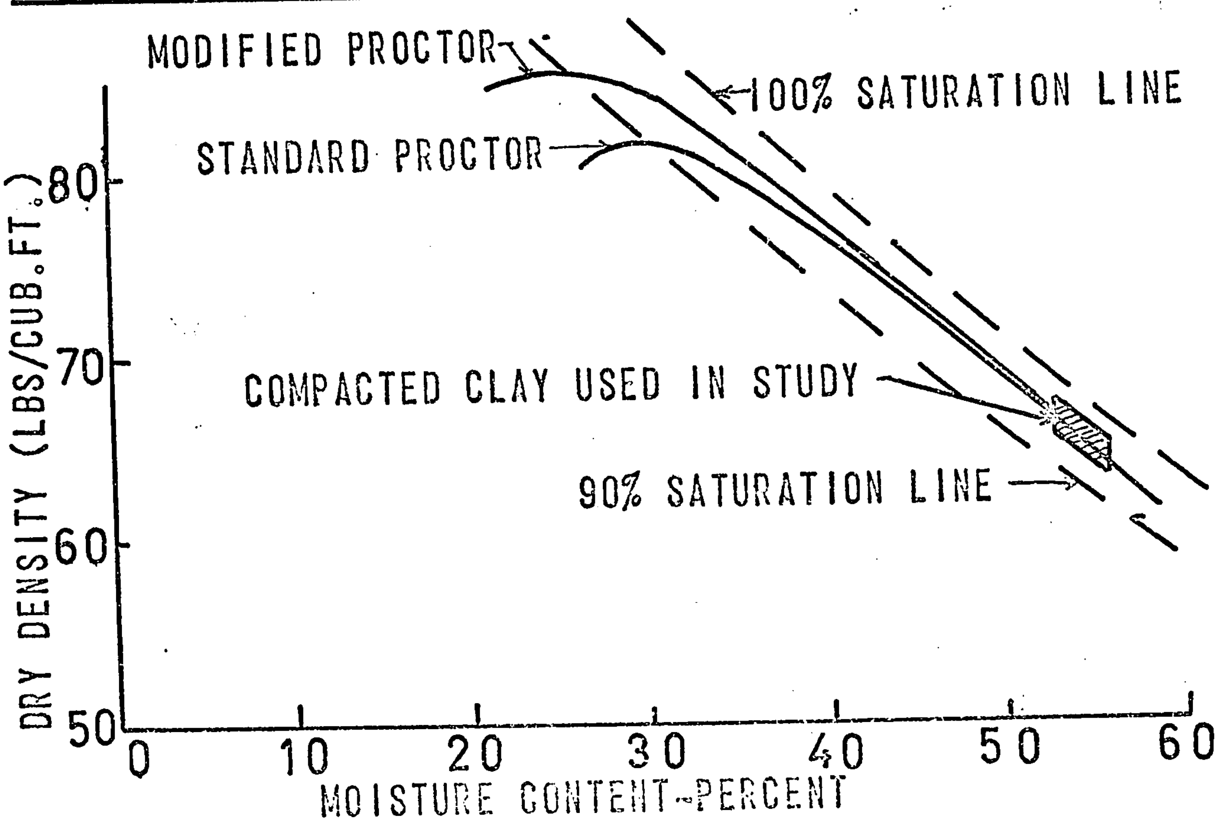

FIG. II-3b. DENSITY - MOISTURE CONTENT RANGE FOR COMPACTED SOIL

Compaction and Properties of Compacted Clay

At such a high moisture content the clay density achieved is not very dependent on input compaction energy. A small vibrator was attached to a small footing as shown in Figure II-3a. The passage of this compactor for a certain number of passes resulted in reproducible densities. The compaction can be described as vibratory kneading and the degree of saturation is limited to about 96% by the presence of entrapped air between the saturated clay matrix. Figure II-3b shows the range of densities and moisture content. Unconfined compression tests gave a strength of 1.65 lb/in while shear tests give a yield strength of 1.0 lb/in.

Test Bed Geometry

Since the x-ray beam geometry of 30 degrees along with the 16.5 inch S.F.D. restricts the area that can be radiographed to approximately 7 inches by 7 inches, the test section must be long enough to ensure that steady state loading pattern is achieved before the wheel passes over the section in front of the pulser, and that there should be no end restraints after passage. The test bed container shown in Figure II-4 has a total length of 8 feet and is 7 inches wide. The two 1 foot end sections were 6 inches deep and the central 6 foot section was 2 feet deep. The side walls of the test bed are 1/4 inch

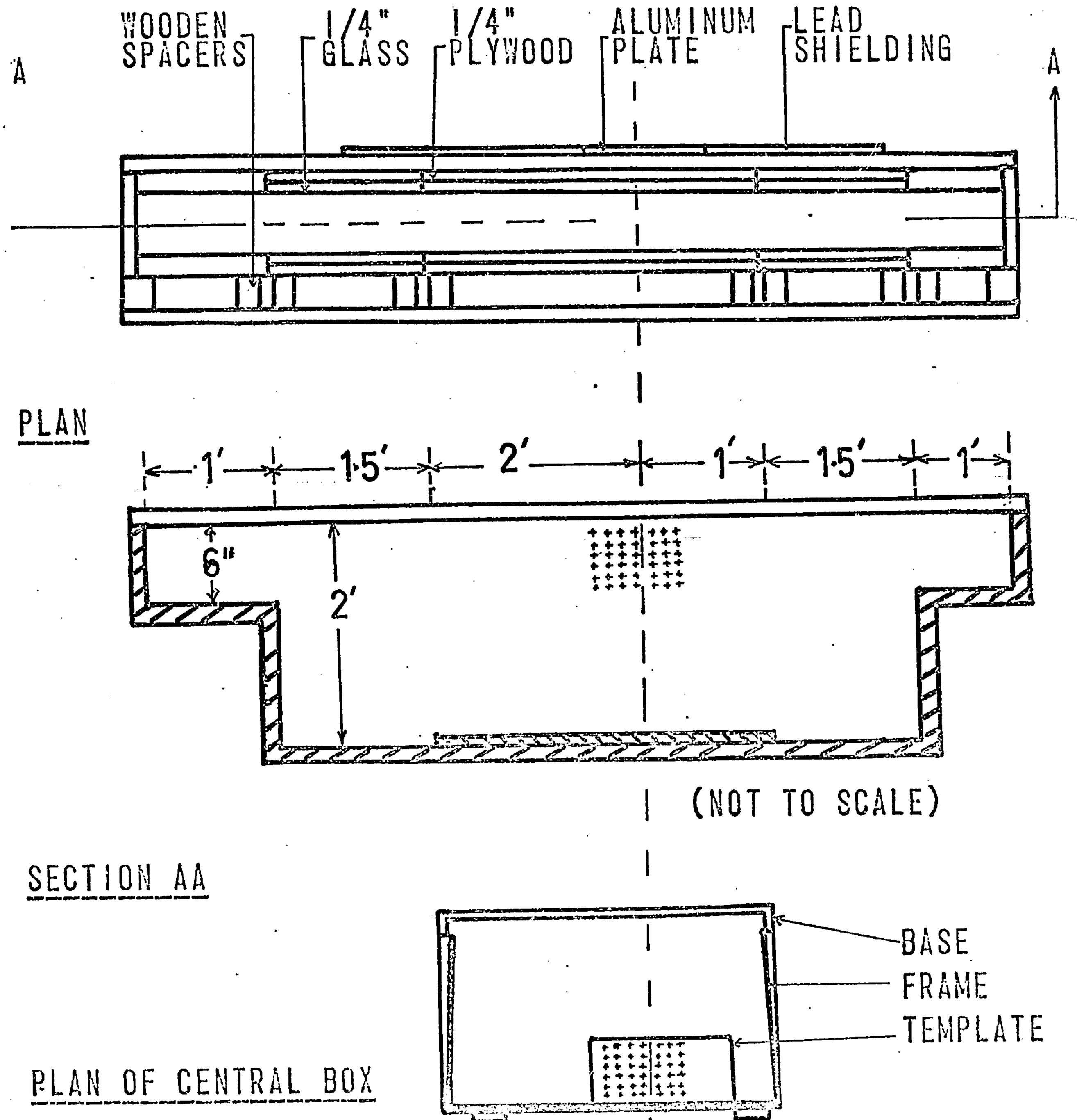

FIGURE II-4. SOIL TEST BED CONTAINER

thick plate glass on a plywood backing. The width of the test section is altered by means of wooden spacers placed behind the front of the test section.

The 3 foot portion of the test section in front of the pulser was designed so that it could be lifted out and compacted flat since preliminary tests had shown that vertical in place compaction caused some layering due to contamination of the edges with the vaseline used to reduce friction at the side walls. Figure II-4 also shows the construction of this section. The top glass side is removed and a three sided rectangular metal frame is filled on the greased bottom glass plate. The clay was compacted in 1 inch finished layers. The matrix of lead markers could be installed in one operation when the levelled depth of the clay was one half the test width. After filling the box, it was levelled with a soil trimmer. The top of the box was clamped and hoisted into place. The metal frame was then removed and the very small gaps left at the ends were filled by vertical compaction. The surface was then levelled by removing the top 1/2 inch with a soil cutter.

Although the test section width was slightly larger than the wheel width, it was observed that the entire width of the soil was deformed. This proved that the vaseline had reduced wall friction to a negligible value.

One of the biggest problems in vehicle-mechanics research on clays is the variability of moisture content at the surface. In large scale testing on clay bins, the soil surface must be covered or sprinkling usually results in an oversoaked soil surface. Since the markers had to be replaced at the end of each test the entire central test section was renewed after each test. Compaction and testing was completed in under 3 hours and therefore excessive drying out of the soil surface was never a problem.

TEST WHEELS AND SYSTEM PARAMETERS

The two wheels used in the previous study on sand were maintained for this series of tests on clay. The dimensions of the small wheel - referred to as the model wheel - are 9.0 inches diameter and 2.5 inches wide, while the larger wheel - hereafter called the prototype - has a diameter of 13.5 inches and a width of 3.75 inches. The geometric scaling ratio λ of the two wheels can be expressed as:-

$$\lambda = \frac{\text{Diameter P}}{\text{Diameter M}} = \frac{\text{Width P}}{\text{Width M}} = \frac{13.5}{9} = \frac{3.75}{2.5} = 1.50$$

The wheels which were made from aluminum were supplied by the De Havilland Company of Canada.

The system parameters which can be varied are load W, wheel radius r, carriage velocity V_c, angular velocity ω, the wheel surface texture and the soil properties. The angular velocity and the carriage velocity in turn define the normal slip.

The same wheel surface texture, i.e. finished aluminum was maintained for all tests. For wheels on clay maintained at the same moisture content and density, the maximum frictional stress is not expected to be affected significantly by the degree of roughness of the wheel surface, the reason being that slipping at some limiting value of the frictional stress can take place either on the surface of contact or on a parallel surface with a thin layer of the soil close to the surface, the thickness of which in the case of a rough surface will be greater than the "friction hills" on the surface. The above points out the fact that in testing of clay soils it is most important that the surface and near surface conditions of the soil should be rigidly controlled if representative results are to be obtained.

Yong et al (1967) postulated that the effects of carriage velocity on soil vehicle interaction at small speeds used in laboratory testing is probably accomodated in the normal slip rate. In the main series of tests it was decided to maintain the carriage velocity at the same value (approximately 5.6 inches per second) while the angular velocity and the resulting torque were varied to cover the slip range from the towed point to about 80% normal slip rate. Supplementary tests performed to try to evaluate speed effects.

The testing schedule adopted is shown in Table II-2.

TABLE II-2

Wheel	Weight	Velocity	Normal Slip	No. of Tests
Model	W_1	V	Towed point to 73%	11
Prototype	$\lambda^2 W_1$	V	Towed point to 78%	10
Prototype	$\lambda^3 W_1$	V	S_1, S_2, S_3, S_4	4
Prototype	λW_1	V	S_1, S_2	2
Prototype	$2\lambda W_1$	V	S_1, S_2	3
Prototype	$\lambda^2 W_1$	λV	S_1	1
Prototype	$\lambda 2 W_1$	$\sqrt{\lambda} V$	S_1	1
Prototype	$\lambda^2 W_1$	$1\sqrt{\lambda} V$	S_1	1
Prototype	$\lambda^2 W_1$	$\frac{1}{\lambda} V$	S_1	1

A few tests were performed on the model wheel, W_2 = 40 lbs. Because of experimental limitations a large portion of the deforming soil could not be included in the radiographs.

The loading for the model wheel of 40 lbs. (W_2) and 23.5 lbs. (W_1) produced deformations which were large enough to be statistically resolved using the cine-radiographic technique. A prototype wheel load of 51 lbs. (W_3) equal to $\lambda^2 W_1$ was chosen for series C. The λ^2 scaling assumes that equal pressures will be exerted on the soil in both systems. This is similar to the assumption that contact pressure is purely radial and equal to the normal pressure beneath a plate at the same depth. Prototype wheel load of 79 lbs. (W_4) assumes a $\lambda^3 W_1$ scaling of forces. This is in agreement with the classical Froude Number $Fr = \frac{V^2}{gl}$, if equal densities are maintained. Supplementary tests were done with loads of 34 lbs., λW_1 and 68 lbs. $2\lambda W_1$.

APPENDIX III

TEST TECHNIQUE AND DATA REDUCTION

Measurement of Soil Response

Figure III-1 shows a schematic diagram of the pulser, test section with marker matrix and the moving cassette holder. Also shown are the wheel positions relative to the undisturbed tracer object matrix when the five shots are taken.

After preparation of the test section, the initial positions of the tracer objects are obtained by firing the first x-ray pulse, with the wheel lying on a metal plate about 6 feet away from the centre line of the pulser. This plate acts as a zero reference point for the sinkage measurement.

Using a voltmeter wired in parallel to the angular velocity tachometer, a voltage versus angular velocity relation was obtained. Since the carriage velocity is known, an approximate slip rate could be determined. The wheel is then passed over the test bed at a predetermined slip range. The spring loaded arm on the dynamometer carriage activates the three limit switches which in turn trigger three consecutive x-ray pulses. The limit switches are placed such that the centre line of the wheel is 6.1 inches before, exactly over and 6.1 inches

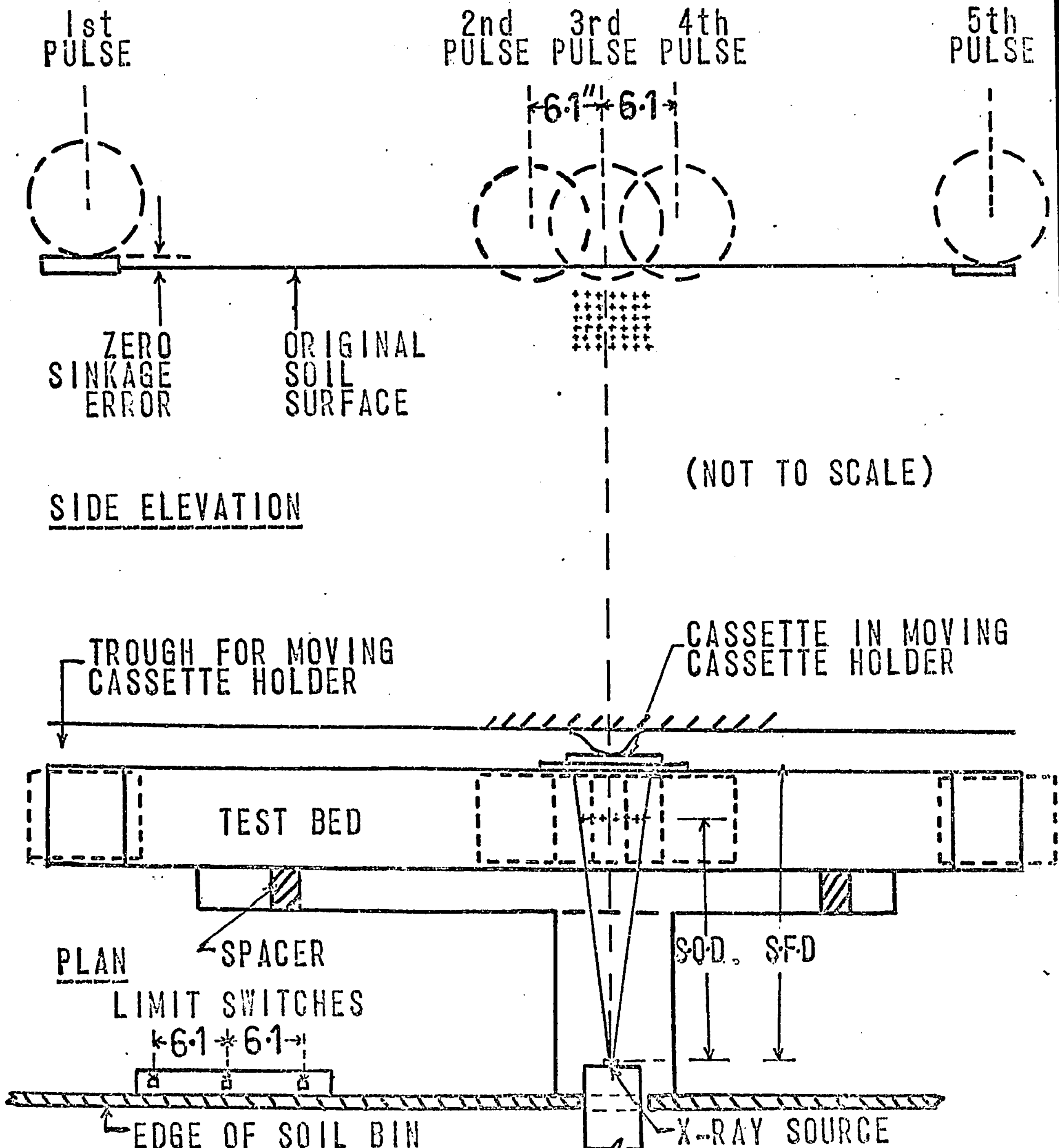

FIG. III-1. THE WHEEL-SOURCE-TRACER-OBJECT-FILM GEOMETRY.

beyond the optical centre of the x-ray beam.

The test is halted with the wheel resting on a wooden plate four feet past the centre line of the pulser. A fifth shot of the final marker position is then taken.

From the U. V. recorder, traces of the following are obtained:-

Torque
Carriage Velocity
Angular Velocity
Sinkage
Drawbar Pull

TEST DATA REDUCTION

System Parameters

A computer programme PARAM listed at the end of this appendix was used to convert the U. V. recorder readings back to the following vehicle parameters, namely:-

Carriage Velocity
Angular Velocity
Normal Slip Rate
Torque
Drawbar Pull
Sinkage and Rut

The following were also included in the computer output, namely:-

Test date and number

Average soil moisture content

Wheel radius, width and axle load.

Transfer of Radiographic Data

A typical radiograph obtained from the third x-ray pulse is shown in Figure III-2. The optical centre marker, other reference makers and wheel rim are visible.

A light table was used to transfer the images on the five radiographs from each test onto a translucent "Matex" acetate sheet. The optical centre marker and the other reference markers that appear on each radiograph were used for alignment. These tracer object images and the optical centre marker image were transfered from the acetate sheet to a sheet of graph paper positioned so that the grid lines coincided with the marker matrix rows.

A data reduction technique developed by Mr. J. L. Vrooman of the Mechanical Engineering Dept.; McGill University was then used. The graph paper was fixed in position on a X-Y plotter and the carriage needle moved manually, by adjusting two heliopotentiometers, to each image location. The voltages corresponding to the horizontal and vertical coordinates of each location are then recorded on a printer by a Dymec 2010B Automatic Scanning Digital Voltmeter. A typical print-out for the five radiographic images of the tracer-object is shown

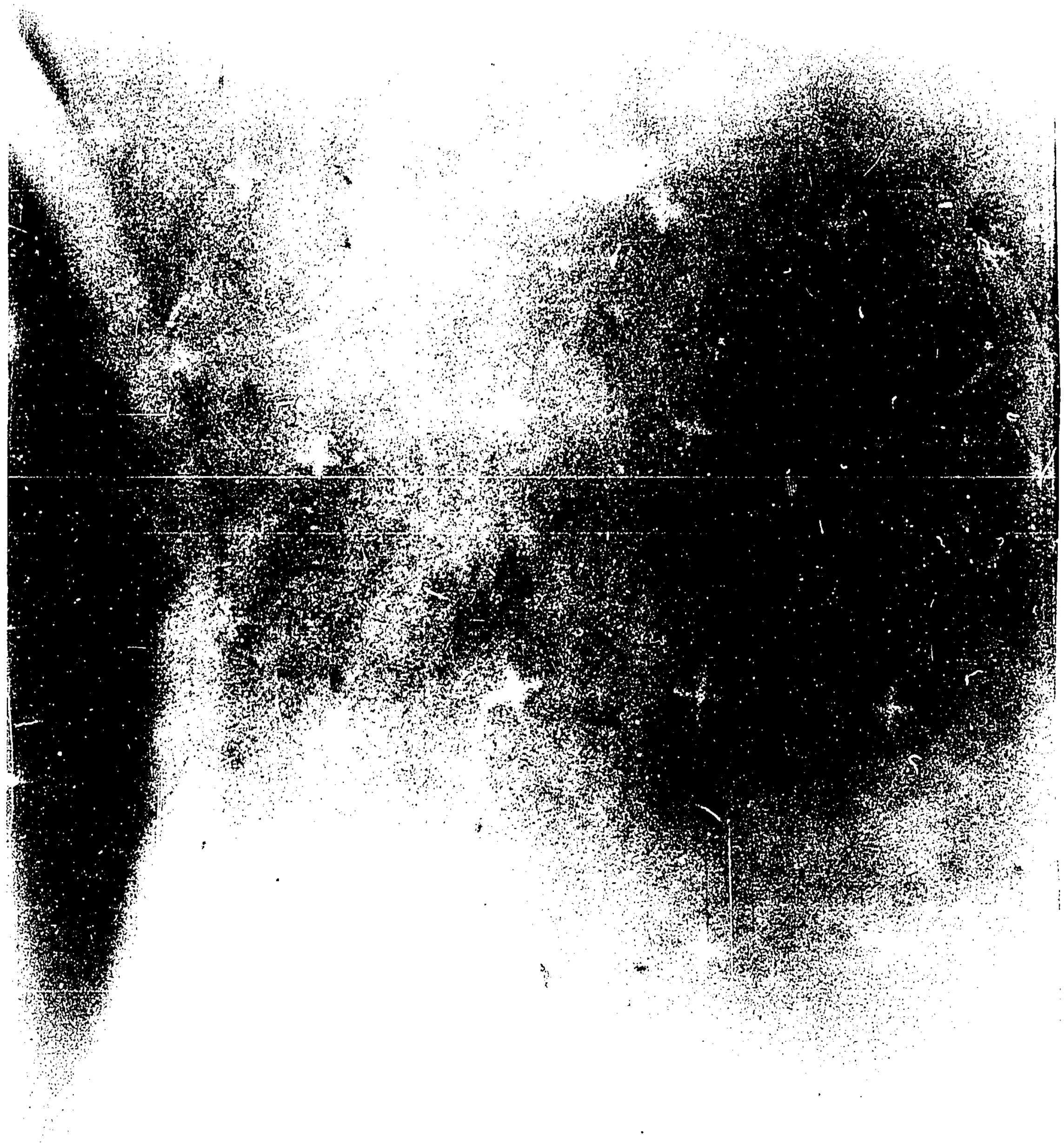

below:-

	25	+ 0 0 4 1 6 3 3	Image from fifth pulse
	24	+ 0 0 1 5 1 2 3	
		T 0 9 4 4 5 6	
	25	+ 0 0 4 1 3 0 3	Image from fourth pulse
	24	+ 0 0 1 4 7 1 3	
		T 0 9 4 4 5 1	
Paper	25	+ 0 0 3 9 2 6 3	Image from third pulse
feed	24	+ 0 0 1 5 8 7 3	
direction ↓		T 0 9 4 4 4 5	
	25	+ 0 0 4 2 2 6 3	Image from second pulse
	24	+ 0 0 2 0 8 0 3	
		T 0 9 4 4 3 8	
	25	+ 0 0 4 3 1 6 3	Image from first pulse
	24	+ 0 0 1 8 9 6 3	
		T 0 9 4 4 2 9	

where T is a time record in hours, minutes and seconds

24 is a channel number referring to X co-ordinate voltage

25 is a channel number referring to Y co-ordinate voltage

Digit 3 in last column in each voltage record is the negative exponent of D.V.M. value.

The voltages are then punched manually onto I. B. M. cards, one card for each tracer object. The card for the above reads as follows:-

4011	1896	4316	2080	4226	1587	3926	1471	4130	1512	4163
Object Identi-fication Code	X	Y	X	Y	X	Y	X	Y	X	Y
	Voltage First Image		Voltage Second Image		Voltage Third Image		Voltage Fourth Image		Voltage Fifth Image	

The first two digits of identification code specify the test number.

The third digit specifies the tracer object matrix row number.

The fourth digit specifies the tracer object matrix column number.

Reduction of Radiographic Data

The computer programs were first written for the McGill I. B. M. 7044. Minor modifications were necessary to adapt these programs for use with the I. B. M. S360 which replaced the 7044.

The computer program LINDA shown at the end of the appendix was used with the punched D. V. M. values. The following operations performed in this program, namely:-

a) The integral values of the voltage records are divided by 1,000, accounting for negative

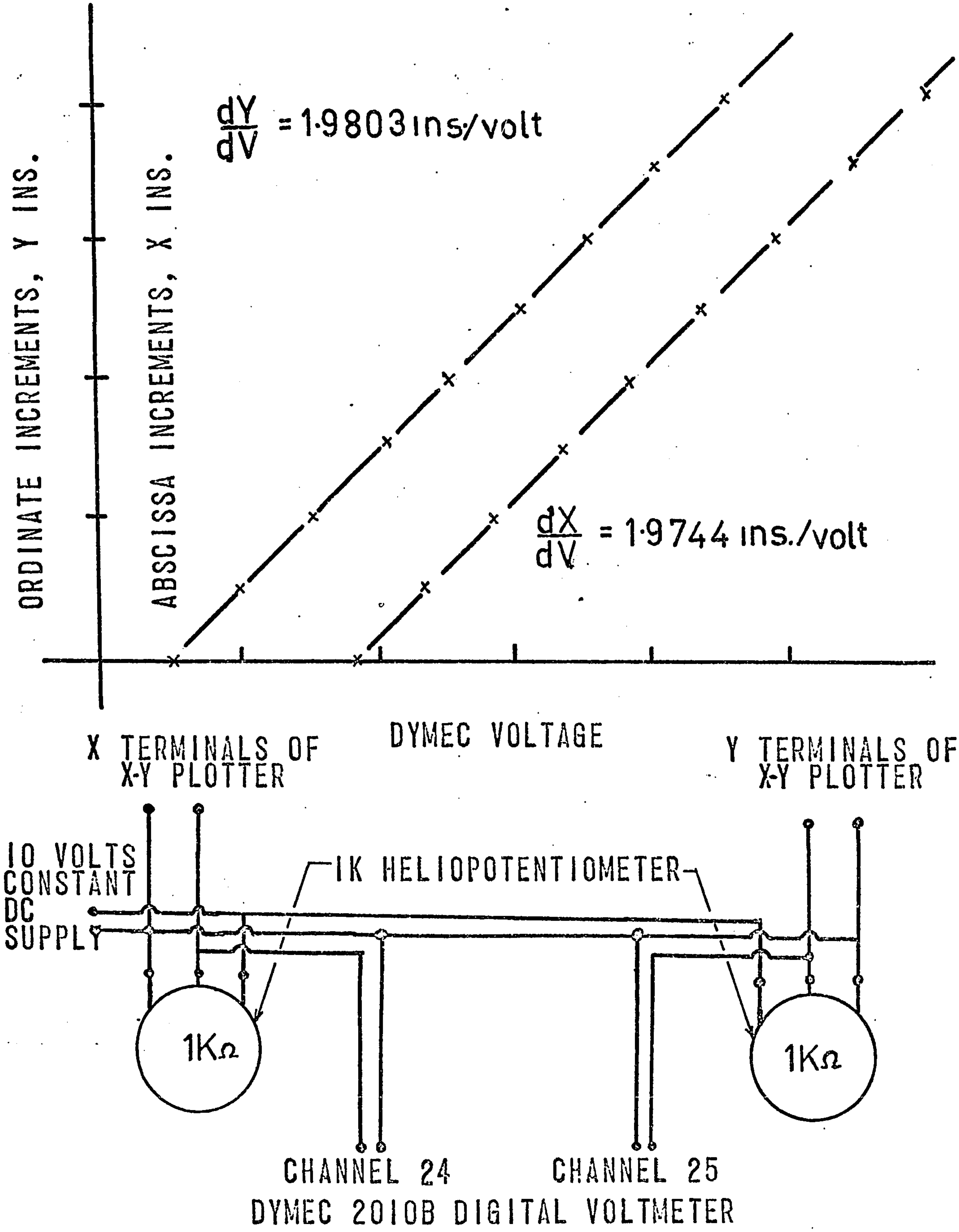

FIG. III-3. CALIBRATION AND CIRCUIT DIAGRAM OF X-Y PLOTTER exponent of 3 in the D. V. M. output and are then converted to co-ordinate values of the images in the plane of the film by means of the voltage-displacement calibrations of the X-Y plotter. The Calibration of the X-Y plotter was performed as follows:-

The system is allowed to warm up for half-an-hour in order to stabilize. A one inch orthogonal grid is placed on the X-Y plotter, the bridge needle placed on a given ordinate and one inch abscissal increments are recorded by the Dymec 2010B Digital Voltmeter. The heliopotentiameter controlling the ordinate value was left untouched in this first phase. An analogous procedure was carried out to obtain the ordinate calibration. It was necessary to calibrate the X-Y plotter for each test to accommodate slight variations in the D. C. supply voltage. The electric circuit diagram and sample calibration curves for a typical test, (Test 40) are shown in Figure III-3.

b) The optical centre of the x-ray beam takes on the co-ordinates (0,0). The co-ordinates of all other points are expressed with respect to the optical centre by using appropriate parallax correction described below. Figure III-4 shows how this correction is obtained. The optical correction $D = \frac{Z_1}{Z_2}$ where Z_1, is the S.O.D. and Z_2, is the S.F.D. The S.F.D. is slightly smaller for the initial and final shots which are taken on two stationary cassettes placed snugly against the rear of the test section. This is accounted for by using the appropriate C values.

The computer output is printed and also punched on I. B. M. cards.

These I. B. M. cards with the co-ordinates given with respect to the optical centre are used with the program JANE listed at the end of this appendix and the following operations are performed:-

i) The material co-ordinates of each object in each row is defined by assigning the value (0,0) to its initial position. The co-ordinates of the other four positions are then expressed with respect to its initial position.

ii) Estimates of the density of the soil contained by four neighbouring tracer objects were obtained.

iii) Velocity computations described in Chapter 4.

Reliability of Computed Results

Initial and Final Tracer-Object Positions

The output of program LINDA shows the co-ordinates

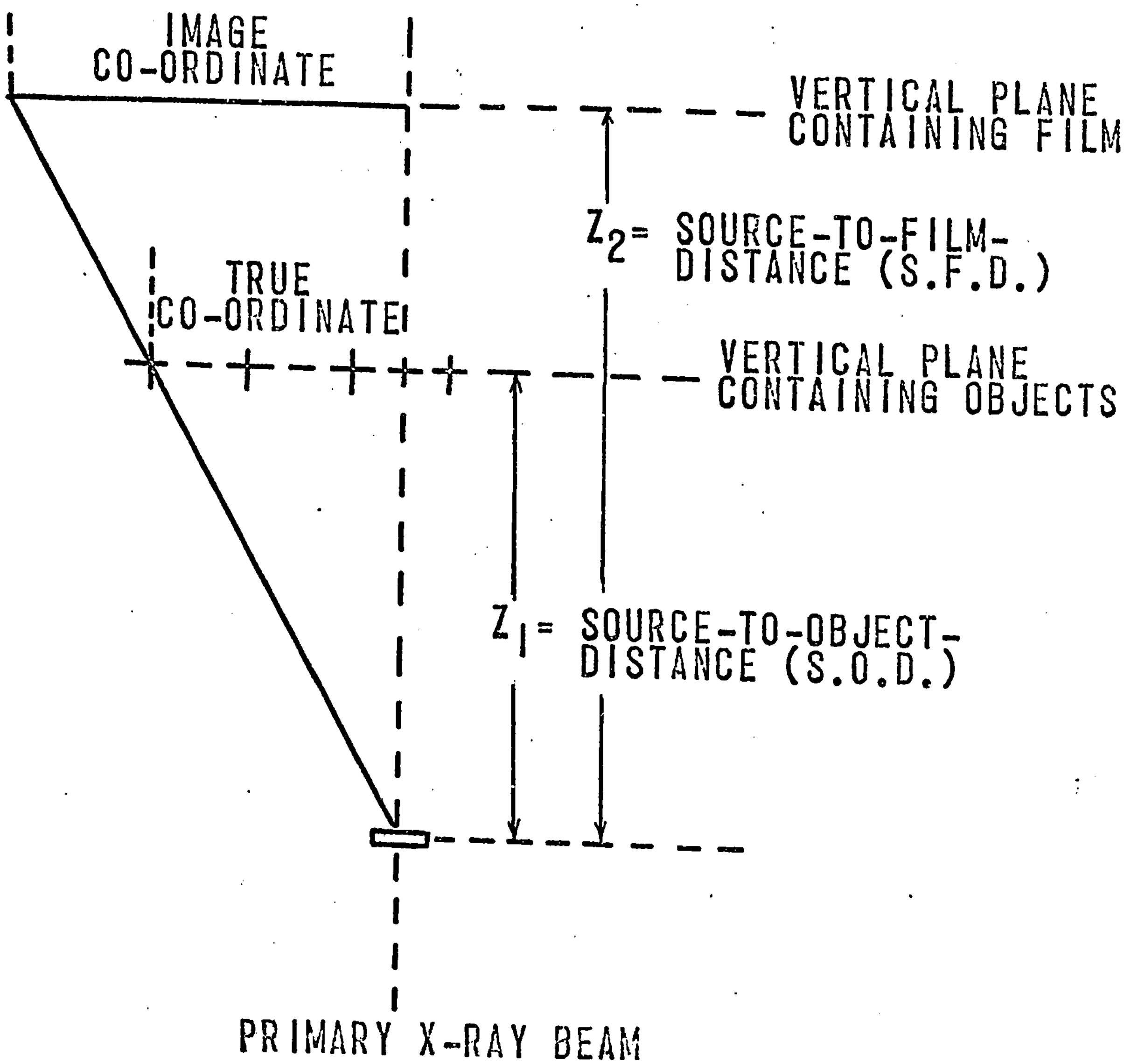

$$\frac{\text{TRUE CO-ORDINATE}}{\text{IMAGE CO-ORDINATE}} = \frac{Z_1}{Z_2} = \text{OPTICAL CORRECTION FACTOR, C.}$$

FIGURE III-4. OPTICAL CORRECTION GEOMETRY USED IN DATA REDUCTION with respect to the optical centre. From a mean depth for each row, a population variance $\hat{\sigma}_i^2$, can be obtained. The principle of supperposition can be applied if the objects are in line and therefore an estimate of the population variance $\hat{\sigma}_f^2$ of the final object positions will include errors which are caused by slight deviation from the initial assumption. The F test, Wallis and Roberts (1956) can be used to compare $\hat{\sigma}_f^2$ with $\hat{\sigma}_i^2$. Results and calculations for a typical test (Test 40), are shown in Table III-1.

The standard deviation calculated from the final object positions will reflect small errors due to the following causes:-

(1) Transferring from radiographs to "Matex" sheet.

(2) Placing needle of X-Y plotter on image points.

(3) Small differences in stressing history due to small differences in the initial depth of tracer objects.

INITIAL DEPTHS	FINAL DEPTHS
2.021	1.777
2.020	1.810
2.060	1.798
2.004	1.700
2.025	1.730
1.937	1.662
1.914	1.693

(Note: co-ordinates are relative to the optical center)

$\hat{\sigma}_i^2 = 0.00236$ $\hat{\sigma}_f^2 = 0.00343$

F statistic $= \hat{\sigma}_f^2/\hat{\sigma}_i^2 = 1.46$

F statistic at 95% confidence level with (6,6) degrees of freedom.......= 4.3

i.e. At 95% confidence level $\hat{\sigma}_f^2$ is small enough to justify superposition.

TABLE III-1. VERIFICATION OF ASSUMPTION OF SUPERPOSITION FOR TOP ROW OF OBJECTS: TEST 40

```
//PARAM        JOB   (F125,000,002,050,000,01),'WEBB                    JOB  13
//S361    EXEC    FORTRAN
//FORT.SYSIN    DD    *
```

```
0001          DIMENSION P(9)
0002          DO 8  M=1,42
0003          READ 1,P(3),P(1),P(2),(P(J),J=6,9),A,B,C,D,E,F,N
0004          IF(N.LT.20) GO TO 13
0005          P(4)=6.75
0006          P(5)=3.75
0007          GO TO 15
0008       13 P(4)=4.5
0009          P(5)=2.5
0010       15 B=0.1391+4.697*B
0011          IF(N.LE.4) GO TO 4
0012          IF(N.GE.14) GO TO 4
0013          A=A/1.93
0014        4 A=0.0051+0.3142*A+0.0061*A**2
0015          C=-0.1059+5.2948*C
0016          D=0.0957+1.8524*D
0017          E=0.0279+0.3083*E+0.00468*E**2+P(8)
0018          IF(N.GE.21) GO TO 14
0019          F=6.6093+28.757*F-0.6796*F**2
0020          GO TO 12
0021       14 F=9.381+49.693*F
0022       12 PULL=C+D
0023          SLIP=(1.0-B/(A*6.2832*P(4)))*100.0
0024          PRINT 2,(P(J),J=1,6),C,D
0025        8 PRINT 3,P(9),A,E,PULL,B,P(7),F,SLIP
0026          STOP
0027        1 FORMAT(A2,A6,A3,10F6.2,I3)
0028        2 FORMAT(1H1,10X,24HRIGID WHEEL TEST ON CLAY,10X,9HTEST DATE,2X,A4,A
           13,10X,11HTEST NUMBER,2X,A2//11X,10HWHEEL DATA,10X,6HRADIUS,F6.2,5H
           2 INS.,5X,5HWIDTH,F6.2,5H INS.//11X,9HSOIL DATA,11X,24HAVERAGE MOIS
           3TURE CONTENT,F8.1,4H 0/0//11X,13HDRAWBAR PULLS,7X,4HLEFT,F8.2,5H L
           4BS.,5X,5HRIGHT,F6.2,5H LBS.)
0029        3 FORMAT(1H-,10X,5HLOAD  F21.2,8H LBS.    ,5X,17HANGULAR VELOCITY ,F9
           1.2,11H REVS./SEC.//11X,11HSINKAGE     ,F15.2,5H INS.,8X,5HPULL ,F21
           2.2,6H LBS. //11X,17HCARRAIGE VELOCITY,F9.2,11H INS./SEC. ,2X,12HDE
           3PTH OF RUT,F14.2,5H INS.//11X,6HTORQUE,F20.2,8H IN.LBS.,5X,17HNORM
           4AL SLIP RATE ,F9.2,4H 0/0)
0030          END
```

TOTAL MEMORY REQUIREMENTS 000678 BYTES

RIGID WHEEL TEST ON CLAY TEST DATE .SEP.67 TEST NUMBER 46

WHEEL DATA	RADIUS 6.75 INS.	WIDTH 3.75 INS.	
SOIL DATA	AVERAGE MOISTURE CONTENT	54.0 0/0	
DRAWBAR PULLS	LEFT -8.10 LBS.	RIGHT -9.33 LBS.	
LOAD	79.00 LBS.	ANGULAR VELOCITY	0.17 REVS./SEC.
SINKAGE	1.18 INS.	PULL	-17.43 LBS.
CARRAIGE VELOCITY	5.68 INS./SEC.	DEPTH OF RUT	0.0 INS.
TORQUE	244.93 IN.LBS.	NORMAL SLIP RATE	19.75 0/0

161

```
//LI...     J...  (...,...,...,...),'W...            J...  55
//S360  EXEC  FORTRAN
//FORT.SYSIN  DD  *
```

```
0001            DIMENSION I(7,7,10),J(10),X(7,7,5),Y(7,7,5),C(5)
0002            READ 6,J4,KX,KY,NN,A,B,(C(M),M=1,5)
0003            PUNCH 5,J4,NN
0004            PRINT 7,J4,KX,KY
0005            DO 200 K=1,7
0006            DO 200 L=1,7
0007            DO 200 M=1,10
0008        200 I(K,L,M)=0
0009            DO 201 N=1,NN
0010            READ 8,J4,K,L,(J(M),M=1,10)
0011            DO 201 M=1,10
0012        201 I(K,L,M)=J(M)
0013            DO 202 K=1,6
0014            DO 203 L=1,7
0015            IF(I(K,L,1).EQ.0) GO TO 203
0016            PRINT 9,J4,K,L,(I(K,L,M),M=1,10)
0017        203 CONTINUE
0018        202 PRINT 10
0019            Z=KX
0020            PX=A*Z/1000.0
0021            Z=KY
0022            PY=B*Z/1000.0
0023            PRINT 12,J4
0024            DO 104 K=1,6
0025            DO 105 L=1,7
0026            IF(I(K,L,1).EQ.0) GO TO 105
0027            DO 103 MM=1,9,2
0028            Z=I(K,L,MM)
0029            M=(MM+1)/2
0030            X(K,L,M)=(A*Z/1000.0-PX)*C(M)
0031            IF(I(K,L,MM).EQ.0) X(K,L,M)=0.0
0032        103 CONTINUE
0033            DO 102 MM=2,10,2
0034            Z=I(K,L,MM)
0035            M=MM/2
0036            Y(K,L,M)=(B*Z/1000.0-PY)*C(M)
0037            IF(I(K,L,MM).EQ.0) Y(K,L,M)=0.0
0038        102 CONTINUE
0039            PRINT 13,K,L,(X(K,L,M),Y(K,L,M),M=1,5)
0040            PUNCH 14,J4,K,L,(X(K,L,M),Y(K,L,M),M=1,5)
0041        105 CONTINUE
0042        104 PRINT 10
0043            STOP
0044          5 FORMAT(A2,I3)
0045          6 FORMAT(A2,2X,2I5,I3,7F7.4)
0046          7 FORMAT(1H1,10X,24HDIGITAL VOLTMETER OUTPUT,66X,12HTEST NUMBER ,A2/
               1/38X,5HPARAX,I8,10X,5HPARAY,I8//10X,6HOBJECT,5X,10HPOSITION 1,8X,1
               20HPOSITION 2,8X,10HPOSITION 3,8X,10HPOSITION 4,8X,10HPOSITION 5/11
               3X,4HCODE,6X,1HX,8X,1HY,8X,1HX,8X,1HY,8X,1HX,8X,1HY,8X,1HX,8X,1HY,8
               4X,1HX,8X,1HY/)
0047          8 FORMAT(A2,I1,I1,10I5)
0048          9 FORMAT(1H ,10X,A2,I1,I1,10I9)
0049         10 FORMAT(/)
0050         12 FORMAT(1H1,10X,24HCORRECTED COORDINATES   ,66X,12HTEST NUMBER ,A2/
```

```
                 1/10X,6HOBJECT,5X,10HPOSITION 1,8X,10HPOSITION 2,8X,10HPOSITION 3,8
                 2X,10HPOSITION 4,8X,10HPOSITION 5/               11X,4HCODE,5X,1HX,8
                 3X,1HY,5X,1HX,8X,1HY,8X,1HX,8X,1HY,8X,1HX,8X,1HY,8X,1HX,8X,1HY/)
0051          13 FORMAT(1H ,1_X,I1,I1,1X,10F9.3)
0052          14 FORMAT(A2,I1,I1,10F7.3)
0053             END

TOTAL MEMORY REQUIREMENTS 00190C4 BYTES
```

TEST NUMBER 40

DIGITAL VOLTMETER OUTPUT

PARAX 3731 PARAY 3052

OBJECT CODE	POSITION 1 X	POSITION 1 Y	POSITION 2 X	POSITION 2 Y	POSITION 3 X	POSITION 3 Y	POSITION 4 X	POSITION 4 Y	POSITION 5 X	POSITION 5 Y
4011	1896	4316	2080	4226	1587	3926	1471	4130	1512	4163
4012	2486	4315	2665	4437	2218	3841	2094	4142	2109	4184
4013	3111	4340	3309	4495	2934	3714	2723	4146	3414	4176
4014	3786	4305	4022	4478	3816	3588	3469	4062	3992	4115
4015	4378	4318	4623	4468	4493	3667	4071	4046	4588	4134
4016	4981	4263	5223	4409	5208	3826	4697	3971	5265	4071
4017	5606	4249	5898	4381	5928	4163	5413	3944		4098
4021	1535	3789	1808	3563	1281	3467	1202	3632	1253	3664
4022	2084	3778	2369	3763	1851	3365	1767	3588	1794	3625
4023	2700	3763	2951	3882	2538	3251	2428	3579	2414	3618
4024	3453	3753	3676	3892	3431	3175	3217	3544	3188	3608
4025	4032	3740	4265	3894	4164	3162	3829	3500	3772	3503
4026	4607	3826	4818	3968	4855	3337	4412	3574	4332	3632
4027	5250	3864	5461	3999	5593	3601	5094	3554	4979	3713
4031	1595	3116	1878	2960	1432	2790	1402	2954	1430	3034
4032	2231	3072	2524	3061	2106	2696	2062	2911	2079	2977
4033	2864	3080	3121	3130	2820	2621	2705	2891	2705	2969
4034	3477	3131	3721	3219	3530	2658	3336	2926	3319	3023
4035	4049	3132	4248	3248	4215	2684	3920	2916	3888	3026
4036	4617	3176	4806	3279	4931	2801	4520	2937	4456	3058
4037	5224	3234	5419	3311	5599	3016	5124	2952	5037	3110
4041	1612	2494	1862	2362	1543	2184	1486	2324	1516	2411
4042	2226	2481	2482	2427	2198	2120	2122	2311	2131	2392
4043	2878	2469	3131	2484	2921	2096	2790	2285	2781	2384
4044	3503	2503	3708	2542	3622	2125	3411	2288	3396	2407
4045	4081	2491	4282	2554	4294	2151	4019	2266	3974	2394
4046	4602	2509	4773	2578	4913	2217	4547	2292	4512	2422
4047	5215	2535	5391	2591	5572	2330	5180	2255	5110	2422
4051	1639	1926	1852	1804	1605	1646	1538	1749	1563	1824
4052	2257	1963	2485	1911	2267	1655	2165	1795	2200	1375
4053	2901	1947	3114	1933	2979	1617	2832	1774	2826	1372
4054	3497	1954	3709	1970	3653	1650	3449	1780	3436	1376
4055	4056	1959	4253	1976	4287	1695	4035	1761	4000	1372
4056	4614	1950	4782	1980	4911	1724	4592	1741	4546	1362
4057	5211	1921	5366	1964	5545	1771	5204	1687	5148	1837
4061	1745	1444	1932	1346	1748	1175	1680	1285	1684	1363
4062	2258	1397	2466	1330	2306	1122	2206	1278	2196	1319
4063	2906	1437	3105	1406	3006	1170	2869	1259	2849	1337
4064	3548	1435	3721	1418	3710	1168	3511	1253	3489	1347
4065	4080	1413	4248	1414	4308	1178	4084	1232	4048	1329
4066	4665	1416	4812	1416	4925	1211	4665	1211	4612	1333
4067	5267	1404	5399	1428	5552	1258	5278	1172	5212	1303

164

CORRECTED COORDINATES TEST NUMBER 40

OBJECT CODE	POSITION 1 X	POSITION 1 Y	POSITION 2 X	POSITION 2 Y	POSITION 3 X	POSITION 3 Y	POSITION 4 X	POSITION 4 Y	POSITION 5 X	POSITION 5 Y
11	-2.943	2.021	-2.583	1.831	-3.354	1.363	-3.536	1.681	-3.559	1.777
12	-1.997	2.020	-1.668	2.150	-2.367	1.231	-2.561	1.700	-2.602	1.810
13	-0.995	2.060	-0.660	2.251	-1.247	1.033	-1.577	1.706	-1.655	1.799
14	0.088	2.004	0.455	2.224	0.133	0.836	-0.410	1.575	-0.508	1.700
15	1.038	2.025	1.395	2.209	1.192	0.959	0.532	1.550	0.419	1.730
16	2.005	1.937	2.334	2.117	2.311	1.207	1.511	1.433	1.375	1.662
17	3.104	1.914	3.390	2.073	3.437	1.733	2.631	1.391	2.461	1.673
21	-3.522	1.179	-3.008	0.797	-3.833	0.647	-3.955	0.905	-3.975	0.979
22	-2.642	1.161	-2.131	1.109	-2.941	0.488	-3.073	0.836	-3.123	0.916
23	-1.654	1.137	-1.220	1.295	-1.866	0.310	-2.038	0.822	-2.113	0.905
24	-0.446	1.121	-0.086	1.310	-0.469	0.192	-0.804	0.767	-0.871	0.889
25	0.483	1.100	0.835	1.313	0.677	0.172	0.153	0.699	0.066	0.989
26	1.405	1.238	1.701	1.429	1.758	0.445	1.065	0.814	0.964	1.008
27	2.437	1.299	2.706	1.477	2.913	0.856	2.132	0.783	2.002	1.057
31	-3.426	0.102	-2.899	-0.143	-3.597	-0.409	-3.644	-0.153	-3.691	-0.029
32	-2.406	0.032	-1.888	0.014	-2.542	-0.555	-2.611	-0.220	-2.650	-0.120
33	-1.391	0.045	-0.954	0.122	-1.425	-0.672	-1.605	-0.251	-1.646	-0.133
34	-0.407	0.126	-0.016	0.260	-0.314	-0.615	-0.618	-0.197	-0.661	-0.046
35	0.510	0.128	0.809	0.306	0.757	-0.574	0.296	-0.212	0.252	-0.042
36	1.421	0.198	1.682	0.354	1.877	-0.392	1.234	-0.179	1.163	0.010
37	2.395	0.291	2.641	0.404	2.922	-0.056	2.179	-0.156	2.095	0.093
41	-3.399	-0.892	-2.924	-1.076	-3.423	-1.354	-3.512	-1.136	-3.553	-1.025
42	-2.414	-0.913	-1.954	-0.975	-2.398	-1.454	-2.517	-1.156	-2.566	-1.072
43	-1.368	-0.932	-0.939	-0.886	-1.267	-1.491	-1.472	-1.196	-1.524	-1.068
44	-0.366	-0.678	-0.036	-0.795	-0.171	-1.446	-0.501	-1.192	-0.537	-1.032
45	0.561	-0.697	0.862	-0.777	0.881	-1.405	0.451	-1.226	0.390	-1.052
46	1.397	-0.868	1.630	-0.739	1.849	-1.302	1.277	-1.185	1.253	-1.008
47	2.380	-0.827	2.597	-0.719	2.880	-1.126	2.267	-1.243	2.212	-1.008
51	-3.356	-1.801	-2.940	-1.947	-3.326	-2.193	-3.431	-2.032	-3.478	-1.964
52	-2.364	-1.742	-1.949	-1.780	-2.290	-2.179	-2.450	-1.961	-2.456	-1.892
53	-1.331	-1.767	-0.965	-1.745	-1.176	-2.238	-1.406	-1.993	-1.452	-1.887
54	-0.375	-1.756	-0.034	-1.698	-0.122	-2.187	-0.441	-1.984	-0.473	-1.881
55	0.521	-1.748	0.817	-1.678	0.870	-2.117	0.475	-2.014	0.431	-1.887
56	1.416	-1.762	1.644	-1.672	1.846	-2.071	1.347	-2.045	1.307	-1.903
57	2.374	-1.809	2.558	-1.697	2.838	-1.998	2.304	-2.129	2.273	-1.943
61	-3.186	-2.572	-2.814	-2.661	-3.102	-2.928	-3.209	-2.756	-3.283	-2.701
62	-2.363	-2.647	-1.979	-2.686	-2.229	-3.010	-2.385	-2.845	-2.462	-2.784
63	-1.323	-2.583	-0.979	-2.567	-1.134	-2.935	-1.349	-2.797	-1.415	-2.743
64	-0.294	-2.586	-0.016	-2.549	-0.033	-2.939	-0.344	-2.806	-0.388	-2.727
65	0.560	-2.621	0.809	-2.555	0.903	-2.923	0.552	-2.839	0.508	-2.756
66	1.498	-2.616	1.691	-2.552	1.868	-2.872	1.461	-2.872	1.413	-2.749
67	2.464	-2.636	2.609	-2.533	2.849	-2.798	2.420	-2.932	2.376	-2.797

```
//JANE        JOB  (F125,000,103,33),150,01),'WEBB              JOB  12
//S360   EXEC   FORTRAN
//FORT.SYSIN   DD    *
```

```
0001          DIMENSION X(7,7,5),Y(7,7,5),XX(7,7,5),YY(7,7,5),P(5),Q(5),DEN(6,6,
             15),AREA(6,6,5),DT(20),U(20),V(20),XXV(20),YYV(20),XV(20),YV(20),T(
             220),XRV(20),Y1(7)
0002          DATA X1,X2,X3/6.1,0.0,-6.1/
0003          DO 120 NXY0=1,4
0004          READ 111,J4,NN,PY,YB
0005      111 FORMAT(A2,I3,2F5.2)
0006          DO 3000 K=1,7
0007          DO 3000 L=1,7
0008          DO 3000 M=1,5
0009          XX(K,L,M)=0.0
0010          YY(K,L,M)=0.0
0011          X(K,L,M)=0.0
0012     3000 Y(K,L,M)=0.0
0013          DO 400 N=1,NN
0014          READ 2,J4,K,L,(P(M),Q(M),M=1,5)
0015        2 FORMAT(A2,I1,I1,10F7.3)
0016          DO 400 M=1,5
0017          X(K,L,M)=P(M)
0018      400 Y(K,L,M)=Q(M)
0019          PRINT 13,J4
0020       13 FORMAT(1H1,10X,24HPARTICLE TRANSLATIONS    ,66X,12HTEST NUMBER ,A2/
             1/10X,6HOBJECT,5X,10HPOSITION 1,8X,10HPOSITION 2,8X,10HPOSITION 3,8
             2X,10HPOSITION 4,8X,10HPOSITION 5/               11X,4HCODE,6X,1HX,8
             3X,1HY,8X,1HX,8X,1HY,8X,1HX,8X,1HY,8X,1HX,8X,1HY,8X,1HX,8X,1HY/)
0021          DO 107 K=1,7
0022          DO 108 L=1,7
0023          IF(ABS(X(K,L,1)).LT.0.00001) GO TO 108
0024          DO 109 M=1,5
0025          IF(ABS(X(K,L,M)).LT.0.00001) GO TO 109
0026          XX(K,L,M)=X(K,L,M)-X(K,L,1)
0027          YY(K,L,M)=Y(K,L,M)-Y(K,L,1)
0028      109 CONTINUE
0029          PRINT 12,K,L,(XX(K,L,M),YY(K,L,M),M=1,5)
0030       12 FORMAT(1H ,11X,I1,I1,1X,10F9.3)
0031      108 CONTINUE
0032          IF(K.EQ.6) PRINT 11
0033       11 FORMAT(1H1)
0034          IF(K.NE.6) PRINT 10
0035       10 FORMAT(/)
0036      107 CONTINUE
0037          PRINT 113,J4
0038      113 FORMAT(1H1,10X,18HRELATIVE DENSITIES,72X,12HTEST NUMBER ,A2//)
0039          DO 300 K=1,6
0040          DO 301 L=1,6
0041          DO 302 M=1,5
0042          AREA(K,L,M)=(ABS((X(K,L+1,M)-X(K,L,M))*(Y(K+1,L+1,M)-Y(K,L,M))-(X(
             1K+1,L+1,M)-X(K,L,M))*(Y(K,L+1,M)-Y(K,L,M)))+ABS((X(K+1,L,M)-X(K,L,
             2M))*(Y(K+1,L+1,M)-Y(K,L,M))-(X(K+1,L+1,M)-X(K,L,M))*(Y(K+1,L,M)-Y(
             3K,L,M))))/2.0
0043          DEN(K,L,M)=AREA(K,L,1)/AREA(K,L,M)
0044          IF(ABS(X(K,L,M)).LT.0.00001) DEN(K,L,M)=0.0
0045          IF(ABS(X(K+1,L,M)).LT.0.00001) DEN(K,L,M)=0.0
0046          IF(ABS(X(K,L+1,M)).LT.0.00001) DEN(K,L,M)=0.0
```

```
0047            IF(ABS(X(K+1,L+1,M)).LT.0.00001) DEN(K,L,M)=0.0
0048        302 CONTINUE
0049        301 PRINT 14,K,L,(DEN(K,L,M),M=1,5)
0050         14 FORMAT(1H ,11X,I1,I1,1X,5F9.3)
0051        300 PRINT 10
0052            PRINT 114,J4
0053            DO 403 K=1,7
0054            S=0.0
0055            R=7.0
0056            DO 402 L=1,7
0057            IF(ABS(X(K,L,1)).LT.0.00001) R=R-1.0
0058        402 S=S+Y(K,L,1)
0059            IF(R.LT.0.00001) GO TO 403
0060            Y1(K)=S/R-PY
0061            PRINT 115,K,Y1(K)
0062        115 FORMAT(1H-,I11,F20.3)
0063        403 CONTINUE
0064            PRINT 16,J4
0065            DO 120 K=1,6
0066            N=6
0067            DO 116 J=1,N
0068            L=N+2-J
0069            M=J+N
0070            MM=J+N*2
0071            DT(J)=(X(K,L,1)-X(K,L-1,1))/YB
0072            U(J)=(XX(K,L-1,2)-XX(K,L,2))/DT(J)
0073            V(J)=(YY(K,L-1,2)-YY(K,L,2))/DT(J)
0074            XXV(J)=(XX(K,L-1,2)+XX(K,L,2))/2.0
0075            YYV(J)=(YY(K,L-1,2)+YY(K,L,2))/2.0
0076            DT(M)=DT(J)
0077            U(M)=(XX(K,L-1,3)-XX(K,L,3))/DT(J)
0078            V(M)=(YY(K,L-1,3)-YY(K,L,3))/DT(J)
0079            XXV(M)=(XX(K,L-1,3)+XX(K,L,3))/2.0
0080            YYV(M)=(YY(K,L-1,3)+YY(K,L,3))/2.0
0081            DT(MM)=DT(J)
0082            U(MM)=(XX(K,L-1,4)-XX(K,L,4))/DT(J)
0083            V(MM)=(YY(K,L-1,4)-YY(K,L,4))/DT(J)
0084            XXV(MM)=(XX(K,L-1,4)+XX(K,L,4))/2.0
0085            YYV(MM)=(YY(K,L-1,4)+YY(K,L,4))/2.0
0086            XV(J)=-X1-(X(K,L,1)+X(K,L-1,1))/2.0
0087            XV(MM)=XV(J)-X3+X1
0088        116 XV(M)=XV(J)-X2+X1
0089            N=N*3
0090            DO 117 J=1,N
0091            T(J)=XV(J)/YB
0092            XRV(J)=XV(J)-XXV(J)
0093            YV(J)=PY+Y1(K)+YYV(J)
0094        117 PRINT 18,K,J,U(J),V(J),XXV(J),YYV(J),XV(J),XRV(J),DT(J),T(J),YV(J)
0095            IF(K.EQ.3) PRINT 11
0096        120 PRINT 10
0097        114 FORMAT(1H1,10X,18HINITIAL DEPTHS     ,72X,12HTEST NUMBER ,A2//10X,3
               1HROW,9H    DEPTH)
0098            STOP
0099         18 FORMAT(1H ,10X,I1,I3,11F9.3)
```

```
0100      16 FORMAT(1H1,10X,23HVELOCITY CALCULATIONS   ,66X,12HTEST NUMBER ,A2//
            19X,8HPOSITION,4X,10HVELOCITIES,7X,12HTRANSLATIONS,3X,25HDISTANCE F
            2ROM WHEEL DELTA,4X,14HTOTAL Y REL TO/11X,4HCODE,4X,5HDX/DT,4X,5HDY
            3/DT,6X,1HX,8X,1HY,4X,16HINITIAL   ACTUAL,4X,4HTIME,5X,4HTIME,4X,5H
            4PARAY/)
0101         END
```

TOTAL MEMORY REQUIREMENTS 00293C BYTES

TEST NUMBER 40

PARTICLE TRANSLATIONS

OBJECT CODE	POSITION 1 X	POSITION 1 Y	POSITION 2 X	POSITION 2 Y	POSITION 3 X	POSITION 3 Y	POSITION 4 X	POSITION 4 Y	POSITION 5 X	POSITION 5 Y
11	0.0	0.0	0.360	-0.190	-0.411	-0.658	-0.593	-0.340	-0.616	-0.244
12	0.0	0.0	0.329	0.140	-0.370	-0.789	-0.564	-0.320	-0.605	-0.210
13	0.0	0.0	0.335	0.191	-0.252	-1.027	-0.582	-0.354	-0.660	-0.262
14	0.0	0.0	0.367	0.220	0.045	-1.168	-0.498	-0.429	-0.596	-0.304
15	0.0	0.0	0.357	0.184	0.210	-1.066	-0.595	-0.475	-0.619	-0.295
16	0.0	0.0	0.329	0.180	0.306	-0.730	-0.494	-0.504	-0.630	-0.275
17	0.0	0.0	0.286	0.159	0.333	-0.181	-0.473	-0.523	-0.643	-0.241
21	0.0	0.0	0.514	-0.382	-0.311	-0.532	-0.434	-0.274	-0.453	-0.200
22	0.0	0.0	0.511	-0.052	-0.299	-0.673	-0.431	-0.325	-0.431	-0.245
23	0.0	0.0	0.434	0.158	-0.212	-0.827	-0.384	-0.315	-0.459	-0.232
24	0.0	0.0	0.360	0.189	-0.023	-0.929	-0.358	-0.354	-0.425	-0.232
25	0.0	0.0	0.352	0.213	0.194	-0.928	-0.330	-0.401	-0.417	-0.211
26	0.0	0.0	0.296	0.191	0.353	-0.793	-0.340	-0.424	-0.441	-0.230
27	0.0	0.0	0.269	0.178	0.476	-0.443	-0.305	-0.516	-0.435	-0.242
31	0.0	0.0	0.527	-0.245	-0.171	-0.511	-0.218	-0.255	-0.265	-0.131
32	0.0	0.0	0.518	-0.018	-0.136	-0.587	-0.205	-0.252	-0.244	-0.152
33	0.0	0.0	0.437	0.077	-0.034	-0.717	-0.214	-0.296	-0.255	-0.178
34	0.0	0.0	0.391	0.134	0.093	-0.741	-0.211	-0.323	-0.254	-0.172
35	0.0	0.0	0.299	0.178	0.247	-0.702	-0.214	-0.340	-0.258	-0.170
36	0.0	0.0	0.261	0.156	0.456	-0.590	-0.187	-0.377	-0.258	-0.188
37	0.0	0.0	0.246	0.113	0.527	-0.347	-0.216	-0.447	-0.300	-0.198
41	0.0	0.0	0.475	-0.184	-0.024	-0.462	-0.113	-0.244	-0.154	-0.133
42	0.0	0.0	0.460	-0.052	0.016	-0.541	-0.103	-0.243	-0.152	-0.159
43	0.0	0.0	0.429	0.046	0.101	-0.559	-0.104	-0.264	-0.156	-0.136
44	0.0	0.0	0.330	0.083	0.195	-0.568	-0.135	-0.314	-0.171	-0.154
45	0.0	0.0	0.301	0.120	0.320	-0.508	-0.110	-0.329	-0.171	-0.155
46	0.0	0.0	0.233	0.129	0.452	-0.434	-0.120	-0.317	-0.144	-0.140
47	0.0	0.0	0.217	0.108	0.500	-0.299	-0.113	-0.416	-0.168	-0.181
51	0.0	0.0	0.416	-0.146	0.030	-0.392	-0.075	-0.231	-0.122	-0.163
52	0.0	0.0	0.415	-0.038	0.074	-0.437	-0.085	-0.219	-0.092	-0.140
53	0.0	0.0	0.366	0.022	0.155	-0.471	-0.075	-0.226	-0.121	-0.120
54	0.0	0.0	0.341	0.068	0.253	-0.431	-0.066	-0.228	-0.098	-0.125
55	0.0	0.0	0.296	0.070	0.349	-0.369	-0.045	-0.266	-0.090	-0.139
56	0.0	0.0	0.228	0.090	0.430	-0.309	-0.069	-0.283	-0.109	-0.141
57	0.0	0.0	0.184	0.112	0.464	-0.189	-0.070	-0.320	-0.101	-0.134
61	0.0	0.0	0.372	-0.089	0.084	-0.356	-0.023	-0.184	-0.097	-0.129
62	0.0	0.0	0.384	-0.039	0.134	-0.363	-0.023	-0.198	-0.099	-0.137
63	0.0	0.0	0.344	0.016	0.189	-0.352	-0.025	-0.214	-0.092	-0.160
64	0.0	0.0	0.278	0.037	0.261	-0.353	-0.050	-0.220	-0.094	-0.141
65	0.0	0.0	0.249	0.066	0.343	-0.302	-0.008	-0.218	-0.052	-0.135
66	0.0	0.0	0.193	0.064	0.370	-0.256	-0.037	-0.256	-0.085	-0.133
67	0.0	0.0	0.145	0.103	0.385	-0.162	-0.044	-0.296	-0.088	-0.161

RELATIVE DENSITIES

TEST NUMBER 40

11	1.000	0.988	1.027	1.011	1.013
12	1.000	0.988	0.962	0.997	1.002
13	1.000	1.001	1.010	1.000	1.014
14	1.000	1.005	1.091	1.054	1.111
15	1.000	1.063	1.100	1.082	1.101
16	1.000	1.042	1.008	1.000	1.040
21	1.000	1.039	1.069	1.055	1.109
22	1.000	1.025	1.060	1.032	1.069
23	1.000	0.986	1.032	1.016	1.034
24	1.000	1.010	1.053	1.043	1.051
25	1.000	1.023	1.034	1.036	1.040
26	1.000	0.975	1.041	1.056	1.051
31	1.000	1.027	1.034	1.004	0.991
32	1.000	1.020	1.038	1.031	1.026
33	1.000	1.038	1.074	1.034	1.033
34	1.000	1.015	1.053	1.001	1.019
35	1.000	1.024	0.998	1.022	1.010
36	1.000	1.002	1.048	1.055	1.061
41	1.000	1.047	1.073	1.021	0.977
42	1.000	1.040	1.052	1.036	1.037
43	1.000	1.046	1.045	1.090	1.022
44	1.000	1.005	1.060	1.070	1.023
45	1.000	1.033	1.050	1.080	1.003
46	1.000	1.013	1.101	1.076	1.035
51	1.000	1.023	1.023	1.050	1.006
52	1.000	1.043	1.057	1.015	0.989
53	1.000	1.025	1.045	1.020	0.956
54	1.000	1.022	0.988	1.001	0.966
55	1.000	1.054	1.013	1.081	1.037
56	1.000	1.025	1.019	1.043	0.988
61	0.0	0.0	0.0	0.0	0.0
62	0.0	0.0	0.0	0.0	0.0
63	0.0	0.0	0.0	0.0	0.0
64	0.0	0.0	0.0	0.0	0.0
65	0.0	0.0	0.0	0.0	0.0
66	0.0	0.0	0.0	0.0	0.0

INITIAL DEPTHS

TEST NUMBER 40

ROW	DEPTH
1	-0.153
2	-0.974
3	-2.018
4	-3.037
5	-3.919
6	-4.759
7	-5.664

VELOCITY CALCULATIONS

TEST NUMBER 40

POSITION CODE	VELOCITIES DX/DT	DY/DT	TRANSLATIONS X	Y	DISTANCE FROM WHEEL INITIAL	ACTUAL	DELTA TIME	TOTAL TIME	Y REL TO PARAY
1 1	0.219	0.107	0.308	0.170	-8.654	-8.962	0.197	-1.548	2.167
1 2	0.162	0.023	0.343	0.182	-7.621	-7.964	0.173	-1.363	2.179
1 3	0.059	0.212	0.362	0.202	-6.663	-7.025	0.170	-1.192	2.199
1 4	-0.165	-0.150	0.351	0.206	-5.646	-5.997	0.194	-1.010	2.203
1 5	-0.033	-0.285	0.332	0.166	-4.604	-4.936	0.179	-0.824	2.163
1 6	0.183	-1.950	0.345	-0.025	-3.630	-3.975	0.169	-0.649	1.972
1 7	-0.137	-2.792	0.320	-0.455	-2.554	-2.874	0.197	-0.457	1.542
1 8	-0.555	-1.942	0.258	-0.898	-1.521	-1.779	0.173	-0.272	1.099
1 9	-0.971	-0.600	0.127	-1.117	-0.563	-0.690	0.170	-0.101	0.880
1 10	-1.533	0.728	-0.103	-1.097	0.454	0.557	0.194	0.081	0.900
1 11	-0.658	1.328	-0.311	-0.908	1.496	1.807	0.179	0.268	1.089
1 12	-0.242	0.774	-0.390	-0.723	2.470	2.860	0.169	0.442	1.274
1 13	-0.107	0.097	-0.483	-0.513	3.546	4.029	0.197	0.634	1.484
1 14	-0.069	0.168	-0.500	-0.490	4.579	5.078	0.173	0.819	1.508
1 15	0.047	0.271	-0.502	-0.452	5.537	6.039	0.170	0.991	1.545
1 16	-0.434	0.387	-0.540	-0.391	6.554	7.093	0.194	1.172	1.606
1 17	0.100	0.190	-0.573	-0.337	7.596	8.169	0.179	1.359	1.660
1 18	-0.171	-0.118	-0.578	-0.330	8.570	9.148	0.169	1.533	1.667
2 1	0.146	0.070	0.282	0.184	-8.021	-8.303	0.185	-1.435	1.361
2 2	0.340	0.133	0.324	0.202	-7.044	-7.368	0.165	-1.260	1.378
2 3	0.048	-0.144	0.356	0.201	-6.118	-6.474	0.166	-1.095	1.377
2 4	0.342	-0.143	0.397	0.174	-5.050	-5.447	0.216	-0.903	1.350
2 5	0.436	-1.188	0.472	0.053	-3.952	-4.425	0.177	-0.707	1.229
2 6	0.019	-2.096	0.512	-0.217	-3.018	-3.531	0.157	-0.540	0.959
2 7	-0.666	-1.896	0.414	-0.618	-1.921	-2.335	0.185	-0.344	0.558
2 8	-0.964	-0.818	0.273	-0.860	-0.944	-1.217	0.165	-0.169	0.316
2 9	-1.306	-0.006	0.086	-0.928	-0.018	-0.104	0.165	-0.003	0.248
2 10	-0.875	0.472	-0.117	-0.878	1.050	1.167	0.216	0.188	0.298
2 11	-0.492	0.871	-0.256	-0.750	2.148	2.403	0.177	0.384	0.426
2 12	-0.076	0.896	-0.305	-0.602	3.082	3.387	0.157	0.551	0.574
2 13	-0.190	0.498	-0.322	-0.470	4.179	4.501	0.185	0.748	0.706
2 14	0.061	0.139	-0.335	-0.412	5.156	5.491	0.165	0.922	0.764
2 15	-0.168	0.283	-0.344	-0.377	6.082	6.425	0.166	1.088	0.799
2 16	-0.120	0.180	-0.371	-0.334	7.150	7.521	0.216	1.279	0.842
2 17	-0.266	-0.057	-0.408	-0.320	8.248	8.655	0.177	1.475	0.856
2 18	-0.019	0.324	-0.433	-0.299	9.182	9.614	0.157	1.643	0.877
3 1	0.086	0.247	0.253	0.135	-8.008	-8.261	0.174	-1.433	0.266
3 2	0.233	0.135	0.280	0.167	-7.065	-7.345	0.163	-1.264	0.299
3 3	0.561	-0.268	0.345	0.156	-6.151	-6.496	0.164	-1.100	0.288
3 4	0.261	-0.324	0.414	0.105	-5.201	-5.615	0.175	-0.930	0.237
3 5	0.446	-0.523	0.477	0.029	-4.201	-4.679	0.182	-0.752	0.161
3 6	0.049	-1.244	0.523	-0.131	-3.184	-3.707	0.182	-0.570	0.000
3 7	-0.407	-1.395	0.492	-0.468	-1.908	-2.399	0.174	-0.341	-0.337
3 8	-1.282	-0.687	0.352	-0.646	-0.965	-1.317	0.163	-0.173	-0.514
3 9	-0.939	-0.238	0.170	-0.721	-0.051	-0.221	0.164	-0.009	-0.590
3 10	-0.721	0.136	0.030	-0.729	0.899	0.869	0.176	0.161	-0.597
3 11	-0.562	0.716	-0.085	-0.652	1.898	1.983	0.182	0.340	-0.520
3 12	-0.192	0.417	-0.154	-0.549	2.916	3.069	0.182	0.522	-0.417
3 13	0.166	0.402	-0.201	-0.412	4.192	4.394	0.174	0.750	-0.280
3 14	-0.166	0.227	-0.201	-0.358	5.135	5.335	0.163	0.919	-0.227
3 15	0.018	0.104	-0.213	-0.331	6.049	6.261	0.164	1.082	-0.200
3 16	-0.017	0.153	-0.212	-0.309	6.999	7.211	0.176	1.252	-0.178
3 17	0.050	0.242	-0.209	-0.274	7.998	8.208	0.182	1.431	-0.142

4	1	0.091	0.119	0.225	0.118	-7.988	-8.213	0.176	-1.429	-0.768
4	2	0.455	-0.060	0.267	0.124	-7.079	-7.346	0.150	-1.266	-0.762
4	3	0.175	-0.223	0.315	0.101	-6.197	-6.513	0.165	-1.109	-0.785
4	4	0.552	-0.206	0.379	0.064	-5.233	-5.612	0.179	-0.936	-0.822
4	5	0.166	-0.577	0.444	-0.008	-4.209	-4.653	0.187	-0.753	-0.895
4	6	0.085	-0.692	0.467	-0.123	-3.194	-3.661	0.176	-0.571	-1.010
4	7	-0.273	-0.768	0.476	-0.366	-1.888	-2.364	0.176	-0.338	-1.253
4	8	-0.883	-0.495	0.386	-0.471	-0.979	-1.365	0.150	-0.175	-1.358
4	9	-0.754	-0.362	0.257	-0.538	-0.097	-0.355	0.165	-0.017	-1.425
4	10	-0.524	0.050	0.148	-0.563	0.867	0.719	0.179	0.155	-1.450
4	11	-0.454	0.096	0.058	-0.550	1.891	1.832	0.187	0.338	-1.437
4	12	-0.227	0.448	-0.004	-0.501	2.906	2.910	0.175	0.520	-1.388
4	13	-0.040	0.563	-0.116	-0.366	4.212	4.328	0.175	0.753	-1.253
4	14	0.067	-0.080	-0.115	-0.323	5.121	5.236	0.150	0.916	-1.210
4	15	-0.151	0.090	-0.123	-0.321	6.002	6.125	0.165	1.074	-1.208
4	16	0.173	0.279	-0.120	-0.289	6.967	7.086	0.179	1.246	-1.176
4	17	0.005	0.112	-0.103	-0.253	7.991	8.094	0.187	1.430	-1.140
4	18	-0.057	-0.006	-0.108	-0.243	9.006	9.114	0.176	1.611	-1.130
5	1	0.257	-0.128	0.206	0.101	-7.995	-8.201	0.171	-1.430	-1.668
5	2	0.425	-0.125	0.262	0.080	-7.068	-7.330	0.160	-1.264	-1.689
5	3	0.281	-0.012	0.318	0.069	-6.173	-6.491	0.160	-1.104	-1.700
5	4	0.146	-0.269	0.353	0.045	-5.247	-5.600	0.171	-0.939	-1.724
5	5	0.265	-0.325	0.390	-0.008	-4.253	-4.643	0.185	-0.761	-1.777
5	6	0.006	-0.609	0.416	-0.092	-3.240	-3.655	0.177	-0.580	-1.861
5	7	-0.198	-0.700	0.447	-0.249	-1.895	-2.342	0.171	-0.339	-2.018
5	8	-0.506	-0.375	0.390	-0.339	-0.968	-1.358	0.160	-0.173	-2.108
5	9	-0.599	-0.387	0.301	-0.400	-0.073	-0.374	0.160	-0.013	-2.169
5	10	-0.573	-0.234	0.204	-0.451	0.853	0.649	0.171	0.153	-2.220
5	11	-0.438	0.184	0.114	-0.454	1.847	1.733	0.185	0.331	-2.223
5	12	-0.248	0.254	0.052	-0.415	2.860	2.808	0.177	0.512	-2.184
5	13	0.006	0.216	-0.069	-0.302	4.205	4.274	0.171	0.752	-2.071
5	14	0.150	0.106	-0.057	-0.275	5.132	5.188	0.160	0.918	-2.044
5	15	-0.131	0.237	-0.056	-0.247	6.027	6.082	0.160	1.078	-2.016
5	16	-0.053	0.012	-0.070	-0.227	6.953	7.023	0.171	1.244	-1.996
5	17	-0.060	0.038	-0.081	-0.222	7.947	8.028	0.185	1.422	-1.992
5	18	0.062	-0.068	-0.081	-0.225	8.960	9.040	0.177	1.603	-1.994
6	1	0.278	-0.226	0.169	0.083	-8.081	-8.250	0.173	-1.446	-2.525
6	2	0.334	0.012	0.221	0.065	-7.129	-7.350	0.168	-1.275	-2.544
6	3	0.190	-0.190	0.263	0.051	-6.233	-6.496	0.153	-1.115	-2.557
6	4	0.359	-0.114	0.311	0.026	-5.291	-5.602	0.184	-0.947	-2.582
6	5	0.215	-0.296	0.364	-0.012	-4.257	-4.621	0.186	-0.762	-2.620
6	6	-0.082	-0.340	0.378	-0.064	-3.325	-3.703	0.147	-0.595	-2.673
6	7	-0.087	-0.544	0.378	-0.209	-1.981	-2.358	0.173	-0.354	-2.818
6	8	-0.161	-0.274	0.356	-0.279	-1.029	-1.385	0.168	-0.184	-2.888
6	9	-0.537	-0.334	0.302	-0.327	-0.133	-0.435	0.153	-0.024	-2.936
6	10	-0.391	0.005	0.225	-0.352	0.809	0.584	0.184	0.145	-2.961
6	11	-0.296	-0.059	0.162	-0.358	1.843	1.681	0.186	0.330	-2.966
6	12	-0.340	0.048	0.109	-0.359	2.774	2.665	0.147	0.496	-2.968
6	13	0.041	0.231	-0.041	-0.276	4.119	4.160	0.173	0.737	-2.885
6	14	0.173	0.226	-0.022	-0.237	5.071	5.093	0.168	0.907	-2.846
6	15	-0.275	-0.013	-0.029	-0.219	5.967	5.996	0.153	1.067	-2.828
6	16	0.130	0.033	-0.038	-0.217	6.908	6.946	0.184	1.236	-2.826
6	17	0.016	0.086	-0.024	-0.206	7.943	7.967	0.186	1.421	-2.815
6	18	0.0	0.095	-0.023	-0.191	8.874	8.897	0.147	1.588	-2.800

```
//INVTS       JOB  (F125,000,001,010,000,01),'WEBB                    '         JOB  13
//S360   EXEC   FORTRAN
//FORT.SYSIN   DD    *
```

175

```
0001          DIMENSION I(13,19),J(13,19),EPSI(13,19),BETA(13,19),GAMMA(13,19),
             1GAMMB(13,19),STRIN(13,19),GAMMX(13,19)
0002          DO 4 L=1,13
0003          READ 3,(I(L,K),K=1,19)
0004        4 READ 3,(J(L,K),K=1,19)
0005        3 FORMAT(19I4)
0006          DO 5 K=2,18
0007          DO 5 L=2,12
0008          EPSI(L,K) =(ABS(FLOAT(I(L,K-1)-I(L,K)))+ABS(FLOAT(I(L,K)-I(L,K+1))
             1))/100.0
0009          GAMMB(L,K)=(ABS(FLOAT(J(L,K-1)-J(L,K)))+ABS(FLOAT(J(L,K)-J(L,K+1))
             1))/100.0
0010          BETA(L,K) =(ABS(FLOAT(J(L-1,K)-J(L,K)))+ABS(FLOAT(J(L,K)-J(L+1,K))
             1))/100.0
0011          GAMMA(L,K)=(ABS(FLOAT(I(L-1,K)-I(L,K)))+ABS(FLOAT(I(L,K)-I(L+1,K))
             1))/100.0
0012          GAMMX(L,K)=GAMMA(L,K)+GAMMB(L,K)
0013        5 STRIN(L,K)=SQRT((EPSI(L,K)**2+BETA(L,K)**2)/2.0+(GAMMX(L,K)**2)/4.
             10)
0014          PRINT 7
0015        7 FORMAT(1H1,10X,5HEDCTX,60X,15HTEST NUMBER 32/)
0016          DO 9 L=2,12
0017        9 PRINT 8,L,(EPSI(L,K),K=2,18)
0018          PRINT 10
0019       10 FORMAT(1H1,10X,5HEDCTY,60X,15HTEST NUMBER 32/)
0020          DO 11 L=2,12
0021       11 PRINT 8,L,(BETA(L,K),K=2,18)
0022          PRINT 12
0023       12 FORMAT(1H1,10X,10HGAMMADCTXY,60X,15HTEST NUMBER 32/)
0024          DO 13 L=2,12
0025       13 PRINT 8,L,(GAMMX(L,K),K=2,18)
0026          PRINT 6
0027        6 FORMAT(1H1,10X,21HSTRAINRATE INVARIANTS,60X,15HTEST NUMBER 32/)
0028          DO 2 L=2,12
0029        2 PRINT 8,L,(STRIN(L,K),K=2,18)
0030        8 FORMAT(1H0,5X,I2,17F6.2)
0031          STOP
0032          END
```

EDOTX

TEST NUMBER 32/

2	0.18	0.24	0.29	0.36	0.37	0.35	0.34	0.30	0.16	0.18	0.35	0.42	0.50	0.59	0.52	0.34	0.19
3	0.18	0.25	0.31	0.35	0.36	0.31	0.20	0.10	0.05	0.10	0.21	0.34	0.45	0.44	0.45	0.38	0.20
4	0.17	0.25	0.31	0.34	0.36	0.32	0.15	0.02	0.04	0.10	0.17	0.30	0.39	0.38	0.37	0.34	0.22
5	0.15	0.21	0.28	0.31	0.31	0.30	0.20	0.07	0.06	0.12	0.18	0.27	0.34	0.33	0.33	0.30	0.20
6	0.14	0.18	0.26	0.30	0.26	0.19	0.12	0.07	0.04	0.07	0.18	0.27	0.27	0.26	0.27	0.27	0.19
7	0.09	0.16	0.24	0.27	0.24	0.20	0.14	0.06	0.03	0.07	0.16	0.23	0.22	0.22	0.23	0.23	0.19
8	0.07	0.14	0.20	0.24	0.22	0.19	0.13	0.06	0.04	0.08	0.14	0.18	0.20	0.18	0.18	0.22	0.18
9	0.06	0.15	0.14	0.17	0.24	0.23	0.15	0.05	0.03	0.08	0.13	0.17	0.20	0.17	0.17	0.17	0.14
10	0.03	0.08	0.12	0.16	0.20	0.17	0.17	0.13	0.04	0.07	0.11	0.15	0.20	0.17	0.13	0.13	0.12
11	0.0	0.05	0.10	0.12	0.15	0.18	0.16	0.09	0.05	0.06	0.11	0.13	0.12	0.11	0.11	0.09	0.10
12	0.0	0.0	0.05	0.09	0.09	0.17	0.16	0.07	0.04	0.04	0.09	0.11	0.09	0.06	0.06	0.08	0.08

EDDTY

TEST NUMBER 32/

2	0.20	0.33	0.37	0.40	0.40	0.42	0.37	0.09	0.02	0.03	0.18	0.39	0.42	0.70	0.85	0.42	0.18
3	0.17	0.25	0.37	0.40	0.40	0.40	0.27	0.06	0.02	0.05	0.16	0.45	0.37	0.50	0.59	0.38	0.27
4	0.20	0.22	0.30	0.38	0.38	0.40	0.18	0.02	0.04	0.09	0.14	0.26	0.36	0.42	0.44	0.35	0.31
5	0.15	0.21	0.26	0.33	0.36	0.30	0.16	0.03	0.05	0.10	0.16	0.11	0.29	0.35	0.35	0.33	0.30
6	0.15	0.22	0.25	0.28	0.32	0.20	0.13	0.05	0.04	0.11	0.17	0.23	0.27	0.29	0.29	0.29	0.30
7	0.12	0.20	0.21	0.25	0.24	0.16	0.08	0.05	0.04	0.14	0.16	0.20	0.25	0.26	0.27	0.27	0.28
8	0.08	0.14	0.15	0.19	0.17	0.11	0.09	0.05	0.04	0.12	0.16	0.20	0.23	0.26	0.26	0.27	0.24
9	0.11	0.13	0.13	0.14	0.13	0.11	0.10	0.04	0.04	0.11	0.16	0.19	0.20	0.23	0.24	0.24	0.24
10	0.11	0.12	0.14	0.13	0.13	0.13	0.06	0.05	0.03	0.11	0.16	0.15	0.16	0.17	0.19	0.18	0.21
11	0.16	0.14	0.15	0.14	0.14	0.13	0.09	0.08	0.03	0.08	0.12	0.17	0.16	0.15	0.14	0.16	0.12
12	0.11	0.12	0.11	0.12	0.10	0.06	0.07	0.04	0.03	0.05	0.09	0.13	0.15	0.11	0.11	0.10	0.06

GAMMADOTXY TEST NUMBER 32/

2	0.52	0.51	0.45	0.25	0.32	0.71	0.89	1.07	1.07	0.98	0.98	0.75	0.54	0.40	0.48	0.55	0.69
3	0.40	0.32	0.32	0.19	0.24	0.60	0.72	0.89	1.00	0.86	0.76	0.67	0.50	0.23	0.25	0.31	0.48
4	0.34	0.24	0.22	0.16	0.26	0.56	0.57	0.69	0.79	0.64	0.46	0.53	0.51	0.18	0.09	0.20	0.35
5	0.29	0.21	0.17	0.13	0.31	0.53	0.53	0.68	0.75	0.59	0.50	0.47	0.34	0.16	0.05	0.12	0.22
6	0.23	0.18	0.17	0.18	0.30	0.44	0.46	0.62	0.72	0.55	0.44	0.43	0.29	0.14	0.05	0.11	0.21
7	0.17	0.17	0.15	0.21	0.29	0.35	0.31	0.48	0.58	0.47	0.41	0.33	0.25	0.15	0.04	0.11	0.16
8	0.09	0.06	0.07	0.16	0.22	0.24	0.23	0.39	0.45	0.37	0.36	0.27	0.19	0.15	0.06	0.09	0.15
9	0.05	0.07	0.08	0.14	0.21	0.24	0.27	0.29	0.35	0.29	0.25	0.21	0.17	0.14	0.10	0.07	0.12
10	0.05	0.09	0.12	0.11	0.20	0.27	0.25	0.31	0.34	0.29	0.29	0.28	0.18	0.10	0.07	0.06	0.14
11	0.06	0.05	0.10	0.13	0.21	0.26	0.19	0.32	0.30	0.26	0.30	0.32	0.23	0.11	0.05	0.07	0.14
12	0.02	0.02	0.07	0.12	0.18	0.20	0.23	0.27	0.28	0.28	0.27	0.25	0.21	0.14	0.12	0.06	0.04

STRAINRATE INVARIANTS TEST NUMBER 32/

2	0.32	0.39	0.40	0.40	0.42	0.52	0.57	0.58	0.55	0.51	0.56	0.55	0.53	0.68	0.74	0.47	0.39
3	0.27	0.30	0.38	0.39	0.40	0.47	0.43	0.45	0.50	0.44	0.42	0.52	0.48	0.48	0.54	0.41	0.34
4	0.25	0.26	0.32	0.37	0.39	0.46	0.33	0.35	0.40	0.33	0.28	0.39	0.45	0.41	0.41	0.36	0.32
5	0.21	0.23	0.28	0.33	0.37	0.40	0.32	0.34	0.38	0.31	0.30	0.31	0.36	0.35	0.34	0.32	0.28
6	0.19	0.22	0.27	0.30	0.33	0.29	0.26	0.32	0.36	0.29	0.28	0.33	0.31	0.28	0.28	0.29	0.27
7	0.14	0.20	0.24	0.28	0.28	0.25	0.19	0.25	0.29	0.26	0.26	0.27	0.27	0.25	0.25	0.26	0.25
8	0.09	0.14	0.18	0.23	0.23	0.20	0.16	0.20	0.23	0.21	0.23	0.23	0.24	0.24	0.23	0.25	0.22
9	0.09	0.14	0.14	0.17	0.22	0.22	0.19	0.15	0.18	0.17	0.19	0.21	0.22	0.21	0.21	0.21	0.21
10	0.08	0.11	0.14	0.16	0.20	0.20	0.18	0.18	0.17	0.17	0.20	0.21	0.20	0.19	0.17	0.16	0.13
11	0.12	0.11	0.14	0.15	0.18	0.20	0.16	0.18	0.16	0.15	0.19	0.22	0.18	0.14	0.13	0.13	0.13
12	0.08	0.09	0.09	0.12	0.13	0.16	0.17	0.15	0.14	0.15	0.16	0.17	0.16	0.11	0.11	0.10	0.07

```
*         GO        END      STEP TIME     .08 MINS       TUE SEP 17, 1968  TIME OF DAY 18.7982 HRS    *

**********************************************************************************************************
* 360/50-1          71-CARDS READ        201-LINES PRINTED          0-CARDS PUNCHED  JOB SEQ NO.     40*
      YOU HAVE  274.86 MINS. LEFT
*     JOB  INVTS    END     TOTAL TIME     .42 MINS       TUE SEP 17, 1968  TIME OF DAY 18.7984 HRS    *
**********************************************************************************************************


H A S P  JOB STATISTICS --      70 CARDS READ --      130 LINES PRINTED --      0 CARDS PUNCHED -- JOB  13 -- INVTS
```

Leaf 181 omitted im page numbering.

APPENDIX IV

SIMPLIFIED METHODS FOR COMPUTING INTERFACIAL ENERGY

Mean Frictional Stress

There is a variation in soil velocity around the area of contact. For example, in Test 38, the soil velocity varies from 6.7 in./sec at inlet to 7.4 in./sec at bottom, dead center and finally to 6.6 in./sec at exit. If an average soil velocity is assumed for the entire contact area, a mean slip velocity for the entire contact area can be obtained and from the stress-slip velocity relationship for the soil, average frictional stress can be selected. The interfacial energy can then be expressed as:-

$$X = \begin{matrix}\text{Average}\\ \text{Frictional}\\ \text{Stress}\end{matrix} \times \begin{matrix}\text{Total Area}\\ \text{of}\\ \text{Contact}\end{matrix} \times \begin{matrix}\text{Average}\\ \text{Slip}\\ \text{Velocity}\end{matrix} \qquad \text{IV-1}$$

Estimation of Frictional (Shear) Stresses from Torque Measurements

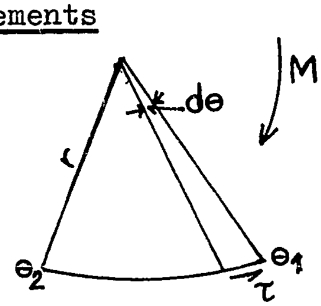

The following Equation can be written for torque:-

$$M = br \int_{\theta_1}^{\theta_2} r\tau d\theta \qquad \text{IV-2}$$

where b = width of wheel

τ = shear stress on an elemental area.

If it is assumed that the shear stress is constant over the interface, Equation (IV-2) reduces to:-

$$M = br^2 \tau \Big|_{\theta_1}^{\theta_2} \qquad \text{IV-3}$$

For clay soils and especially at higher slips the assumption of a uniform shear stress is reasonable since the soil velocity over the entire interface is similar, the shear stresses defined by the slip velocity will be similar.

In Equation (IV-3) all the terms except for τ are known and stresses calculated from the torque are in close agreement with mean frictional stress calculated by assuming an average slip velocity.

Calculation of Interfacial Energy from Torque

As stated before, the torque can be expressed as:-

$$M = br \int_{\theta_1}^{\theta_2} r\tau d\theta \qquad \text{IV-4}$$

The area of contact is given by:-

$$A = b \int_{\theta_1}^{\theta_2} rd\theta \qquad \text{IV-5}$$

If Equation (IV-4) is divided by Radius, r, we obtain:-

$$\frac{M}{r} = b \int_{\theta_1}^{\theta_2} \tau rd\theta \qquad \text{IV-6}$$

Therefore using Equation (IV-5), Equation (IV-6) becomes:-

$$\frac{M}{r} = A\tau \qquad \text{IV-7}$$

where $A\tau$ = Average shear force over the area of contact.

The Interfacial Energy can then be expressed as:-

$$X = A\tau V_s = \frac{M}{r} V_s \qquad \text{IV-8}$$

where V_s is the average slip velocity.

Equation (IV-8) was used by Fitzpatrick-Nash (1968) to calculate the interfacial energy. For cohesive soils at higher slips where the shear stress is fairly uniform over the contact surface $\frac{M}{r}$ represents a very useful approximation. Calculations of interfacial energy by this method were in close agreement with the method described in Chapter 4.

BIBLIOGRAPHY

Bekker, M.G., (1956) "Theory of Land Locomotion", University of Michigan Press, Ann Arbor.

Bekker, M.G., (1960) "Off-the-Road Locomotion; Research and Development in Terramechanics", University of Michigan Press, Ann Arbor.

Bekker, M.G., (1959) "Mobility of Cross Country Vehicles", Machine Design Vol. 31; No. 26; pp. 92-96 and Vol. 32, No. 1; (1960) pp. 145.

Bloedow, F.H., (1962) "Radiographic Instrumentation Study", Report No. AFSWC-TDR-62-44, U. S. Air Force Special Weapons Center, Kirtland Air Force Base, New Mexico.

Boyd, C.W., & Windisch, S.J., (1966) "A Technique for Measuring Deformations Within a Sand Under Controlled Wheel Loads", Proc. 2nd Int. Conf. I.S.T.V.S., Quebec.

Fano, U., Spencer, L.V., & Berger, M.J., (1959) "Penetration and Diffusion of X-Rays", "Neutrons and Related Gamma Ray Problems", Ency. of Physics., Vol. XXXVIII/2 pp. 660-817, Edited by S. Flugge, Springer-Verlag, Berlin.

Fitzpatrick-Nash, J.D., (1968) "Energy Dissipation in Clays Beneath Moving Rigid Wheels", M.Eng. Thesis, McGill University.

Frietag, D.R., Green, A.J., & Murphy Jr., N.R., (1965) "Normal Stresses at the Tire-Soil Interface in Yielding Soils", Highway Research Record, No. 74, pp. 1-18.

Frietag, D.R., (1965) "Wheels on Soft Soils; An Analysis of Existing Data", Tech. Report No. 3-670, U. S. Army Eng. Wat. Expt. Sta., Vicsburg, Miss.

Freudenthal, A.M., & Geiringer, H., (1950) "The Mathematical Theories of the Inelastic Continuum", Elasticity and Plasticity, Ency. of Physics., Vol. VI, pp. 229-432, Edited by S. Flugge, Springer-Verlag, Berlin.

Hegedus, E., (1960) "A Simplified Method for Determination of Bulldozing Resistance", Rep. No. 61, O.A.T.C., Detroit Arsenal.

Hegedus, E., (1965) "Pressure Distribution Under Rigid Wheels", Trans. Am. Soc. Agric. Eng., Vol. 8, No. 3, pp.305.

Hencky, H., (1924) "z. angew. Math-Mech. 4", pp. 323, Reviewed by Freudenthal and Geiringer (1950).

Hill, R., (1950) "The Mathematical Theory of Plasticity", Oxford University Press.

Janosi, Z., (1961) "An Analysis of Pneumatic Tire Performance on Deformable Sand", Proc. 1st Int. Conf. I.S.T.V.S., Turin, pp.737-762.

Japp, R.D., (1968) "An Investigation of the Dynamic Behaviour of Inelastic Materials", Ph.D. Thesis, McGill University.

Leflaive, E.M., (1966) "Description of Wheel Performance on Dry Sand in Terms of Energy Parameters", paper presented at 2nd Int. Conf. I.S.T.V.S., Quebec.

Love, A.E.H., (1946) "A Treatise on the Mathematical Theory of Elasticity", Dover, New York.

McKibben, E.G., (1938) "Some Kinematic and Dynamic Studies of Rigid Transport Wheels for Agricultural Equipment", Iowa State College of Agriculture, Research Bulletin 231, Ames, Iowa.

McKyes, S.E., (1969) "An Investigation of the Deformation Behaviour of Clay Soils", Ph.D. Thesis, McGill University.

McMaster, R.C., (1959) "Non Destructive Testing Handbook", Volume I, Ronald Press, New York.

Nadai, A., (1950) "Theory of Flow & Fracture of Solids", Volume I, McGraw Hill, New York.

Onafeko, O., (1964) "Measuring Radial & Tangential Stress Beneath Rigid Wheels", J. Terramechanics, Vol. 1, No. 3, pp. 61.

Onafeko, O., & Reece, A.R., (1967) "Soil Stresses and Deformation Beneath Rigid Wheels", J. Terramechanics, Vol. 4, No. 1, pp. 59-80.

Phillips, J.R., (1961) "The Powered Vehicular Wheel Plane-Rolling in Equilibrium; A Consideration of Slip and Rolling Resistance", Proc. 1st Int. Conf. I.S.T.V.S., Turin, pp.541-557.

Poletayev, A.F., (1964) "The Compaction of Soil Under a Rolling Wheel", J. Terramechanics, Vol. 1, No. 3, pp. 7-17.

Prager, W., (1961) "Introduction to Mechanics of Continua", Ginn & Co., Boston.

Prager, W., & Hodge, P.G., (1951) "Theory of Perfectly Plastic Solids", John Wiley & Sons, New York.

Reece, A.R., (1965) "Principles of Soil-Vehicle Mechanics", Proc. Inst. Mech. Eng., London. Vol. 180, Part 2A, pp. 45.

Reece, A.R., (1961) Discussion on paper by Phillips (1961).

Roscoe, K.G., Arthur, J.R.F., & James, R.G., (1963) "The Determination of Strains in Soils by an X-Ray Method", Civ. Eng. and Pub. Wks. Rev. 58, pp. 873-876 and 1009-1012.

Sela, A.D., (1961) "On the Slip & Tractive Effort", Proc. 1st Int. Conf. I.S.T.V.S., Turin, pp. 587-604.

Schuring, D., (1966) "The Energy Loss of a Wheel", Proc. 2nd Int. Conf. I.S.T.V.S., Quebec, pp. 391-424.

Sylvestre-Williams, R., (1969) "Velocity and Strain Rate Fields Under Action of a Grouser in Sand", M.Eng. Thesis, McGill University.

Thomsen, E.G., and Lapsley, J.T., (1954) "Experimental Stress Determination with a Metal During Plastic Flow", Proc. Am. Soc. of Exptl. Stress Analyses, Vol. 11, No. 2, pp. 59-68.

Thomsen, E.G., Yang, C.T., and Bierbower, J.B., (1964) "An Experimental Investigation of the Mechanics of Plastic Deformation of Metals", University of California Publication in Engineering, Vol. 5, No. 4, pp. 89-144.

Thomsen, E.G., Yang, C.T., & Kobayashi, S., (1965) "Mechanics of Plastic Deformations in Metal Processing", MacMillan, New York, pp. 486.

Uffelmann, F.L., (1961) "The Performance of Rigid Cylindrical Wheels on Clay Soil", Proc. 1st Int. Conf. I.S.T.V.S., Turin, pp. 111-125.

Victoreen, J.A., (1949) "The Calculation of X-Ray Mass Absorption Coefficients", J. App. Phys. Vol. 20, pp. 1141.

Wallis, W.A., and Roberts, H.U., (1956) "Statistics: A New Approach", The Free Press, New York.

Wills, B.M.D., (1966) "The Load Sinkage Equation in Theory and Practice", Proc. 2nd Int. Conf. I.S.T.V.S., Quebec, pp. 199-246.

Wilson, N., & Krzywicki, H.R., (1966) "Soil Mechanics as it Affects Vehicle Performance", Can. Geo. Jr., Vol. 3, pp. 204-216.

Wismer, R.D., (1966) "Performance of Soils Under Tire Loads", Report 3, "Tests in Clay Through Nov. 1962", Tech. Report No. 3-666, U.S. Army Eng. Wat. Expt. Sta., Vicsburg, Miss.

Wong, J.Y., & Reece, A.R., (1966) "Soil Failure Beneath Rigid Wheels", Proc. 2nd Int. Conf. I.S.T.V.S., Quebec, pp. 425-445.

Yong, R.N., Boyd, C.W., & Simonsen, O.F., (1964) "Fundamental Research Considerations in Soil-Vehicle Interaction", McGill University, Soil Mechanics Series, No. 11.

Yong, R.N., Boyd, C.W., & Webb, G.L., (1967) "Experimental Study of Behaviour of Sand Under Moving Rigid Wheels", McGill University, Soil Mechanics Series, No. 20.

Yong, R.N., & Osler, J.C., (1966) "On the Analysis of Soil Deformation Under a Moving Rigid Wheel", Proc. 2nd Int. Conf. I.S.T.V.S., Quebec, pp. 339-352.

Yong, R.N., & McKyes, S.E., (1967) "Yielding of Clay in a Complex Stress Field", Proc. 3rd Int. Pan Am. Cont., Caracas, pp.131-143

Yong, R.N., & Warkentin, B.P., (1966) "Introduction to Soil Behaviour", MacMillan, New York, pp.